**Dissertations in Forestry
and Natural Sciences**

UNIVERSITY OF
EASTERN FINLAND

ANNINA SAUKKO

Triple Contrast Method for Computed Tomography Diagnostics of Cartilage Injuries

Annina Saukko

TRIPLE CONTRAST METHOD FOR COMPUTED TOMOGRAPHY DIAGNOSTICS OF CARTILAGE INJURIES

ACADEMIC DISSERTATION

To be presented by the permission of the Faculty of Science and Forestry for public examination in the Auditorium CA101 in Canthia Building at the University of Eastern Finland, Kuopio, on August 27th, 2021, at 12 o'clock.

Author's address: University of Eastern Finland
                      Department of Applied Physics
                      P.O.Box 1627
                      70211 KUOPIO
                      FINLAND
                      email: annina.saukko@uef.fi

Supervisors: Professor Juha Töyräs
                      University of Eastern Finland
                      Department of Applied Physics
                      Kuopio, Finland
                      Kuopio University Hospital
                      Kuopio, Finland
                      email: juha.toyras@kuh.fi

                      Dean Jukka Jurvelin
                      University of Eastern Finland
                      Faculty of Forestry and Natural Sciences
                      Kuopio, Finland
                      email: jukka.jurvelin@uef.fi

                      Juuso Honkanen, PhD
                      Center of Oncology
                      Kuopio University Hospital
                      Kuopio, Finland
                      email: juuso.honkanen@kuh.fi

Reviewers: Adjunct Professor Mika Kortesniemi
                      University of Helsinki and Helsinki University
                      Hospital
                      HUS Medical Imaging Center
                      Helsinki, Finland
                      email: mika.kortesniemi@hus.fi

                      Assistant Professor Ketan Ghaghada
                      Texas Children's Hospital
                      Department of Pediatric Radiology
                      Houston, USA
                      email: ghaghada@bcm.edu

Opponent: Research Director Harri Sievänen
                      UKK-Institute
                      Tampere, Finland
                      email: harri.sievanen@ukkinstituutti.fi

ABSTRACT

Post-traumatic osteoarthritis (PTOA) is a joint disease associated with the gradual erosion of cartilage covering the ends of articulating joints. It can result from a single traumatic incident, repetitive injurious incidents, or due to excessive mechanical stress and strain. Resulting abnormal mechanical function and biochemical alterations may lead to post-traumatic changes in cartilage structure and composition. In PTOA, these changes may eventually worsen and lead to a progression of osteoarthritis (OA). Identification of incipient post-traumatic changes is crucial for the selection of the optimal conservative, such as exercise, losing weight, pain relief medicines, steroid injections, non-steroidal anti-inflammatory drugs, or surgical intervention, but effective means to identify them are still limited.

Superficial collagen disruption, proteoglycan (PG) loss, and increased water content are the first signs of OA. These alterations in tissue structure and composition increase tissue permeability and decrease the fixed charge density in cartilage matrix. Contrast-enhanced computed tomography (CECT) is an imaging technique that utilises contrast agents. With CECT, the detection of OA-related changes is possible as the degenerative changes alter the diffusion and accumulation of contrast agents in articular cartilage. Contrast agents may also be exploited for segmentation of cartilage tissue in CT images since contrast agents enhance the interface between synovial fluid and cartilage as the natural contrast at this interface is almost non-existent.

Current CECT of a knee joint includes two subsequent CT scans acquired immediately and 45 minutes after the intra-articular injection of an anionic contrast agent. The scan acquired immediately after contrast agent administration allows segmentation of the articulating surface and lesions, while the latter scan enables detection of internal cartilage changes related to the initiation of PTOA. This method includes two drawbacks. Firstly, recent studies suggest that a recently developed cationic contrast agent has a superior sensitivity for PG content at diffusion equilibrium compared with conventional anionic agents. However, a critical weakness of cationic agent occurs at clinically feasible time points (< 120 min after injection) as the diffusion of cationic contrast agent is controlled by degeneration related factors (i.e., loss of PG, increase in water content, and increased permeability) having opposite effects on diffusion and leading to diminished sensitivity. We hypothesize that this drawback is solved by adding a non-ionic contrast agent that is sensitive to increases in tissue permeability and water content. The second drawback is related to contrast agent diffusion-induced loss of contrast at the synovial fluid-cartilage interface. To overcome this drawback, we propose the use of nanoparticles (NPs) that, due to their size, are too large to diffuse into cartilage tissue. Consequently, the NPs can maintain a high contrast at the synovial fluid-cartilage interface even at later imaging time points.

The aim of this thesis was to introduce a triple contrast agent method that, to-

gether with a quantitative dual-energy CT (QDECT), enables simultaneous quantification of PG and water contents in articular cartilage and enables the accurate segmentation of the articulating surfaces. To this end, we first studied the suitability of two different dual contrast methods for the detection of different types of cartilage injuries. This research then led to the development of the triple contrast agent. In study **I**, the potential of the dual contrast agent consisting of anionic, iodine-based contrast agent and a suspension of bismuth(III) oxide nanoparticles (BiNPs) to detect different types of articular cartilage injuries was evaluated. Also, the ability to facilitate a high contrast at articular surfaces for improved segmentation was examined. The dual contrast agent consisting of cationic, iodine-based and non-ionic, gadolinium-based contrast agents was examined in study **II**. The ability of this dual contrast agent to allow simultaneous determination of PG and changed permeability at clinically feasible time points (i.e., 1 h and 2 h after contrast agent administration) was determined. In study **III**, a triple contrast agent, being a mixture of three contrast agents (cationic, iodine-based and non-ionic, gadolinium-based contrast agents together with BiNP suspension), was studied for simultaneous determination of cartilage PG content, water content, and changed permeability and segmentation of the articulating surfaces. Finally, the capability of the dual contrast agent based on cationic and non-ionic contrast agents to detect post-traumatic changes in equine cartilage tissue around the surgically-induced lesions was evaluated in study **IV**.

BiNPs were found to maintain a high contrast at articulating surfaces. This was shown to allow an accurate segmentation of the cartilage surfaces at the same time as anionic contrast agent enabled the detection of cartilage degeneration. Further, the cartilage lesions caused by the mechanical impact were visualized (study **I**). The findings of study **II** suggest that the simultaneous evaluation of cationic, iodine-based and non-ionic, gadolinium-based contrast agent partitions is possible with QDECT. As the cationic contrast agent is sensitive to PG, tissue permeability as well as water content and non-ionic agent to tissue permeability and water content, their mixture allows subsequent quantitative determination of PG and water contents. As a result, a significant correlation ($P < 0.001$) between cationic contrast agent partition and PG content was obtained, enabling differentiation between the intact and injured cartilage. In study **III**, the triple contrast agent measurements demonstrated that the benefits of the two dual contrast agents also were present in triple contrast agents; accurate determination of articulating surface was possible with simultaneous quantification of PG and water contents. In study **IV**, significant differences in partition of cationic, iodine-based agent between post-traumatic and control samples were seen at 30 min ($P = 0.004$), 60 min ($P = 0.028$), and 20 h ($P < 0.001$) and in partition of non-ionic contrast agent at 60 min ($P < 0.001$) and 120 min ($P = 0.002$) after immersing the samples in contrast agent bath. Further, significant Spearman correlations between the cationic agent partitioning and PG content were obtained at 20 h ($\rho = 0.69$, $P < 0.001$) and 24 h ($\rho = 0.63$, $P < 0.001$) diffusion time points.

In light of the findings presented in this thesis, the triple contrast method enables improved characterisation of cartilage composition, i.e., PG and water contents can be evaluated simultaneously together with accurate segmentation of the articulating surfaces. Thereby, for example, the evaluation of post-traumatic degeneration around a lesion site is possible with a single scan. These improvements in CECT may allow a more effective selection of patient-specific surgical treatment options and prevention of PTOA.

To my parents Nina and Asko

ACKNOWLEDGEMENTS

Turku, June 17, 2021

Annina Saukko

ABBREVIATIONS

2D	Two-dimensional
3D	Three-dimensional
AU	Arbitrary unit
AuNP	Gold nanoparticle
BiNP	Bismuth(III) oxide nanoparticle
CA	Contrast agent
CA4+	Contrast agent bearing four positive charges
CCD	Charged-coupled device
CT	Computed tomography
CECT	Contrast-enhanced computed tomography
DD	Digital densitometry
dGEMRIC	Delayed gadolinium enhanced magnetic resonance imaging of cartilage
ECM	Extracellular matrix
EDTA	Ethylenediaminetetraacetic acid disodium salt
FCD	Fixed charge density
GAG	Glycosaminoglycan
Gd	Gadolinium
HU	Hounsfield unit
I	Iodine
ICRS	International Cartilage Repair Society
LM	Light microscope
microCT	X-ray microtomography
MRI	Magnetic resonance imaging
NP	Nanoparticle
NSAID	Nonsteroidal anti-inflammatory drug
OA	Osteoarthritis
OD	Optical density
PBS	Phosphate buffered saline
PCD	Photon counting detector
PEG	Polyethylene glycol
PG	Proteoglycan
PTOA	Post-traumatic osteoarthritis
QDECT	Quantitative dual-energy computed tomography

SYMBOLS AND NOTATIONS

[...]	Concentration
A	Atomic mass
α	X-ray attenuation
C	Concentration
d	Diameter
E	X-ray photon energy
E_{dyn}	Dynamic modulus
E_{eq}	Equilibrium modulus
F	Faraday constant
I	Intensity
I_0	Initial intensity
J	Diffusion flux
M	Molar mass
μ	Mass X-ray attenuation coefficient
μ_l	Linear X-ray attenuation coefficient
n	Number of samples
N	Number of knee joints
ν	Poisson's ratio
P	Level of statistical significance
Ψ	Membrane potential
q	Electric charge
r	Donnan ratio
R	Gas constant
ρ	Spearman's rho
ρ_d	Density
t	Time
T	Temperature
x	Distance
z	Valence of the ion
Z	Atomic number

LIST OF PUBLICATIONS

This thesis consists of the present review of the author's work in the field of medical imaging and the following selection of the author's publications:

I Saukko, A. E., Honkanen, J. T., Xu, W., Väänänen, S. P., Jurvelin, J. S., Lehto, V. P. & Töyräs, J. (2017). Dual contrast CT method enables diagnostics of cartilage injuries and degeneration using a single CT image. Annals of Biomedical Engineering, 45(12), 2857–2866.

II Saukko, A. E., Turunen, M. J., Honkanen, M. K., Lovric, G., Tiitu, V., Honkanen, J. T., Grinstaff, M. W., Jurvelin, J. S. & Töyräs, J. (2019). Simultaneous quantitation of cationic and non-ionic contrast agents in articular cartilage using synchrotron microCT imaging. Scientific Reports, 9(1), 1–9.

III Honkanen, M. K.*, Saukko, A. E.*, Turunen, M. J., Xu, W., Lovric, G., Honkanen, J. T., Grinstaff, M. W., Lehto, V. & Töyräs, J. (2020). Triple contrast CT method enables simultaneous evaluation of articular cartilage composition and segmentation. Annals of Biomedical Engineering, 48(2), 556–567.
(*Equal contribution)

IV Saukko, A. E., Nykänen, O., Sarin, J., Nissi, M., te Moller, N. C., Weinans, K., Mancini., I. A., Visser, J., Brommer, H., van Weeren, P. R., Malda, J., Grinstaff, M. & Töyräs, J. Dual contrast CT technique can reveal equine post-traumatic osteoarthritis *in vitro*.
Accepted to Journal of Orthopaedic Research (2021).

Throughout the thesis, these papers will be referred to by Roman numerals.

AUTHOR'S CONTRIBUTION

The publications selected in this dissertation are original research papers on contrast-enhanced computed tomography of articular cartilage injuries utilizing dual and triple contrast agents. In study **I**, the author contributed to the design and implementation of the research, conducted the measurements and analysed and interpreted the data, and wrote the first draft of the manuscript. In study **II**, the author prepared the samples, analysed the data, and drafted the manuscript. The measurements were conducted together with Miitu H and Mikael T. In study **III**, the author prepared the samples for the X-ray microtomography measurements, which were conducted together with the author, Miitu H, Mikael T, and Juha T. The author also aided in interpreting of the results, and worked on the manuscript. In study **IV**, the author manufactured the samples, performed the measurements, processed the experimental data, and drafted the manuscript. In all studies, each co-author has made substantial scientific contributions to the reported work.

TABLE OF CONTENTS

1 Introduction

Articular cartilage is a highly specialized connective tissue that covers the ends of articulating bones. The function of articular cartilage is to provide a smooth surface for low-friction movements, thus allowing proper functioning of a healthy joint. Acute cartilage injuries, such as sports injuries or sudden impact from a fall, can lead to subchondral bone contusions, torn ligaments, and meniscal tears [1]. Moreover, these changes can cause abnormal joint function that can create excessive mechanical stresses and strains in cartilage, which in turn can lead to a progressive loss of joint cartilage and subsequent post-traumatic osteoarthritis (PTOA). The tissue changes related to late-stage PTOA are similar to idiopathic osteoarthritis (OA). Articular cartilage is prone to degeneration resulting from its limited capacity for self-regeneration due to its avascular nature. The degenerative changes in articular cartilage include PG depletion, alterations in the collagen fibril network, and reduction in the collagen content [2–4]. Further, these structural changes in proteoglycans (PGs) and collagen fibrils result in cartilage swelling, increased water content and tissue permeability that allow free water and other molecules to flow in and out of the tissue.

PTOA causes pain and reduced physical activity at an individual level but also induces huge economic losses for the society. In Finland, the annual economic burden of OA is estimated to be hundreds of millions of euros, and 6% of the disability pensions are granted based on OA [5]. PTOA represents approximately 12% of all cases of OA [6], and it primarily affects young individuals [7]. PTOA usually develops to clinically diagnosable OA in 2 to 5 years after certain articular fractures and in decades after less severe joint injuries [1]. The probability of PTOA after a significant joint injury is estimated to vary from 20% to 50% [7]. Surgical, pharmaceutical intervention, and conservative methods (e.g., weight loss, exercise therapy, or knee bracing), may prevent or slow down the development of PTOA after acute cartilage injury provided that the early signs of initiation are observed in time, thus allowing the early preventive actions [1, 8]. To this end, sensitive techniques to detect acute cartilage lesions and early post-traumatic degenerative changes are needed to allow these actions.

Magnetic resonance imaging (MRI) and contrast-enhanced computed tomography (CECT) provide excellent tools to diagnose cartilage injuries and the initiation of PTOA. MRI provides excellent soft tissue contrast and is thus an important clinical tool in cartilage imaging. MRI can identify cartilage tissue properties, such as proteoglycan (PG) content, collagen orientation, and water content [9,10]. However, in some cases, the use of MRI is hindered due to its relatively low spatial resolution and long image acquisition times [10, 11]. On the other hand, CECT exhibits higher spatial resolution and shorter scan times at approximately half the cost of MRI. Downsides of CECT include the use of ionizing radiation; however, in clinical extremity imaging, low radiation doses with effective doses ranging between 27 and 48 μSv (equal to exposure of approximately 3 – 6 days of background radiation in Finland) [12] are achieved. Further, an injection of an iodine-based contrast agent is required and comes with the possibility of adverse side effects.

CECT imaging is based on the use of X-ray positive contrast agents. In knee CT arthrography, contrast agent enhances the visualisation of synovial fluid-cartilage interface. Without the agent the contrast is nonexistent due to similar X-ray absorption characteristics of synovial fluid and cartilage. Contrast agents are also used to study the degeneration-related changes in cartilage as their uptake into cartilage is dependent on the severity of the degeneration [13–19]. Commercially available contrast agents include anionic and non-ionic contrast agents. A decrease in cartilage fixed charge density (FCD) via the loss of PG macromolecules is a degenerative change that can be detected with anionic contrast agents. These contrast agents with negative molecular charges are repelled from cartilage due to the negative FCD in tissue and are thus distributed into cartilage inversely proportional to the PG content. Further, as the negative FCD decreases along with degeneration, the uptake of anionic contrast agents into tissue increases, thus revealing degenerated tissue through elevated uptake. These degenerative changes also include an increase in water content and the disruption of the superficial collagen network [20, 21]. These changes can be studied with both anionic and non-ionic contrast agents as the uptake of these contrast agents increases with increased water content and disruption of the collagen network with increased tissue permeability.

Recently, cationic contrast agents have raised interest as potential contrast agents in cartilage imaging. Recent studies have reported that cationic contrast agent CA4+, at diffusion equilibrium, increases sensitivity for tissue PG content compared to commercially available anionic and non-ionic contrast agents [11, 13, 22, 23]. As a positively charged molecule, CA4+ distributes into cartilage proportionally to the PG content. This is due to the electrostatic attraction between the CA4+ and the negative FCD of PG molecules. Even though CA4+ exhibits high sensitivity at diffusion equilibrium towards PG content, CA4+ has shown diminished sensitivity at clinically feasible time points (i.e., imaging time points from 30 minutes up to 2 hours from the administration of the contrast agent) [24]. The lack of performance at early-stage of diffusion results from two degeneration-related factors that have opposite effects on the CA4+ diffusion; the diffusion decreases with the loss of PGs and increases with decreased steric hindrance (i.e., the physical diffusion barrier of the tissue orchestrated by collagen network architecture and PGs in the matrix) and increased water content. To remedy this shortcoming, we propose a quantitative dual-energy CT technique (QDECT) allowing quantitative simultaneous imaging of the diffusion of two contrast agents.

QDECT is a technique that utilizes two X-ray imaging energies and a mixture of two contrast agents. In this thesis, the contrast agent mixture is composed of a cationic, iodine-based contrast agent (CA4+) and a non-ionic, gadolinium-based contrast agent (gadoteridol). As mentioned above, CA4+ distributes into cartilage proportionally to the PG distribution. However, as gadoteridol has no molecular charge, it distributes into cartilage following the water content and steric hindrance. Based on this, the effect of water and a steric hindrance on the CA4+ diffusion may be minimized by normalizing the partition of CA4+ with that of gadoteridol. To simultaneously obtain the CA4+ and gadoteridol distributions within cartilage, the samples need to be imaged with two different X-ray energies. Element-specific absorption k-edges of iodine (33.2 keV) and gadolinium (50.3 keV) are used to select the optimal imaging energies. X-ray sources produce either monochromatic or polychromatic energy. With a monochromatic X-ray source, that produces X-rays with an extremely narrow energy band, the two X-ray energies in QDECT are selected from both sides of either iodine or gadolinium k-edge. For example, energies of 25

keV 37 keV could be used. However, with a polychromatic X-ray source producing a continuous spectrum of photon energies, the X-ray tube voltages in QDECT should be selected so that the effective energies of the spectra fall in both sides of the iodine or gadolinium k-edge. In this case, the X-ray tube voltages could be for example 70 kV and 140 kV. Clinical CT devices currently produce polychromatic X-rays.

When studying superficial cartilage lesions together with internal tissue changes, the current clinical CECT of a knee joint includes two subsequent scans; the first scan (arthrography) is acquired immediately and the second scan (delayed arthrography) in 30 minutes to 2 hours after the contrast agent administration into the joint space [23–25]. The first scan enables the accurate segmentation of articulating surfaces together with the identification of surface lesions. The second scan, on the other hand, allows the detection of internal changes on the lesion site as well as evaluation of PTOA initiation in the surrounding tissue by observing the partitioning of contrast agent within the tissue. These two scans are essential due to contrast agent diffusion-induced loss of contrast at the cartilage-synovial fluid interface in the latter scan. This prevents the accurate segmentation and delineation of lesions. At the same time, the assessment of internal degenerative changes in cartilage is impossible based on the first scan as the contrast agent has not had enough time to diffuse into the tissue. In addition to being logistically challenging, need for two scans increases the radiation dose to a patient. To overcome this issue, we developed bismuth(III) oxide nanoparticles (Bi_2O_3-NP, later abbreviated as BiNP) coated with polyethylene glycol (PEG) that, due to their size, are too large to be able to diffuse into cartilage. The BiNPs are thus able to maintain the contrast at articulating surfaces even at delayed imaging time points. BiNPs are hence allowing simultaneous segmentation of articulating surfaces and surface lesions together with the assessment of internal cartilage integrity from the delayed arthrography, thus eliminating the need for two separate CT scans.

In this thesis, we developed two different dual contrast agents. The first dual contrast agents utilized commercial anionic contrast agent mixed with BiNPs to allow simultaneous segmentation of the articular cartilage surface and quantitative characterization of tissue properties and health. The second contrast agent allowed separate determination of cartilage PG and water contents based on simultaneous quantification of iodine-based, cationic and gadolinium-based, non-ionic contrast agents using QDECT. Lastly, the advantages of the two dual contrast gents were combined into one solution leading to the introduction of a triple contrast agent. The triple contrast agent is a mixture of three contrast agents: 1) cationic, iodine-based CA4+, 2) non-ionic, gadolinium-based gadoteridol, and 3) BiNP suspension. The development of the triple contrast agent included several steps, and each of these steps is briefly introduced below in the descriptions of the publications this thesis is based on.

In study **I**, the potential of nanoparticles in cartilage imaging is studied by mixing them with commercially available anionic, iodine-based contrast agent (ioxaglate). Study **II** focuses on the evaluation of another dual contrast agent being a mixture of cationic, iodine-based contrast agent (CA4+) and non-ionic, gadolinium-based contrast agent (gadoteridol). The ability for simultaneous evaluation of water and PG contents based on quantification of cationic and non-ionic contrast agent partitions at clinically relevant diffusion time points is studied. In study **III**, the potential of the QDECT technique and its ability to monitor the end result of surgical repair of chondral injuries and to detect post-traumatic degeneration in the tissue around the repaired lesion is determined. Finally, in study **IV**, a triple contrast agent composed

3

of CA4+, gadoteridol, and BiNPs is introduced. In this study, our aim was to show that the triple contrast method allows a simultaneous and quantitative evaluation of interstitial water and PG contents in articular cartilage based on CA4+ and gadoteridol distributions within tissue similarly as with the dual contrast agent consisting of CA4+ and gadoteridol. Our second aim was to demonstrate that BiNPs enable simultaneous segmentation of the articulating surfaces and lesions at all imaging time points, thus removing the need for the first arthrography.

2 Knee Joint

In this chapter, the anatomy of the knee joint and especially articular cartilage with its structure, composition, and mechanical properties are described. Further, PTOA together with degenerative changes is introduced. The clinical diagnosis and treatment of PTOA are also briefly discussed.

The knee (Fig. 2.1) is the largest joint in the body and is a hinge type synovial joint. It mainly allows flexion and extension as well as a small degree of medial and lateral rotation. Knee is a complex structure consisting of bones, cartilage, ligaments, tendons, bursae, joint capsule, synovial fluid, and menisci. The knee joints femur (thigh bone) to the tibia (shin bone). A smaller bone, fibula, runs along the tibia while the patella articulates with the femur covering and protecting the anterior articular surface of the joint. Bones are connected to the leg muscles (quadriceps and hamstring muscles) by tendons. These muscles and tendons are vital to motion and provide most of the power and control for the knee joint. Ligaments join the knee bones while also providing stability. Patellar ligament is a continuation of the quadriceps femoris tendon and is attached to the tibial tuberosity (a ridge-like prominence). Anterior and posterior cruciate ligaments connect the femur and the tibia. Medial and lateral collateral ligaments, on the other hand, can be found on the sides of the joint and they stabilise the hinge motion of the knee, preventing exces-
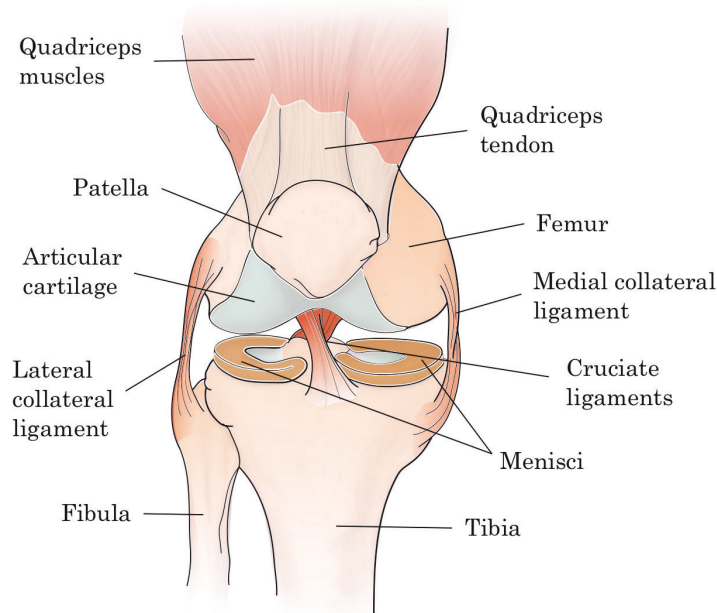

Figure 2.1: Schematic drawing of the human right knee joint.

sive medial or lateral movement. The moving structures of the joint are surrounded by a sac called bursa. Four bursae are found in the knee joint. The bursae are filled with synovial fluid. This fluid circulates around the patella, tibia, and femur and lubricates and provides nutrients to the joint. In a healthy knee, articular cartilage covers the dorsal surface of the patella and ends of the femur and tibia.

2.1 ARTICULAR CARTILAGE

Articular cartilage is elastic, highly specialized connective tissue that covers the articulating bone surfaces of diarthrodial joints. It allows a low friction surface enabling bones to glide smoothly against each other. In addition, articular cartilage facilitates the transmission of loads and absorbs shocks protecting the underlying bone from impacts. By reducing wear, stress, and friction, the articular cartilage enables a range of motions needed in daily living and in athletic endeavors.

2.1.1 Structure and Composition

Articular cartilage is hyaline cartilage, which is a porous, viscoelastic fiber-reinforced tissue [26]. In humans, thickness of the articular cartilage in the knee joint varies from 2 to 4 mm [27]. Cartilage tissue is mainly comprised of extracellular matrix (ECM) surrounding by a sparse distribution of highly specialized cells called chondrocytes (1-2% of the total tissue volume). The ECM is composed of collagen (15–22% of the wet weight), PGs (4–7% of the wet weight) [28], interstitial water (60–80% of the wet weight), and electrolytes [29]. PGs, collagen, and electrolytes are crucial for maintaining the water within the ECM, thus preserving cartilage's unique mechanical properties. Cartilage has no blood vessels, nerves, or lymphatics, unlike most other tissues [28]. Due to the absence of these tissue components, nutrients are transported to the cartilage through diffusion. Synovial fluid acts as the main source of nutrition. Further, this absence also results in slow or no regeneration of articular cartilage after an injury.

Water is the main component of cartilage. Most of the water can freely diffuse in and out from the cartilage while approximately 30% of this water is bound within the intrafibrillar space of the collagen, and the remaining part is contained in the pore space of the matrix. The relative water content is highest at the superficial zone (80%) and decreases towards the deep zone (65%) [29, 30]. Inorganic ions such as sodium, calcium, chloride, and potassium are dissolved into water. The concentration of cationic ions is much higher than that of anionic ions to balance the negative FCD induced by PGs.

Water serves many important functions, such as maintaining the transportation of nutrients and ions to chondrocytes across the cartilage tissue. The avascular structure ensures that the water can freely transport in and out from cartilage through diffusion and convection. Also, mechanical properties depend on water content and tissue permeability on water flow. Cartilage's ability to withstand significant loads derives mainly from two factors: the frictional resistance to the water flow and the pressurization of water within the matrix.

Collagen is the most abundant structural macromolecule in ECM, forming the internal skeleton of articular cartilage tissue. Collagen represents 10–22% of the
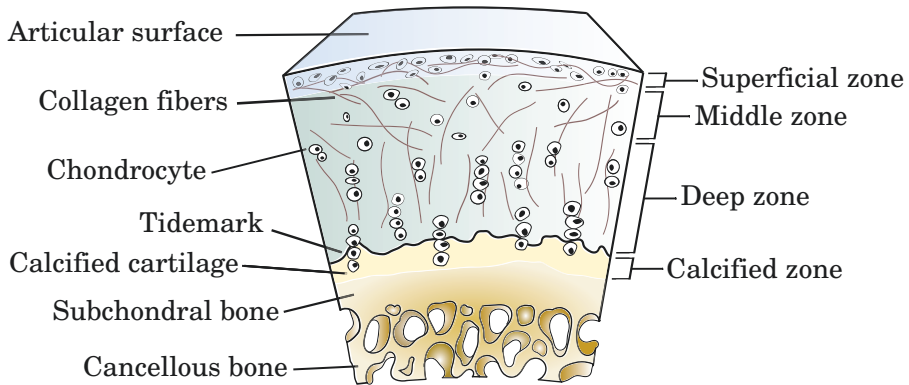
Figure 2.2: Schematic illustration of articular cartilage structure and composition. Cartilage can be divided into four zones: 1) superficial zone (5-20% of the cartilage thickness), 2) middle zone (20-60% of the cartilage thickness), 3) deep zone (50-75% of the cartilage thickness), and 4) calcified zone [31].

wet weight of cartilage [32]. Collagen is primarily of type II collagen. Type II collagen contributes up to 95% of the collagen in ECM. Type II collagen forms fibrils and fibers tightly packed, specifically aligned, and extensively cross-linked. Other collagen types also exist, such as types I, IV, V, VI, IX, and XI, but they contribute only a minor proportion of the collagen in cartilage. Their main function is to form and stabilize the type II collagen fibril network. The orientation of collagen fibrils varies between the cartilage zones. In the superficial zone of articular cartilage, the collagen fibrils are densely packed and orientated parallel to the surface. In the middle zone, the fibrils are oriented in a more randomly fashion but bend over to merge more perpendicularly to the surface. In the deep cartilage, the fibrils are arranged perpendicular to the underlying subchondral bone being attached to the bone through the calcified cartilage [29, 33]. In addition, secondary collagen fibrils are orienting randomly throughout the cartilage. The collagen concentration is lowest in the middle zone but increases both towards the deep and the superficial zones [34].

PG is a heavily glycosylated protein that is composed of a core protein and one or more covalently attached glycosaminoglycan (GAG) chains [35]. PGs contribute 5–10% of the articular cartilage wet weight representing the second-largest macromolecule group in ECM after collagen [32]. In articular cartilage, the highest PG content is at the deep zone, and the content decreases towards the superficial zone [28, 36]. A variety of PGs, including aggrecan, decorin, biglycan, and fibromodulin, exists in articular cartilage. PGs inflict a negative fixed charge for the tissue due to negatively charged functional sulphate ($-SO_4$) and carboxyl (-COOH) groups [37]. The negative fixed charge creates osmotic pressure in the ECM, resulting in water and cations to be drawn into cartilage tissue's extracellular space. This causes swelling of the tissue, which in turn is constrained by the collagen network [38]. This swelling pressure contributes to the mechanical properties of the cartilage, especially, to cartilage tissue's compressive stiffness [28].

Chondrocytes are the only cell type that is found in cartilage tissue, and they account only for 1-2% of the total volume of articular cartilage [39]. Chondrocytes,

in normal conditions, are stable, highly specialized, metabolically active cells that maintain the ECM [27, 40]. They also synthesize ECM components to repair and maintain the structural integrity of the tissue. However, as chondrocytes possess the limited potential for replication, they can respond only to minor tissue changes, thus contributing to the limited intrinsic healing capacity of cartilage. Chondrocytes vary in their shape, size, and number, depending on the anatomical regions. The chondrocytes near the surface at the superficial zone are more flattened and smaller while the deeper cells are spheroidal and align into columns perpendicular to the articulating surface. The superficial zone has a greater number of chondrocytes compared with the deep layers [27, 30].

Articular cartilage can be structurally divided into four zones; 1) superficial or tangential zone, 2) middle or transitional zone, 3) deep or radial zone, and 4) calcified zone. These zones vary in composition and structure (Fig. 2.2) [41, 42]. A thin superficial zone makes up approximately 5-20% of the articular cartilage thickness and provides most of the cartilage tissue's tensile properties [31]. The main function of the superficial zone is to resist shear and compressive forces and to provide the integrity that is imperative to protect and maintain the deeper layers. Immediately below the superficial zone is the middle zone that represents 20-60% of cartilage thickness. In the middle zone, as the collagen fibrils in this zone are organized in a more random manner, they provide resistance to compressive stresses applied to the joint [43]. The deep zone represents approximately 50-75% of the total cartilage thickness [31]. The deep zone provides cartilage with great resistance for compressive forces [41]. The deep zone and calcified zone are distinguished by the tidemark. The calcified zone is responsible for securing the cartilage to the underlying subchondral bone. In practice, this is done by anchoring the collagen fibrils of the deep zone to the subchondral bone.

2.1.2 Function and Mechanical Properties

Articular cartilage distributes the load directed to it to the underlying subchondral bone, and its unique mechanical properties and structure enable the cartilage to adapt under frictional, compressive, shear, and tensile loading [44, 45]. Also, cartilage tissue possesses good resilience and viscoelastic properties [46]. These features are crucial for maintaining the normal articular cartilage structure and function as inactivity of the joint can results in degeneration of the cartilage tissue [29].

During rapid joint loading, the collagen network and increase in interstitial fluid pressure control the deformation by stiffening the cartilage. Collagen network provides resilience to the cartilage deformation under loading, and the low permeability prevents the fast fluid outflow from the matrix [38, 47–49]. Increase in the interstitial fluid pressure enhances the fluid flow out of the ECM which results in a large frictional drag caused by the matrix [37, 50]. As the load is removed, the fluid flows back into the cartilage tissue. Under static loading, on the other hand, cartilage tissue softens while it distributes the load to a larger area by allowing the fluid flow within and out from the area. When subjected to a constant load or deformation, the articular cartilage is viscoelastic and changes in a time-dependent manner. Finally, at the end of deformation, an equilibrium is reached between the load and forces resisting the cartilage deformation. Here, PGs play an important role in supporting the load by providing cartilage with its osmotic properties [47, 51]. When the static load is released, interstitial fluid flows back into matrix and cartilage returns back to its original state. After mechanical injury or due to arthritic degeneration, the

collagen fibril network is damaged and results in subsequent expansion of PGs and increase in water content. These changes increase the matrix permeability and decreases the cartilage stiffness leading to impaired capability of cartilage to support load [52].

In addition to distributing loads and managing stresses, articular cartilage provides a smooth, lubricated, and low friction surface for articulation. Two main mechanisms ensure that minimal friction between articulating surfaces is achieved. In first line macromolecules, such as lubricin, provide lubrication in the synovial fluid [53]. Secondly, during dynamic loading, interstitial fluid pressure increases and forms a thin fluid film between the articulating surfaces minimizing friction [54].

2.2 POST-TRAUMATIC OSTEOARTHRITIS OF A KNEE

Traumatic injuries of cartilage in the knee are common in young adults, especially in athletes [55]. Cartilage injuries may cause pain, swelling, and occasionally a "catching sensation" caused by loose cartilage or bone fragments. Injuries may also trigger a lengthy remodelling process in the cartilage and as well as in subchondral bone [56]. The magnitude of mechanical impact and the severity of tissue damage determine the extent of pathological response and the following traumatic injury. High-energy injuries, such as ligament and meniscal injuries, e.g., resulting from vehicle accident, usually cause articular cartilage damage with a possible contusion of subchondral bone.

PTOA is a joint disease associated with a gradual erosion of articular cartilage [6, 57], accounting for 12% of all cases of OA [6]. Superficial collagen disruption, PG loss, and increased tissue water content are the first signs of PTOA [20, 21]. These changes increase tissue permeability, elevating the diffusion of soluble mobile ions into articular cartilage [17, 58]. In addition to articular cartilage damage, PTOA also involves the degeneration of other tissue components. Whole-joint biologic responses trigger, for example, the release of inflammatory mediators that initiate progressive tissue destruction, as well as repair responses [1, 59]. These changes in articular cartilage lead to disruption of periarticular muscles, ligaments, subchondral bone, and synovial membrane [60]. PTOA develops on average within a 10-to-15 years' time window. In contrary to primary osteoarthritis, PTOA is typically diagnosed earlier in life, and the progression of the disease is faster, increasing the joint-related morbidity period [61].

Mechanical causes of PTOA can be divided into two categories: 1) acute structural damages and 2) chronic loading abnormalities of injured joints [62]. A patient may either have a combination of structural cartilage damage caused by an acute injury and chronic joint abnormality or primarily have only one of these causes. Acute structural damages occur after a high-energy joint injury. These acute damages initiate, in most cases, clinically apparent joint inflammation and result in macroscopic structural disruption of articular cartilage and subchondral bone. The risk of developing PTOA after acute injury is related to the magnitude of the mechanical impact subjected to the joint. A study by Anderson *et al.* showed that when the energy of impact in intra-articular fractures of the tibial plafond exceeded a certain threshold, the injury predictably leads to OA within two years [63]. Acute damages are usually

single events that cause immediate structural damage and cell death, accompanied by acute inflammatory and repair responses [64–66].

Chronic loading abnormality of injured joint induces gradual-onset of structural damages together with cartilage compositional degradation, which may not induce visible disruption of the articular surface. In addition, gradual-onset of structural damages initiate biological responses causing progressive cell death at the lesion site and around it [1]. Metabolic disturbances, triggered by the cells that survived the damage, may also further amplify the degradation of the cartilage matrix and lower its tolerance for mechanical stress [1, 67]. Secondly, in addition to biological responses, chronic loading abnormalities caused by acute injury mechanically and gradually degrade the joint and articular cartilage [62]. For example, residual surface incongruity caused by intra-articular fracture results in the wear out of cartilage first from those areas of the highest cumulative contact stress [63]. Residual instability and incongruity usually result from repeated small mechanical damages. Cell death and pronounced inflammatory responses are mostly absent in injuries causing chronic loading abnormalities.

Even though the pathways to joint degradation have been studied extensively, development of accurate methods to estimate whether an acute joint injury will progress to PTOA has been challenging. Further, development of clinical techniques to evaluate the internal cartilage changes after cartilage injury has been challenging. These shortcomings inevitably have led to hindered development of treatment and mitigation options and efforts to prevent the progression of PTOA.

2.3   CLINICAL DIAGNOSIS AND TREATMENT OF POST-TRAUMATIC OSTEOARTHRITIS

Articular cartilage has only limited capability for regeneration due to both its avascular nature and its unique and complex structure [68]. Therefore, for effective treatment of cartilage injuries, and prevention of PTOA, early detection of degenerative changes is important. However, physicians currently have only limited options to evaluate the severity of a joint injury.

OA is usually diagnosed based on patient symptoms and clinical examination. To verify the diagnosis and assess the severity of the damage to articular cartilage, several methods exist, including arthroscopy, X-ray radiography, computed tomography, and MRI. Arthroscopy allows visual inspection and probing of cartilage using small incisions through the skin and other soft tissues [69]. During the arthroscopic examination, the joint health is assessed visually as well as palpating the cartilage surface with a metallic hook. As a downside of arthroscopy; the technique is heavily subjective and relies on the surgeon's assessment skills and experience, leading to potentially suboptimal treatment decisions. Furthermore, especially at the early-stage degeneration, the visual inspection can be misleading as cartilage tissue may undergo initial structural and compositional changes prior to any visibly detectable changes emerge. Complementing a conventional arthroscopy, arthroscopically applicable imaging techniques, such as near-infrared spectroscopy, optical coherence tomography, and ultrasound imaging can also be applied during the examination. These techniques allow imaging with high resolution, but despite this, they are not yet disembarked in wide clinical use [70–72].

X-ray radiographs and CT scans are unable to directly visualize the articular cartilage. Instead, they can be used to identify changes in subchondral bone and joint-space narrowing. In comparison, MRI enables the detection of changes in articular cartilage composition and mechanical properties [73–76] together with the possibility to evaluate surface lesions and loose fragments, thus enabling improved treatment planning. During recent years, researchers have gained more understanding of the changes in MRI signal after acute cartilage injuries and subsequent development of PTOA.

Many of these current techniques, including clinical examination, native X-ray imaging, and arthroscopic examination, lack the capability for early detection of PTOA. Indeed, these techniques can only detect major tissue changes. However, CECT and delayed gadolinium-enhanced MRI of cartilage (dGEMRIC) have shown promise for the early diagnostics of PTOA [14,58,77,78]. These techniques are based on contrast agents and their solute transport properties to assess tissue composition and function. MRI is sensitive to the state of the water in cartilage tissue, the 3D architecture of the collagen scaffold, and to changes in PG content [9,10]. However, the use of MRI is hindered due to its relatively long *in vivo* image acquisition times and high costs [10,11]. CT, on the other hand, provides better spatial resolution than MRI, short acquisition times with approximately half the cost of MRI, thus, providing an alternative imaging method for PTOA diagnostics.

Cartilage injuries can be evaluated based on the severity of the cartilage lesion using certain classification systems, such as the International Cartilage Repair Society (ICRS) system. However, the poor reliability of the current classification systems has hindered their usage [79–81]. In this regard, the classification systems have been known useful in characterizing injuries but not in selecting the optional treatment [82].

The treatment of PTOA is exceedingly challenging, and current treatment options frequently fail to prevent PTOA. In this context, for a successful outcome, the treatment has to be delivered in the early stage of PTOA to prevent or alter the course of the disease. Current efforts to treat or delay PTOA of a knee are multimodal, including patient education and self-management as well as pharmacological treatments and surgical interventions. Patient education and self-management focus on weight loss, encouraging the patient for moderate exercises and including physical therapy and occupational therapy. Pharmacological treatments include acetaminophen (paracetamol), nonsteroidal anti-inflammatory drugs (NSAIDs), COX-2 inhibitors, opioid analgesics, and intra-articular drugs (such as corticosteroids and hyaluronic acid) [83].

Surgical total knee replacement is typically limited to patients with end-stage OA. However, surgical interventions, that stimulate the growth of new cartilage, have evolved during the past years and can be used in PTOA treatment. The most commonly used method to stimulate the growth and repair cartilage injuries is bone marrow stimulation [84]. In surgery, the bone marrow is stimulated by creating multiple holes to the subchondral bone plate to enable stem cells entering from the bone marrow into the cartilage lesion. These stem cells can differentiate into fibrochondrocytes that have similar features to fibroblasts and chondrocytes. Fibrochondrocytes are cells that generate collagen type I as do fibroblasts and possess similar rounded morphology protected by a territorial matrix as also chondrocytes do.

Autologous chondrocyte transplantation [85] and autologous osteochondral mosaicplasty [86] are also options in surgical intervention. In autologous chondrocyte transplantation, the cartilage in the repair site is restored in three stages. At first,

healthy cartilage is harvested arthroscopically from areas with less weight-bearing, after which the healthy cartilage cells are cultivated *in vitro*. In the third stage, the cultivated cells are injected into the lesion site below the periosteal flap that is sutured to cartilage tissue. In contrast to autologous chondrocyte transplantation, an autologous osteochondral mosaicplasty can be performed with only one operation. During the operation, multiple small cylindrical osteochondral grafts are obtained from a less weight-bearing area. The grafts are then transplanted into the lesion site to promote healing. Recent studies have also focused on the development of pharmaceutical interventions to decrease or prevent the progress of PTOA [1,8].

PTOA is often detected in the advanced stage after it becomes radiographically apparent by the altered alignment of the major bones caused by severe cartilage damage. Thus, even though multiple treatment options exist for the repair of cartilage injuries, they are largely ineffective due to late diagnosis past the "treatment window". To this end, effective techniques to detect and assess the cartilage integrity immediately after the acute injury are warranted.

3 Contrast-Enhanced Computed Tomography

In this chapter, the concepts of CECT is described in the context of knee imaging. First, a brief overview of CT is provided. Then, the role of contrast agents in CECT imaging is highlighted, and the physics behind the diffusion of contrast agents into articular cartilage is described. Lastly, QDECT, the key technique used in this doctoral thesis, is explained.

3.1 X-RAY COMPUTED TOMOGRAPHY

CT is a medical imaging modality that utilizes ionizing radiation, X-rays, to produce 2D axial slices of an object that can be viewed in 3D. X-rays are electromagnetic radiation with wavelengths in the range from 0.01 to 20 nanometers. CT imaging is based on different attenuation of X-rays in different tissues. X-rays attenuate according to the Beer-Lambert law:

$$I(x) = I_0 e^{-\mu_l x}, \tag{3.1}$$

where I is the intensity of the X-ray beam at a distance x, I_0 the initial intensity, and μ_l the linear attenuation coefficient, which depends on the energy of the photon as well as the atomic number of the medium.

In general, the production of CT images from X-rays includes two steps: acquisition and reconstruction. In CT image acquisition, the X-ray tube rotates around a subject positioned in the rotation axis. The X-ray source is mounted on the opposing side of the detector, and X-rays are emitted in a collimated fan- or cone-shaped beam. In some X-ray microtomography (microCT) systems, the imaged object is rotated while the X-ray source and detector remain stationary. As the X-rays pass through the subject, the X-rays are attenuated depending on the properties of the tissues and X-ray energy. In the diagnostic energy range (20 – 150 kV), the combination of the two X-ray interactions produces the overall attenuation of the X-ray beam: photoelectric effect and Compton scattering. In the photoelectric effect, an X-ray photon collides with an atom transferring all of its energy to an electron, resulting in the ejection of that electron and subsequent ionization of the atom. The photoelectric effect produces high contrast in the X-ray image. Compton scattering, on the other hand, occurs when an incident X-ray photon interacts with an outer shell (valence) electron and is deflected from its original path. The incident photon imparts energy for the electron, which results in the electron to be ejected from its orbital. After the interaction, the X-ray photon continues to travel through the material along an altered path with decreased energy. In addition to the photoelectric effect and Compton scattering, X-rays can also interact with matter through Rayleigh scattering. This interaction occurs when the energy of the X-ray photon is smaller than the binding energy of the electron. In Rayleigh scattering, the X-ray photon interacts with the atom and is scattered. In this collision process, no energy

is lost or deposited and thus also no radiation dose is deposited on the medium. As the X-rays leave the subject, they reach the detector and are detected at a single angular position. In this way, several hundreds of projections around the subject are acquired per rotation.

Collected CT projections are mathematically converted into 2D tomographic image slices in a process called reconstruction. Reconstruction can be performed either analytically or iteratively. In analytical reconstruction, the attenuation coefficients within a cross-section are calculated from sine waves that consist of ray sums taken at differing angles of the imaging object. The most commonly used analytical algorithm is the filtered back-projection method. In this method, the attenuation profiles are collected from different directions and filtered before back-projected across the image plane. The filtering is performed to remove any blurriness of the image (star-like artefacts) and is done by convolving the attenuation profiles using a filter function with "negative wings" [87]. The strength of the analytical reconstruction is its computational efficiency and numerical stability. In the iterative reconstruction, images are reconstructed by iteratively optimizing an objective function, which typically involves a data fidelity term and an edge-preserving regularization term [88]. Generally, iterative optimization includes iterations of forward projection and back-projection between image space and projection space. From these two reconstruction methods, iterative reconstruction algorithms have become the preferred method. The downside of iterative reconstructed images is their plastic-like, paint-brushed unfamiliar image appearance, which is not for most radiologists' liking [89,90]. Thus, vendors have provided a possibility to use variable user-specified iterative strength levels or blending of iterative and filtered back projection images to mitigate this unfamiliar appearance. After reconstruction, the CT images can be viewed and analysed.

3.2 CONTRAST AGENTS

Radiocontrast agents are used to enhance the visualization of internal structures and their boundaries in CT imaging. Positive radiocontrast agents are substances that effectively attenuate X-rays. They are more radiopaque to X-rays than the surrounding tissue and decrease exposure on the X-ray detector. Negative contrast agents (such as air, carbon dioxide, and oxygen) on the other hand are less radiopague than the surrounding tissue and predominantly appear black on radiographic images due to their low X-ray attenuation. Either intravenous or direct injection into the area of interest is used to administer the contrast agent.

Radiocontrast agents have to meet several requirements before they can be applied clinically [15,91]. The first requirement for radiocontrast agents is their ability to attenuate X-rays. Linear X-ray attenuation coefficient (μ_l) describes how effectively the material attenuates X-rays and, to better understand this concept, the following relation can be derived:

$$\mu_l \approx \frac{\rho_d Z^4}{AE^3},$$

(3.2)

where ρ_d is the material density, Z the atomic number, A the atomic mass, and E the X-ray photon energy. To generalize, radiocontrast agents with high atomic number

and/or high density tend to provide a better contrast to the image (with negative contrast agents low atomic number and/or low density) [15]. By increasing the attenuation difference between the target tissue and its surroundings, at least by a factor of two, a radiocontrast agent can significantly improve the visualization of the target tissue. In addition to their ability to attenuate X-rays, contrast agents should be easily administered to a patient. This requires that the contrast agent forms a stable suspension or is soluble at aqueous physiological conditions, has suitable pH and osmolality, and has a low viscosity. Also, the contrast agent and its metabolic end-products should preferably be non-toxic, and they should have favourable biodistribution and pharmacokinetic profiles. Furthermore, to reduce the potential toxicity, the contrast agent should be excreted from the body within a reasonable time (<24 hours). At the same time, the retention time should be long enough (2–4 hours) to allow enough time for CT imaging [15]. Lastly, the production costs should remain tolerable, and the compound should be chemically stable.

Contrast agents are usually classified as ionic or non-ionic (usually organic compounds) agents based on their charge. Ionic contrast agents consist either of the negatively charged anions or positively charged cations. Radiocontrast agents are typically iodine-, barium-, or gadolinium-based compounds. These materials possess relatively high attenuation and advantageous k-edge in the diagnostic X-ray energy range, making them effective X-ray contrast agents. k-edge is a material-specific steep increase in photoelectric absorption and represents the binding energy of the innermost and most strongly bound (i.e., k-shell) electron. With photon energies just above the k-edge, the material will have a substantially higher attenuation coefficient compared with photon energies just below the k-edge. Also, outer shell electrons have absorption edges, but the corresponding energies are too low to have any importance at clinical energies.

Iodine-based contrast agents are widely used in medical X-ray imaging. Iodine has a high atomic number ($Z = 53$) and a k-edge of 33.2 keV that is near the effective energy of most diagnostic X-ray beams (kVp = 80–140 keV). For this reason, iodine has an optimal attenuation capacity for clinical applications. Iodine-based contrast agents usually possess good solubility and low toxicity [92]. Another advantage of iodine-based contrast agents is their low osmolality reducing serious acute systemic side effects compared to high osmolality agents. A downside of iodine-based radio-contrast agents is their rapid renal clearance restricting their use in imaging where long circulation times are required. Furthermore, they are known to sometimes induce serious allergic or adverse effects and renal toxicity in patients with pre-existing renal impairment. Finally, when using high-energy X-rays (for example, with obese patients), the attenuation induced by iodine can be insufficient.

Gadolinium-based contrast agents are widely used in MRI imaging owing to their unique magnetic properties. Additionally, due to the high atomic number of gadolinium ($Z = 64$), they can also provide desirable contrast as a CT contrast agent, although the optimal dose in CT imaging is higher than is used in MRI. Free gadolinium ions (Gd^{3+}) are extremely toxic; thus, gadolinium ions are often chelated with polyaminocarboxylic acid, forming non-toxic and stable complexes. Gadolinium-based contrast agents are less likely to produce an allergic reaction than the iodine-based contrast agents, with the incidence of severe allergic reactions to gadolinium-based contrast agents being as low as 0.1% [93].

Recently, nano-sized, metallic contrast agents have drawn scientific interest [15]. They usually possess high atomic numbers providing favourable X-ray attenuation properties [94]. As an example, gold nanoparticles (AuNPs) provide approximately

2.7 times greater contrast per unit weight at 100 keV energy than iodine [95]. In addition to gold, other heavy atoms such as lanthanide, tantalum, and bismuth have been studied as possible contrast media [15]. Nanoparticles (NPs) are generally unstable, and they tend to aggregate due to their high surface energy and high ionic strength of many biological fluids. For these reasons, inorganic nanoparticles are usually coated with an organic capping layer preventing them to come into close contact with each other. Thus, the organic capping layer can improve the physicochemical properties of inorganic nanoparticles.

Bismuth nanoparticles, as a contrast agent, have raised interest during the last years. Bismuth has a high attenuation coefficient due to its high atomic number (Z = 83). Moreover, manufacturing bismuth-based NPs is cost-effective, and they are also low in toxicity [15]. The low toxicity of bismuth is further supported by the fact that it is widely used as an ingredient in pharmaceuticals and cosmetics and that bismuth(III) salts have shown no adverse side effects when used in therapy for peptic ulcer disease [96].

3.3 DIFFUSION OF CONTRAST AGENTS

Due to the avascular structure of articular cartilage, nutrients are transported from the synovial fluid through diffusion [33]. Similarly, contrast agents injected inside the joint cavity are diffused into cartilage. Diffusion is a process where molecules from high concentration move towards lower concentration until the concentration gradient has disappeared. Diffusion is the main form of transportation at the sub-micron scales [97, p. 64-140]. The diffusion of particles is essentially a type of random fluctuations that are called Brownian motion. Diffusing particles are constantly undergoing small, random fluctuation, and their movement in the cartilage and synovial fluid can be described with Fick's laws of diffusion [98]. Fick's first law describes the relationship between the diffusive flux and concentration under a steady state. Diffusion flux J defines the net movement of the soluble molecules across the unit area. According to Fick's first law, the diffusion flux is proportional to the concentration gradient and can be expressed as:

$$J = -D\frac{\partial C}{\partial x} \ ,$$

(3.3)

where D is the diffusion coefficient or diffusivity, C the concentration, and x the position along with the tissue depth. In the equation (3.3), the diffusion coefficient is a specific constant that describes the interaction of the solute with the tissue through which the solute is transported. Thus, the diffusion coefficient defines the rate at which the diffusion equilibrium is achieved.

In many cases, the concentration changes with time. Since the Fick's first law has no time dependency, it can not be utilized in the time-varying cases. However, with time-varying diffusion flux, the diffusion can be described with Fick's second law, also called diffusion law as:

$$\frac{\partial C}{\partial t} = D\frac{\partial^2 C}{\partial x^2} \ ,$$

(3.4)

where t is the time.

The Gibbs-Donnan equilibrium is a state of equilibrium that charged particles exhibit when they are separated with a semipermeable membrane. Specifically, it describes the electrostatic potential and osmotic forces needed to balance the system and to restore equilibrium [97, p. 414]. In the presence of electrostatic potential, the mobile ions to distribute unevenly across the membrane at diffusion equilibrium. To this end, the Nernst equation enables the determination of ion distribution across the membrane when the gradient of the potential is similar for all the ions. The membrane potential $\Delta\Psi$ can be solved using the Nernst equation:

$$\Delta\Psi = -\frac{RT}{zF} \ln \frac{[C]_1}{[C]_2} \ , \tag{3.5}$$

where R is the gas constant, T the temperature, z the valence of the ion, F the Faraday constant, $[C]_1$ the concentration on one side of the membrane, and $[C]_2$ the concentration on the other side. This equation describes the difference between the concentration of molecules and charges on both sides of the membrane and the resting potential of the system. Donnan ratio is achieved by rearranging the equation of membrane potential:

$$r = \left(\frac{[C]_1}{[C]_2} \right)^{1/z} \ . \tag{3.6}$$

Subsequently, by combining the Nernst equation and Donnan ratio the following equation for the membrane potential can be derived

$$\Delta\Psi = -\frac{RT}{F} \ln r \ . \tag{3.7}$$

Now, we can notice that the presence of a fixed charges create an osmotic gradient across the membrane [99].

Let us now consider three species of small ions Na^+, K^+, and Cl^- with concentrations of $[C]_i$. In diffusion equilibrium, each of these ion species must separately be in Nernst equilibrium at the same value of $\Delta\Psi$:

$$\Delta\Psi = -\frac{RT}{F} \ln \frac{[C]_{1,Na^+}}{[C]_{2,Na^+}} = -\frac{RT}{F} \ln \frac{[C]_{1,K^+}}{[C]_{2,K^+}} = -\frac{RT}{F} \ln \left(\frac{[C]_{1,Cl^-}}{[C]_{2,Cl^-}} \right)^{-1} \ . \tag{3.8}$$

By solving this, we notice that the Donnan ratio can be rewritten as the Gibbs-Donnan relations:

$$\Delta\Psi = \frac{[C]_{1,Na^+}}{[C]_{2,Na^+}} = \frac{[C]_{1,K^+}}{[C]_{2,K^+}} = \frac{[C]_{2,Cl^-}}{[C]_{1,Cl^-}} \ . \tag{3.9}$$

This is called the Donnan equilibrium and the $\Delta\Psi$ is called the Donnan potential for the system.

Finally, the above-described theory can also be applied to the cartilage tissue. To simplify the discussion, the cartilage tissue is assumed to be homogenous. It contains mobile ions and an ionized solid matrix and is surrounded by ion solution (e.g., saline or synovial fluid). In cartilage, the partitioning and the concentration of mobile ions are affected by the fixed charge caused by PGs in the extracellular matrix [75]. Thus, an equation can be derived from describing the interactions between

the mobile ions and the FCD. Applying the Gibbs-Donnan theory and by assuming that the distribution of mobile ions obeys ideal Donnan equilibrium conditions (Eq. 3.6), we can write the following equation [100]:

$$\left(\frac{[\text{cation}]_{\text{bath}}}{[\text{cation}]_{\text{cartilage}}}\right)^{z_{\text{cation}}} = \left(\frac{[\text{anion}]_{\text{bath}}}{[\text{anion}]_{\text{cartilage}}}\right)^{z_{\text{anion}}}. \tag{3.10}$$

Now, as cartilage tissue is assumed to be externally electroneutral, the following conditions must stand:

$$z_{\text{cation}}[\text{cation}]_{\text{bath}} = z_{\text{anion}}[\text{anion}]_{\text{bath}} \tag{3.11}$$

and

$$z_{\text{cation}}[\text{cation}]_{\text{cartilage}} = z_{\text{anion}}[\text{anion}]_{\text{cartilage}} + \text{FCD}, \tag{3.12}$$

where FCD is the fixed charge density caused by negatively-charged PGs [37].

Contrast agent diffusion within the cartilage tissue is affected by a variety of structural and compositional features of the tissue. The diffusion coefficient varies between the different layers of cartilage based on the collagen network integrity and architecture, as well as PG and water contents [101]. High collagen content and especially the thicker collagen fibers in the deep cartilage are known to create a steric hindrance to the contrast agent diffusion [14, 102]. On the other hand, variations in the concentration of negatively-charged PG molecules can either decrease or increase the diffusion of the contrast agent depending on whether an anionic or a cationic contrast agent are used [103]. Also, specific features of the contrast agents affect the diffusion. Increasing molecular size is known to decrease the diffusion rate into the tissue [104]. Possible steric interactions between the diffusing molecule and tissue arising from the mutual impenetrability of finite-size particles may modulate the diffusion. The shape of the diffusing molecule also influences the diffusion. Planar molecules are generally shown to diffuse faster than spherical solutes if the diffusing molecule is small [105,106]. However, with bigger molecules, the effect is opposite; the diffusion rates of planar solutes are reduced compared with spherical molecules [107]. Also, the charge of the molecule can change the uptake of the contrast agents. For example, cationic contrast agents possessing a higher positive charge have greater equilibrium partition values in articular cartilage than the agents with a smaller charge [19,108]. On the other hand, with anionic contrast agents the higher the negative charge, the lower the equilibrium partition in articular cartilage [18].

3.4 DELAYED CONTRAST-ENHANCED COMPUTED TOMOGRAPHY

CECT utilizes radiocontrast agents and their solute transport properties to visualize and evaluate the cartilage tissue structures and composition. In CECT, anionic contrast agents are most commonly used. At diffusion equilibrium, anionic contrast agents distribute into cartilage inversely proportional to the spatial distribution of FCD but also according to the depth-dependent water content and structural integrity of the tissue matrix [18,109–112]. In the cartilage matrix, FCD is due to the

highly negative net charge governed by the PGs. Since the PG content decreases as the cartilage degenerates, the partitioning of charged contrast agents varies based on the degree of cartilage degeneration. Prohibitively long times, depending on the cartilage thickness as well as the charge and the molecular size of the radiocontrast agent are often needed to reach diffusion equilibrium. For example, with iodine-based contrast agent, ioxaglate, studies have reported equilibrium times of over 8 hours in human and bovine articular cartilage [17,18,58]. Therefore, reaching equilibrium in clinical circumstances is unattainable. Thus, in the early-diffusion stage, the concentration distribution does not reflect the true PG distribution. However, significant correlations between the contrast agent concentration and the tissue PG content have been reported *in vitro* already at an early stage of diffusion i.e., during clinically feasible imaging times [17,113].

The clinical CECT of a knee joint is based on the acquisition of two subsequent images [24,25,113]. The first scan (arthrography) is acquired immediately after the contrast agent administration. Arthrography enhances the visualisation and enables reliable delineation of articulating surface and superficial lesions. The second scan (delayed arthrography) is acquired in 30 minutes to 2 hours after the intra-articular injection of a radiocontrast agent. Based on the partitioning of the radiocontrast agent within the tissue, the latter scan allows the evaluation of internal changes in cartilage tissue e.g., those related to initiation of PTOA. However, diffusion diminishes contrast at the cartilage-synovial fluid interface and the accurate delineation of the articulating surface is impossible. This is also the reason why the two subsequent scans are needed. No interpretation of the cartilage integrity can be made from arthrography also since the contrast agent has not had enough time to diffuse into cartilage. In time points after 2 hours, no reliable interpretation of cartilage condition can anymore be made since the contrast agent concentration in the synovial fluid has decreased due to physiological clearance and uptake by other tissues. In practice, need for two scans can be logistically demanding and doubles the radiation dose to a patient. In general, radiation doses are relatively low when clinical cone-beam CT devices are used. In extremity imaging, the dose induced in one helical knee CT scan is approximately 160 µSv, but with cone-beam CT, as low doses as 27 to 48 µSv can be reached [12].

Cationic, iodine-based contrast agents have recently raised interest due to their increased sensitivity for PG loss [13,108,109]. Along with Gibbs-Donnan theory, the electrostatic interactions between the cationic contrast agent and the negative PGs enable the cationic contrast agent to achieve higher equilibrium concentrations in the cartilage tissue compared with currently available negatively charged contrast agents. For example, a recent study has observed that the mean attenuation values of the cationic contrast agent were approximately 2.9 times higher than the more commonly used ioxaglate at diffusion equilibrium [15].

The problem of cationic contrast agent appears in the early-stage diffusion, i.e. when the diffusion is controlled by degenerative factors having opposite effects on the diffusion; decreased PG content reduces the diffusion while the increased water content and decreased steric hindrance caused by the ECM increase the diffusion. For this reason, the diagnostic sensitivity of cationic contrast agent may be limited when using clinically feasible imaging time points. However, recent studies have proposed that this shortcoming could be solved by using quantitative dual-energy computed tomography [114].
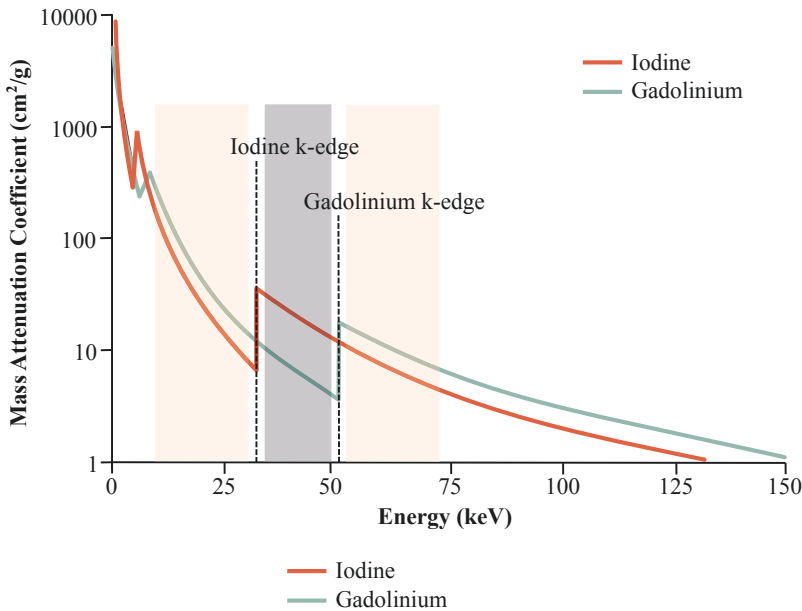
Figure 3.1: Mass attenuation coefficients for iodine and gadolinium as a function of photon energy. The *k*-edge of iodine occurs at 33.2 keV, and the *k*-edge of gadolinium is at 50.2 keV. In quantitative dual-energy computed tomography (QDECT), the two X-ray tube voltages should be chosen so that most of the energy spectrum obtained with the first X-ray tube voltage is on energies below 33.2 keV or above 50.2 keV (illustrated in red color) and the energy spectrum produced by the second X-ray tube voltage is between the iodine and gadolinium *k*-edges (illustrated in gray). The energies are thus selected to maximize the difference between the iodine and gadolinium attenuation coefficients. The mass attenuation coefficient data were obtained from the reference [115].

Quantitative Dual-Energy Computed Tomography

The capability of CECT utilizing cationic contrast agents can be improved by implementing QDECT [114]. This technique applies two X-ray energies and a mixture of two contrast agents: a cationic, iodine-based contrast agent, such as CA4+, and a non-ionic, gadolinium-based contrast agent, such as gadoteridol.

Simultaneous quantification of iodine and gadolinium can be achieved by applying two X-ray tube voltages selected based on the element-specific *k*-edges (Fig. 3.1). Two energies are selected based on *k*-edges to maximize the difference between iodine and gadolinium attenuation coefficients. Conventional μCT and clinical CT scanners possess relatively wide energy spectra. Thus, the photon energies can spread on both sides of iodine or gadolinium *k*-edges, deteriorating the technique's accuracy. To this end, the spectra with the two energies need to be filtered to obtain narrow energy spectra and to improve the difference between the attenuation coefficients. With a monochromatic X-ray beam, produced for example using a synchrotron, this problem intrinsically does not exist. Usage of monochromatic beams enables the energies to be selected exactly below and above contrast agents' *k*-edges with no problems related to the wide energy spectra of conventional CT devices.

After imaging with two energies, the partitioning of iodine and gadolinium within the sample can be calculated based on Beer-Lambert law (3.1) and Bragg's additivity law presented below:

$$\alpha_E = \mu_{I,E}[C]_I + \mu_{Gd,E}[C]_{Gd} \, ,$$ (3.13)

where α_E is the X-ray attenuation with the energy E, $\mu_{I,E}$ and $\mu_{Gd,E}$ are the mass attenuation coefficients, and $[C]_I$ and $[C]_{Gd}$ the concentrations of iodine (I) and gadolinium (Gd), respectively. To determine the concentrations of iodine and gadolinium, the sample must be imaged using two different photon energy spectra E_1 and E_2. Thus, the concentrations can be calculated from the following equations:

$$[C]_I = \frac{\alpha_{E_2}\mu_{Gd,E_1} - \alpha_{E_1}\mu_{Gd,E_2}}{\mu_{I,E_2}\mu_{Gd,E_1} - \mu_{I,E_1}\mu_{Gd,E_2}} \, ,$$ (3.14)

$$[C]_{Gd} = \frac{\alpha_{E_1}\mu_{I,E_2} - \alpha_{E_2}\mu_{I,E_1}}{\mu_{I,E_2}\mu_{Gd,E_1} - \mu_{I,E_1}\mu_{Gd,E_2}} \, .$$ (3.15)

Finally, in the QDECT technique, the effect of water content and steric hindrance into iodine-based cationic contrast agent diffusion is taken into account by normalizing (e.g., dividing) the iodine-based contrast agent partition with that of gadolinium-based contrast agent. QDECT technique provides an advantage over conventional CECT. It allows simultaneous quantification of interstitial water and PG contents in articular cartilage based on iodine-based and gadolinium-based contrast agent partitioning within the tissue. Lastly, it is worth noting that the QDECT technique is not limited to the use of iodine- and gadolinium-based contrast agents. Instead, any combination of cationic and non-ionic agents based on elements with k-edges suitable to each other may be used, providing that two corresponding X-ray tube voltages can be selected to perform QDECT.

4   Aims and Hypothesis

The main aim of this thesis was to introduce a triple contrast agent for CECT diagnostics of cartilage composition and evaluation of post-traumatic changes. The specific aims of each individual study were:

1. to investigate the feasibility of BiNPs to enhance contrast at synovial fluid-articular cartilage interface and thereby facilitate accurate segmentation of the articulating surfaces and superficial cartilage lesions together with the determination of cartilage condition through simultaneous use of an anionic contrast agent.

2. to combine cationic and non-ionic contrast agents, and by using QDECT to simultaneously determine the partition of the two contrast agents for subsequent evaluation of articular cartilage PG and water contents.

3. to develop a triple contrast agent consisting of iodine-based, cationic and gadolinium-based, non-ionic contrast agents and BiNPs, enabling simultaneous evaluation of cartilage composition and delineation of articulating surfaces.

4. to investigate the potential of triple contrast agents to detect post-traumatic degeneration around a surgically-induced lesion.

5   Materials and Methods

In this chapter, the materials and methods of the four independent studies (**I-IV**) are described. The materials and methods are summarised in Table 5.1. For complete descriptions of materials and methods, see the original publications (studies **I–IV**).

Table 5.1: Summary of the materials and methods utilized in studies **I–IV**.

Study	Species, number of joints	Sample groups	Methods
I	Bovine cartilage, $N = 10$	intact, mechanically injured, PG-depleted	CECT, digital densitometry
II	Bovine cartilage, $N = 11$	intact, mechanically injured + PG-depleted, PG-depleted	CECT, QDECT, digital densitometry
III	Bovine cartilage, $N = 9$	intact, mechanically injured, PG-depleted	CECT, QDECT, digital densitometry
IV	Equine cartilage, $N = 14$	intact, post-traumatic degeneration	CECT, QDECT, digital densitometry, biomechanical testing

N = number of joints, PG = proteoglycan, CECT = contrast-enhanced computed tomography, QDECT = quantitative dual-energy computed tomography

5.1   SAMPLE PREPARATION

Studies **I** and **III** utilized the same set of samples. Osteochondral samples ($n = 30$) obtained from a local abattoir (Savo-Karjalan liha Oy, Finland) were extracted from the bovine knee joints ($N = 10$) and divided into three groups: 1) intact, 2) PG-depleted, and 3) mechanically injured. Osteochondral samples were prepared from the upper lateral quadrant of the patella by extracting an osteochondral disc ($d = 2.65$ cm). From that disc, three adjacent osteochondral plugs ($n = 30$ in total, $d = 7$ mm) were punched (Fig. 5.1). Enzymatic degradation was performed using
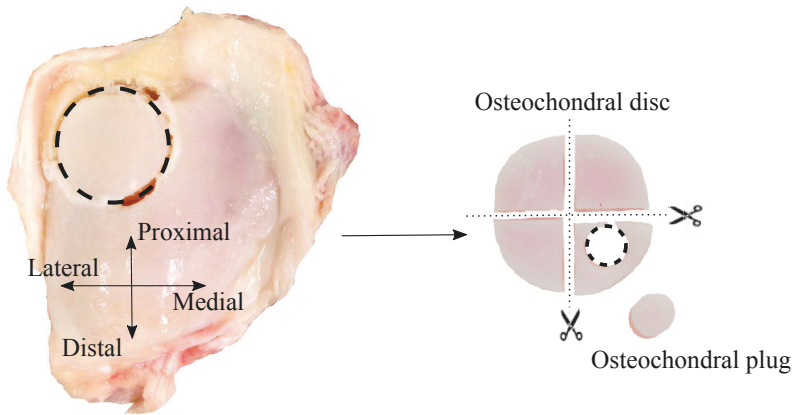
Figure 5.1: Preparation of osteochondral plugs utilized in studies **I** – **III**. At first, an osteochondral disc was drilled from the upper lateral part of the patella. Secondly, the disc was divided into four quadrants, and three osteochondral plugs were punched from these quadrants. Subsequently, the underlying subchondral bone was trimmed to thickness of approximately 1 mm.

a trypsin solution immersion (0.5 mg/ml, Sigma-Aldrich, USA) for 15 h at 37.5 °C in an incubator for nearly complete depletion of the PGs [116]. Here, trypsin was used to create the characterised signs of early-stage OA by digestion of PGs [117]. The mechanical injury was induced with a custom made drop tower by dropping a stainless steel impactor (m = 500 g) with a polished face on the sample from the height of 20 cm. The third osteochondral plug served as an intact reference sample.

Sample preparation in study **II** was similar to that described in studies **I** and **III**. Three adjacent osteochondral plugs (n = 33, d = 4 mm) were extracted from the upper lateral quadrant of the patellae from bovine knee joints (N = 11) obtained from the local grocery store (Prisma, Kuopio, Finland). The osteochondral plugs were also divided into three groups: 1) intact, 2) PG-depleted, and 3) mechanically injured + PG-depleted. The enzymatic degradation and mechanical injury were induced similarly as in studies **I** and **III**, but samples in group 3 were also PG-depleted in addition to the mechanical injury. No ethical permission or approval for the experimental protocol and tissue collection in studies **I** – **III** were needed.

In study **IV**, both femoropatellar joints of Shetland ponies ($N_{experimental}$ = 7, age = 8.8 ± 3.5 years, 6 females and 1 male) were artificially injured by creating two full-thickness cylindrical chondral lesions (d = 9 mm) on the medial femoral ridges (total number of lesions = 28). During a 12-month treatment period, different combinations of chondrons and mesenchymal stem cells in different carrier hydrogels were used to treat the lesions [118,119]. After the treatment period, the ponies were euthanized, and osteochondral samples, including the lesions and surrounding tissue, were extracted post-mortem from the medial trochleae (Fig. 5.2). In addition, equivalent healthy samples were extracted from the femoropatellar joints of healthy ponies ($N_{control}$ = 3, age = 10.3 ± 4.7 years) obtained from a local abattoir (van de Veen Nijkerk, The Netherlands) as control samples. The resulting total number of samples was 20 (14 experimental and 6 control). The measurement protocol was approved by the Ethics Committee of Utrecht University for Animal Experiments
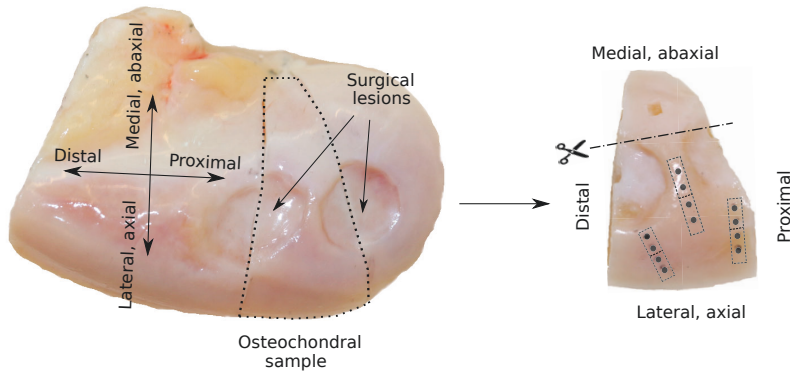
Figure 5.2: Preparation of the experimental samples in study **IV**. The surgical lesions and the extraction location of the experimental sample are indicated in the medial view of a left trochlea. Prior to microCT measurements, the medial, abaxial aspect was trimmed as indicated in the image in the right side. The boxes in the experimental sample illustrate the extraction of the histological sections, and the black dots illustrate the anatomical locations of the biomechanical measurement points.

in compliance with the Institutional Guidelines on the Use of Laboratory Animals (Permission DEC 2014.III.11.098).

In all studies, the samples were stored in phosphate-buffered saline (PBS) at -25 °C until the experiments. Prior to microCT imaging, the sides and the bottom of each osteochondral sample were sealed with cyanoacrylate (Loctite, Henkel Norden AB, Germany) to ensure contrast agent diffusion only through the articular surface.

5.2   PREPARATION OF BISMUTH(III) OXIDE NANOPARTICLES

PEG coated BiNPs were developed in this thesis and utilized as contrast agent in studies **I** and **III**.

Bismuth(III) oxide powder (Bi_2O_3 nanopowder, Sigma-Aldrich, USA) was prepared in a ball mill (Planetary Micro Mill, Pulverisette 7, Fritsch GmbH, Germany). Milling bowls contained 10 g of Bi_2O_3 nanopowder, 70 g of 1 mm milling balls, and 40 mL of distilled water. Milling was performed in 10 min cycles at a speed of 700 rpm. A cooling time of 15 min was applied in between each milling round. The total milling time in study **I** was 4 hours and in study **III** 2 hours.

In study **I**, the stabilization of the suspension was achieved by coating the BiNPs with PEG (M = 12,000 g/mol, Alfa Aesar, USA). The coating was prepared by adding the PEG into the BiNP suspension and stirring the suspension in a flask for 1 h. The concentrations were 100 mg/ml for bismuth(III) oxide and 25 mg/ml for PEG. The obtained mean diameter of BiNP suspension was 260 nm, and surface charge 59 mV measured using a Malvern Zetasizer Nano ZS instrument (Malvern Instruments Ltd., UK). Finally, the pH of the suspension was adjusted to 7.4 with acetic acid (Sigma-Aldrich, USA).

In study **III**, changes in BiNP suspension preparation were made to improve the stability of the suspension. Here, the PEGylated BiNPs were prepared in a one-pot reaction system containing 0.5 kDa PEG-silane (2-[Methoxy(polyethy-leneoxy)9-12propyl]trimethoxysilane, tech-90, Fluorochem, Old Glossop, UK) and ball milled Bi_2O_3 powder. Before the reaction, the milled Bi_2O_3 nanoparticles were washed with ethanol and then mixed with PEG-silane. The mass ratio of PEG-silane to BiNP was 1:6. The BiNP-PEG-silane mixture was heated up to 260 °C and maintained at a constant temperature for 2.5 h in a flask under N_2 atmosphere. Subsequently, the obtained BiNPs were washed with ethanol three times with centrifuge separation (10,000 rpm, 10 min) and ultrasound re-dispersion to remove residual chemicals. The PEG-BiNPs were stored in ethanol until the synchrotron microCT measurements. The PEG-BiNPs in study **III** had a mean diameter of 194 nm and a surface charge of -3.5 mV (Zetasizer Nano ZS, Malvern Instruments Ltd., Malvern, UK).

5.3   CONTRAST-ENHANCED COMPUTED TOMOGRAPHY

CECT images were acquired using two different microCT scanners (studies **I** and **IV**) and a synchrotron-based microCT (studies **II** and **III**). The detailed descriptions of the image acquisitions are described below. The image and data analyses in studies **I** – **IV** were conducted with MATLAB (R2014a/2016b, MathWorks, Inc., USA). Table 5.2 summarises the contrast agents and imaging parameters used in this thesis.

Table 5.2: Summary of the contrast agents and the microCT scanners used in studies **I–IV**.

Study	Contrast agents (charge)	Concentration (mg/ml)	Voxel size (μm^3)	Scanner
I	BiNP ($q = 0$)	100	$15.98 \times 15.98 \times 15.98$	microCT
	ioxaglate ($q = -1$)	48		
II	CA4+ ($q = +4$)	5	$6.5 \times 6.5 \times 6.5$	Synchrotron microCT
	gadoteridol ($q = 0$)	10		
III	BiNP ($q = 0$)	10	$6.5 \times 6.5 \times 6.5$	Synchrotron microCT
	CA4+ ($q = +4$)	5		
	gadoteridol ($q = 0$)	10		
IV	CA4+ ($q = +4$)	10	$59.0 \times 59.0 \times 59.0$	microCT
	gadoteridol ($q = 0$)	20		

BiNP = bismuth(III) oxide nanoparticle, q = charge of the molecule, CA4+ = contrast agent bearing four positive charges, microCT = X-ray microtomography

5.3.1 X-ray Microtomography

In study **I**, the performance of three contrast agents in the detection of cartilage injuries and segmentation was compared. The three contrast agents utilized in study **I** were: (1) ioxaglate solution (48 mg I/ml, M = 1269 g/mol, Hexabrix, Mallinckrodt Inc., USA), (2) BiNP suspension (preparation described above), and (3) a mixture of iodine solution and BiNP suspension, i.e., the dual contrast agent. Prior to the microCT measurement, the solutions were adjusted to be isotonic (approx. 308 mOsm/kg) with PBS supplemented with proteolytic inhibitors [5 mM ethylenediaminetetraacetic acid (EDTA, VWR International, France) and 5 mM benzamidine hydrochloride hydrate (Sigma-Aldrich Inc., USA)] to prevent general degradation of proteins in tissue.

In study **I**, contrast agent diffusion and distribution within the cartilage was examined using a microCT scanner (Skyscan 1172, SkyScan, Belgium). 15.98 $\times$ 15.98 $\times$ 15.98 μm^3 isotropic voxel size, 100 kV tube voltage, 10 mA tube current, and 158 ms pulse length were used. Intact, PG-depleted, and mechanically injured samples were imaged immediately after the contrast agent immersion and after 45 minutes of diffusion. Further, the immersion bath was agitated in between the image acquisitions. The contrast agent bath volume was 3 ml/sample. The order of the immersion in the three contrast agents was randomly varied between the samples. After each imaging session, the contrast agents were washed out by immersing the samples in PBS (308 mOsm/kg, 100 ml) for 2 h at 7 °C before immersing the samples into the following contrast agent.

In study **IV**, the signs of post-traumatic osteoarthritis (PTOA) surrounding the lesion were examined using a mixture of CA4+ (q = +4, M = 1499 g/mol) and gadoteridol (q = 0, M = 559 g/mol, ProHanceTM, Bracco Diagnostic Inc., USA). The iodine concentration in the contrast agent mixture was 10 mg I/ml, and gadolinium concentration was 20 mg Gd/ml. To prevent general degradation of the tissue, the contrast agent mixture was supplemented with proteolytic inhibitors [5 mM EDTA (VWR International, France) and 5 mM benzamidine hydrochloride hydrate (Sigma-Aldrich Inc., USA)] and penicillin-streptomycin (100 units/ml penicillin, 100 μg/ml streptomycin; Life Technologies, USA).

The samples in study **IV** were imaged using a microCT scanner (Quantum FX, Perkin Elmer, USA) with X-ray tube voltages of 90 kV and 50 kV, a tube current of 200 μA, and 180 ms pulse length. Isotropic voxel size of 59 $\times$ 59 $\times$ 59 μm^3 was used. To shape the X-ray spectra, custom-made copper filters of 2 mm and 0.588 mm in thickness were applied for 90 and 50 kV acquisitions, respectively. Seven calibration phantoms with the following concentrations were utilized: one distilled water, three CA4+ phantoms with iodine concentrations of 8, 16, and 32 mg I/ml, and three gadoteridol phantoms with gadolinium concentrations of 8, 16, and 32 mg Gd/ml. The osteochondral samples were first imaged in the air to obtain a baseline image. After the baseline acquisition, the samples were immersed in an isotonic ($\sim$308 mOsm/kg) mixture of CA4+ and gadoteridol diluted in PBS. The samples were imaged at five imaging time points (30 min, 1 h, 2 h, 20 h, and 24 h). The bath volume was 20 ml, and it was stirred gently in between the image acquisitions.

5.3.2 Synchrotron X-ray Microtomography

Synchrotron-based microCT images were acquired in studies **II** and **III** with a third-generation synchrotron-based X-ray source (X02DA TOMCAT beamline of the Swiss

Light Source, PSI, Switzerland).

In study **II**, a mixture of cationic contrast agent CA4+ and gadoteridol was utilized. Osteochondral samples were imaged in the air before contrast agent immersion and at 1 h and 2 h after contrast agent immersion. The concentration of iodine in contrast agent baths was 5 mg I/ml and gadolinium 10 mg Gd/ml. The contrast agent mixture was supplemented with proteolytic inhibitors [5 mM EDTA (VWR International, France) and 5 mM benzamidine hydrochloride hydrate (Sigma-Aldrich Inc., USA)].

In study **III**, two contrast agent mixtures were prepared. The first contrast agent mixture, a dual contrast agent, composed of CA4+ and gadoteridol, and the second contrast agent, a triple contrast agent, composed of CA4+, gadoteridol, and BiNPs. In both contrast agent mixtures, the iodine concentration was 5 mg I/ml and gadolinium 10 mg Gd/ml. In the triple contrast agent, the BiNP concentration was 10 mg/ml. Proteolytic inhibitors [5 mM EDTA (VWR International, France) and 5 mM benzamidine hydrochloride hydrate (Sigma-Aldrich Inc., USA)] were added to suppress the general protein degradation in cartilage tissue. The osteochondral samples were imaged before contrast agent immersion and at 2 h after immersion.

MicroCT images were obtained by combining a 1:1 magnifying visible light optics microscope (Optique Peter, France), a 300 µm thick scintillator (LuAg, CRYTUR spol.s.r.o., Czech Republic), and a scientific complementary metal-oxid-semiconductor (sCMOS) detector (pco.Edge 5.5, PCO AG, Germany). A double-multilayer monochromator ensured a spectral bandwidth of about 2–3%. Two monochromatic X-ray imaging energies were used: In study **II**, the utilized energies were 25 keV and 37 keV, and in study **III**, the energies were 32 keV and 34 keV. The energies were selected based on iodine k-edge (33.2 keV) to maximize the difference in the mass attenuation coefficients of iodine (CA4+). $6.5 \times 6.5 \times 6.5$ µm^3 isotropic voxel size was used in both studies. Imaging geometry resulted in the field of view of 17.07 $\times$ 2.75 mm^2 in study **II** and 16.6 $\times$ 3.5 mm^2 in study **III**. The off-beam alignment system was utilized to minimise radiation exposure [120]. The image reconstruction was performed using a highly optimized algorithm based on Fourier methods [121].

5.4 HISTOLOGICAL AND BIOMECHANICAL ANALYSES

In studies **I–IV** optical density (OD) of Safranin-O stained sections were measured employing digital densitometry (DD) and served as a reference parameter indicating cartilage proteoglycan content. In study **IV**, in addition to OD, also biomechanical measurements were conducted.

5.4.1 Digital Densitometry

Digital densitometry (DD) measurements were performed after microCT measurements. The frozen samples were thawed and cut appropriately. Osteochondral samples in studies **I–III** were cut in half while the samples in study **IV** were prepared based on twelve biomechanical testing locations (see Fig 5.2). Subsequently, the samples were fixed in 10% formalin and dehydrated in an ascending series of ethanol. Following dehydration, decalcification of the samples was performed in EDTA to soften the samples for histological sectioning. Next, samples were embed-

ded in paraffin, and three sections with a thickness of 3 μm were prepared utilizing a microtome. The sections were stained with Safranin-O, which reveals the FCD distribution (i.e., PG content) in cartilage. After staining, OD was measured quantitatively with DD measurements using a light microscope (Nikon Microphot-FXA, Nikon Co., Japan) equipped with a monochromatic light source and a 12-bit CCD camera (ORCA-ER, Hamamatsu Photonics K.K., Japan). System calibration was performed using neutral density filters with optical densities ranging from 0 – 3.0 (Schott, Germany). The settings of the microscope were objective x1, zoom x2, and binning 1. Before the OD was calculated, the subchondral bone was segmented and removed from the images. Then the OD profiles were determined in the direction perpendicular to the articulating surface and interpolated to a length of 100 points. A custom-made Matlab script (Matlab 2016b, Mathworks, Inc.) was used to perform the analysis. In addition to the DD measurement, histological images of Safranin-O stained sections were acquired with a light microscope (Leica MZ75, Leica Microsystems Ltd., Switzerland) fitted with a CCD camera (Nikon digital sight DS-Fi2, Nikon Co., Japan).

5.4.2 Biomechanical Testing

In study **IV**, equilibrium and dynamic moduli were obtained through biomechanical indentation testing. An indentation testing system with a 250 g load cell (accuracy ± 0.25%, Model 31, Honeywell Sensotec Sensors, Columbus, USA) and an actuator (displacement resolution 0.1 μm, PM500-1 A, Newport, Irvine, USA) was used. Four locations were examined from proximal, central, and distal parts with respect to the position of the joint, resulting in a total of twelve biomechanical testing locations in one specimen (less than 12 locations were tested for two samples due to the shape of the sample). Prior to the measurements, the samples were glued on a custom-made sample holder mounted on a goniometer (#55-841, Edmund Optics Inc., Barrington, USA), which enabled perpendicular alignment of the cartilage surface with a plane-ended cylindrical indenter (d = 0.53 mm).

To begin the measurements, the indenter was driven carefully into contact with cartilage surface. To ensure the established contact, the samples were indented five times to 2% of cartilage thickness. Subsequently, four consecutive 5% stress-relaxation steps with the ramp velocity of 100%/s relative to cartilage thickness and a relaxation time of 600 seconds were performed. The indentation was followed by dynamic sinusoidal loading (f = 1.0 Hz) with the amplitude of 1% of the remaining cartilage thickness. The equilibrium (E_{eq}) and dynamic moduli (E_{dyn}) were calculated according to the Hayes equation [122] with a Poisson's ratios of ν = 0.1 for equilibrium modulus and ν = 0.5 for dynamic modulus.

5.5 STATISTICAL ANALYSIS

SPSS (IBM, SPSS Statistics, v.24-25, USA) was employed in statistical analysis. The limit of significance was set to be at $P < 0.05$.

The differences in contrast agent partitioning between healthy and injured/degenerated cartilage were compared through using the non-parametric Mann-Whitney U test. Non-parametric tests were chosen due to a relatively small number of samples,

and since based on the Shapiro-Wilk test, the populations underlying the data sets were found to deviate from being normally distributed. The correlation coefficient and the P-value between the calculated and the measured iodine and gadolinium concentrations in the test tubes were calculated using Pearson's correlation analysis. The Shapiro-Wilk test indicated that the osteochondral sample data is not normally distributed. Thus, Spearman's rank correlation coefficient was used to identify the correlation between the reference parameters (e.g., OD, equilibrium moduli, and dynamic moduli) and contrast agent partitions.

6 Results

This chapter highlights the essential findings of studies **I**- **IV**. Original publications are attached to this thesis as appendices for additional details and complete results.

6.1 DUAL CONTRAST CT

Study **I** focused on the development of a dual contrast agent (BiNPs and ioxaglate) for the simultaneous segmentation of the articulating surfaces and evaluation of the cartilage condition from a single delayed CT image. Developed BiNPs were unable to diffuse into cartilage regardless whether the cartilage was intact, PG-depleted, or mechanically injured (Fig. 6.1). In this context, BiNPs enabled accurate segmentation of articulating surfaces and detection of cracks in the cartilage surface at 45 minutes after the contrast agent immersion. Values of cartilage thickness were determined based on BiNP suspension-, ioxaglate- and dual contrast-enhanced images and compared with the thickness values obtained from the light microscopy of the histological sections. Significant difference in cartilage thickness between the ioxaglate-enhanced images and histological sections was observed ($P < 0.05$ for all sample groups). The cartilage thickness was 7.0% less in ioxaglate-enhanced images obtained immediately after the contrast agent immersion and 9.3% less at 45 min after immersion. The corresponding values for BiNP suspension-enhanced images were 0.6% and 0.7% and for dual contrast-enhanced images 2.3% and 2.3%, respectively.

In addition to maintaining high contrast at articulating surfaces, BiNPs were found to allow ioxaglate diffusion into cartilage tissue without interference, thus enabling the detection of tissue condition. The uptake of ioxaglate was higher in mechanically injured (+86.6%, $P = 0.005$) and PG-depleted (+60.0%, $P = 0.005$) injured samples than in the intact samples at 45 min after contrast agent immersion (Fig. 6.2). In dual contrast agent, the uptake of ioxaglate in mechanically injured samples was +113.1% ($P = 0.013$) and in PG-depleted samples +70.3% ($P = 0.013$) when compared with the intact sample at the same time point. In DD measurements, the PG content was significantly lower in mechanically injured ($P = 0.009$) and PG-depleted samples ($P = 0.0005$) compared with the intact samples.
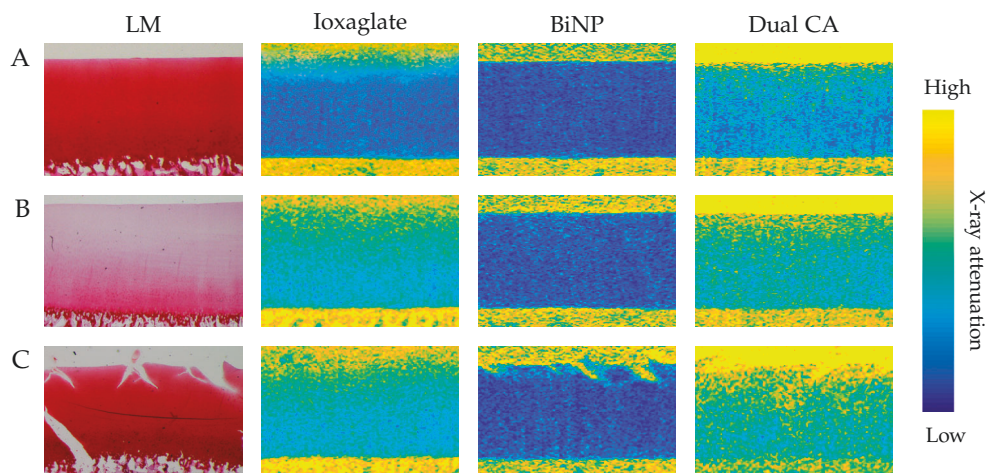
Figure 6.1: Light microscope (LM) imaged Safranin-O stained histological sections and corresponding contrast-enhanced microCT images of (A) intact, (B) proteoglycan (PG)-depleted, and (C) mechanically injured sample images acquired 45 minutes after the contrast agents (CAs) immersion. Visualization of articulating surfaces and superficial lesions is enhanced with the usage of bismuth(III) oxide nanoparticles (BiNPs). The differences in surface features within LM and contrast-enhanced CT images are due to the fact that achieving exactly the same slice position through all the images was found impossible. The detection of degeneration in mechanically injured and PG-depleted cartilage samples is possible based on higher X-ray attenuation (i.e. ioxaglate diffusion) of cartilage when compared with intact cartilage.
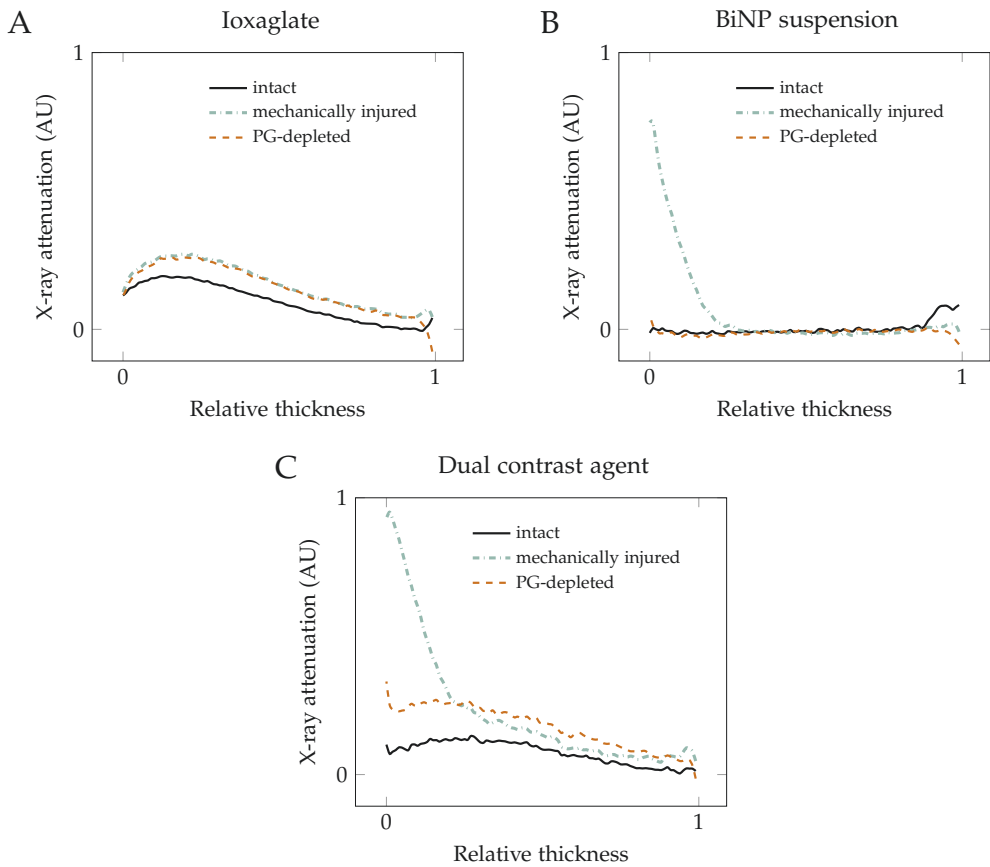
Figure 6.2: Mean depth-wise contrast agent X-ray attenuation profiles in articular cartilage at 45 minutes after the contrast agent immersion for intact, mechanically injured, and proteoglycan (PG)-depleted samples The samples were imaged immersed in (A) ioxaglate, (B) bismuth(III) oxide nanoparticles (BiNP) suspension, and (C) dual contrast agent. The horizontal axis presents the relative distance from articular surface (0) to the cartilage-bone interface (1). Arbitrary units (AUs) are used as the microCT utilized in this study yielded data in 16-bit gray scale values instead of standard 12-bit Hounsfield Unit scale.

6.2 QUANTITATIVE DUAL-ENERGY CT

In study **II**, QDECT was shown to enable simultaneous quantification of partitions of two contrast agents, CA4+ and gadoteridol, and subsequent evaluations of cartilage PG and water contents. Gadoteridol uptake in cartilage was higher in the mechanically injured + PG-depleted samples ($P < 0.008$) than in the intact samples at both imaging time points (1 h and 2 h) (Fig. 6.3 A). However, no significant difference in gadoteridol partition between PG-depleted and intact samples was observed. The uptake of CA4+ was lower at both time points with mechanically injured + PG-depleted and PG-depleted samples when compared with intact samples ($P < 0.011$, Fig. 6.3 B). Normalization of the CA4+ partition with the gadoteridol partition was observed to increase the difference between the injured and intact samples (Fig. 6.3 C). Partitioning maps of CA4+ and gadoteridol at both imaging time points are presented in Fig. 6.4.

Water content analysis showed no significant differences ($P > 0.05$) between mechanically injured + PG-depleted samples or PG-depleted samples when compared with the intact samples. However, lower PG content was observed with the mechanically injured + PG-depleted samples ($P = 0.008$) and PG-depleted samples ($P = 0.008$) than in the intact samples (Fig. 6.3 D). Significant correlations ($P < 0.001$) between OD (i.e., PG content) and CA4+ partition values were found when determined for the superficial cartilage layer (20% of the cartilage thickness). The corresponding Spearman's rhos for CA4+ partitions after 1 h immersion was $\rho = 0.683$ and after 2 h immersion $\rho = 0.738$. For normalized CA4+ partitions the Spearman's rhos after 1 h and 2 h were $\rho = 0.734$ and $\rho = 0.662$, respectively.
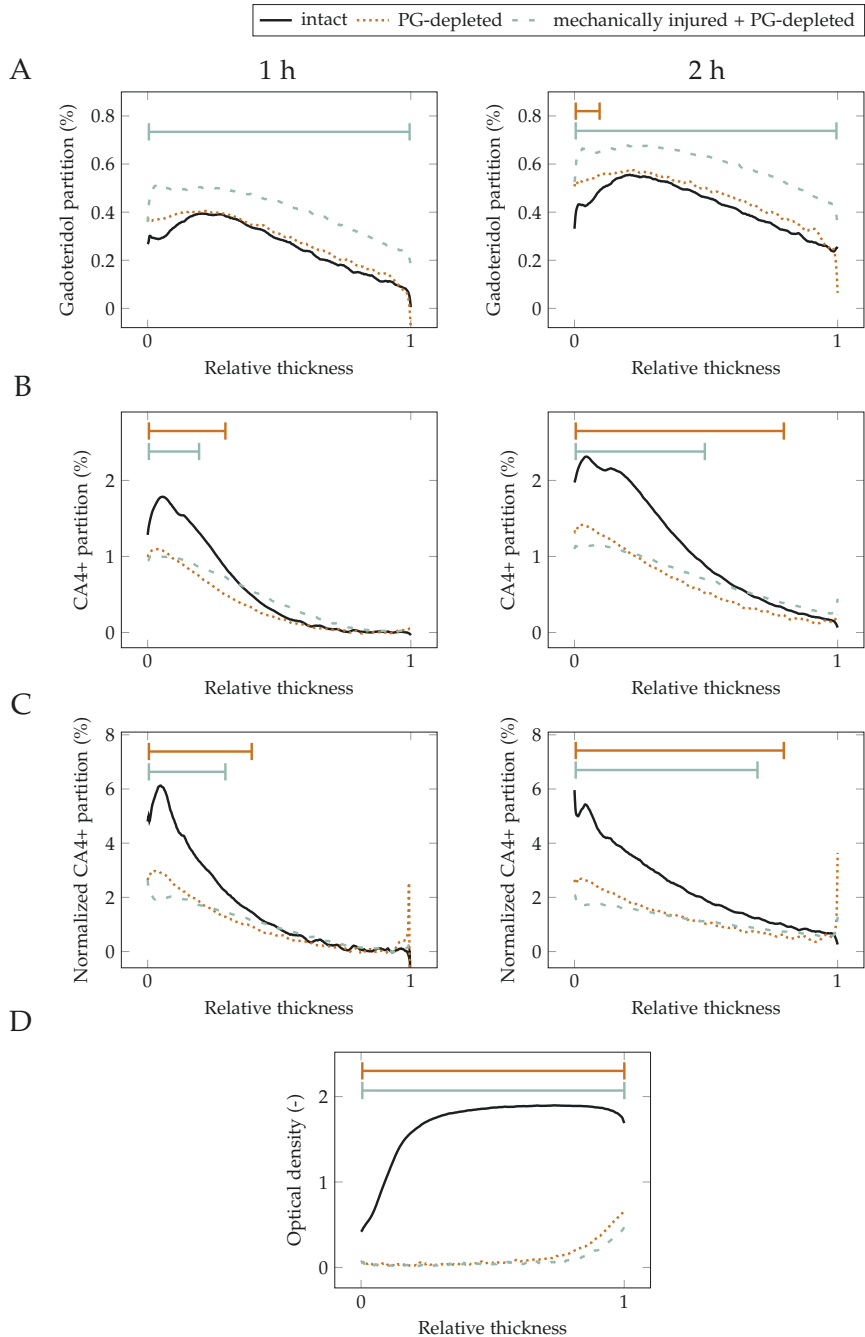
Figure 6.3: Mean depth-wise partitions of (A) gadoteridol, (B) CA4+, and (C) normalized CA4+ at 1 h and 2 h after contrast agent immersion. (D) Mean depth-wise optical density. Statistically significant difference ($P < 0.05$) between the mechanically injured + proteoglycan (PG)-depleted samples (blue) or PG-depleted samples (brown) and intact samples are presented with lines (⊢⊣) above the profiles with corresponding colors. No statistical difference in gadoteridol partition between intact and PG-depleted samples were observed (subfigure (A) 1 h). Cartilage surface is denoted with 0 and cartilage-bone interface with 1.
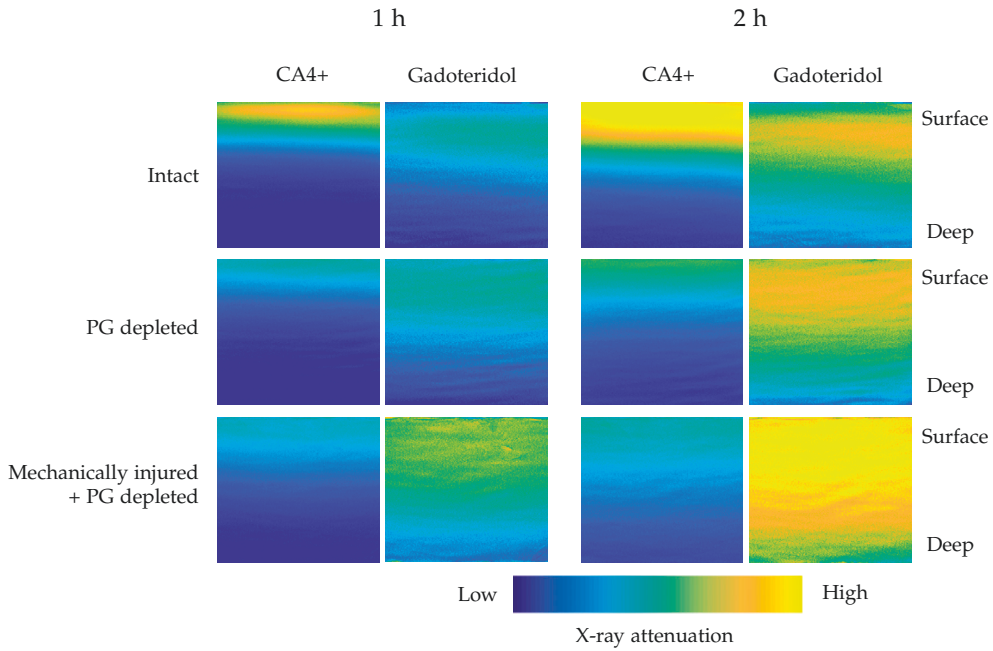
Figure 6.4: CA4+ and gadoteridol partitioning within intact, proteoglycan (PG)-depleted, and mechanically injured + PG-depleted cartilage samples at 1 h and 2 h after contrast agent immersion. The highest CA4+ partition is observed in intact samples as a result of higher PG content of healthy cartilage. On contrary, the gadoteridol partition is lowest in the intact sample, while in the PG-depleted and mechanically injured + PG-depleted samples, the uptake of gadoteridol is increased owing to reduced steric hindrance of the tissue.

6.3 TRIPLE CONTRAST CT

In study **III**, the stability of the BiNPs was measured at multiple time points (0 min, 30 min, 1 h, 2 h, 3 h, 7 h, 11 h and 24 h) after mixing the BiNPs with CA4+ and gadoteridol. The mean particle diameter was 195 $\pm$ 2 nm immediately after the mixing, and no statistically different change ($P > 0.05$) were observed at the later time points.

The visualisation of articulating surfaces and surface lesions was challenging with the dual contrast agent. However, owing to BiNPs, the visualisation of articulating surfaces was enhanced with triple contrast agents at 2 h after the contrast agent immersion (Fig. 6.5). Furthermore, the detection of surface lesion in mechanically injured samples was improved. Statistically significant differences ($0.008 < P < 0.028$) for gadoteridol, CA4+ and normalized CA4+ partitions between the intact samples and PG-depleted/mechanically injured samples in the full cartilage thickness were observed with dual contrast agent. With triple contrast agent, significant difference ($0.008 < P < 0.011$) with gadoteridol, CA4+ and normalized CA4+ partitions was observed only with PG-depleted samples.

The uptake of CA4+ was higher in the superficial and middle zones of intact samples than in PG-depleted samples with both contrast agents (Fig. 6.6). When compared with mechanically injured sample, the difference in the superficial and deep zones was significant with the dual contrast agent and in the superficial zone with the triple contrast agent. The normalization of CA4+ partition with the gadoteridol partition increased the difference between the intact and PG-depleted/mechanically injured samples at superficial and middle zone (Fig. 6.6). Compared with intact sample, the uptake of gadoteridol into PG-depleted sample was higher in middle and deep zones for the dual contrast agent and in all zones for the triple contrast agent. In the mechanically injured samples, the significant differences was found in all zones with the dual contrast agent and in superficial and middle zones with the triple contrast agent.

The linear correlation between CA4+ partition and PG distribution was statistically significant in superficial and middle zones ($0.504 < \rho < 0.766$, $0.0001 < P < 0.007$) with dual and triple contrast agents. The correlation of gadoteridol partition and PG content was significant only in the deep zone and full thickness cartilage ($-0.442 < \rho < -0.428$, $0.021 < P < 0.026$) with dual contrast agent. The normalization of CA4+ improved the correlation between the CA4+ and PG contents significantly in the middle zone with both dual and triple contrast agents.
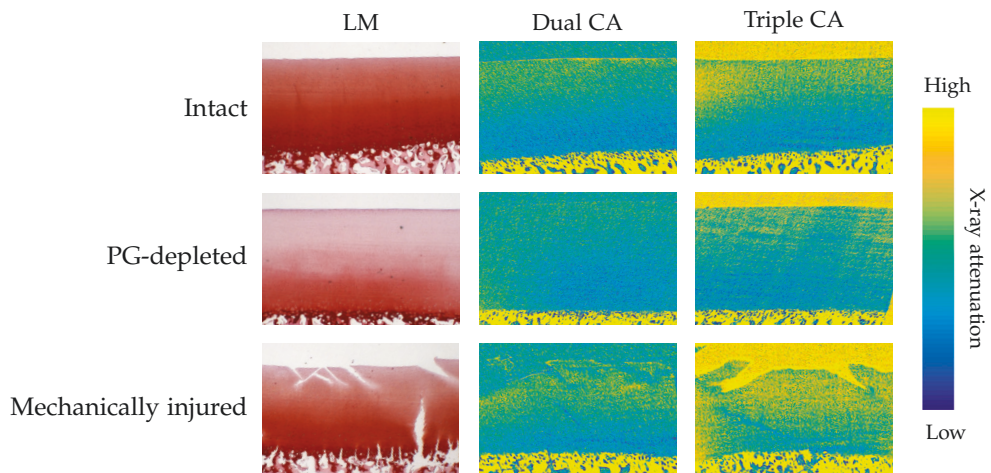
Figure 6.5: Light microscope (LM) images of Safranin-O stained histological sections of representative intact, proteoglycan (PG)-depleted, and mechanically injured samples and corresponding dual contrast agent (CA) and triple contrast agent synchrotron microCT images (32 keV imaging energy, average of five consecutive 6.5 µm thick slices) acquired 2 h after the contrast agent immersion. Triple contrast agent improves visualisation of articulating surfaces and surface lesions owing to bismuth nanoparticles (BiNPs) that are too large to diffuse into cartilage.
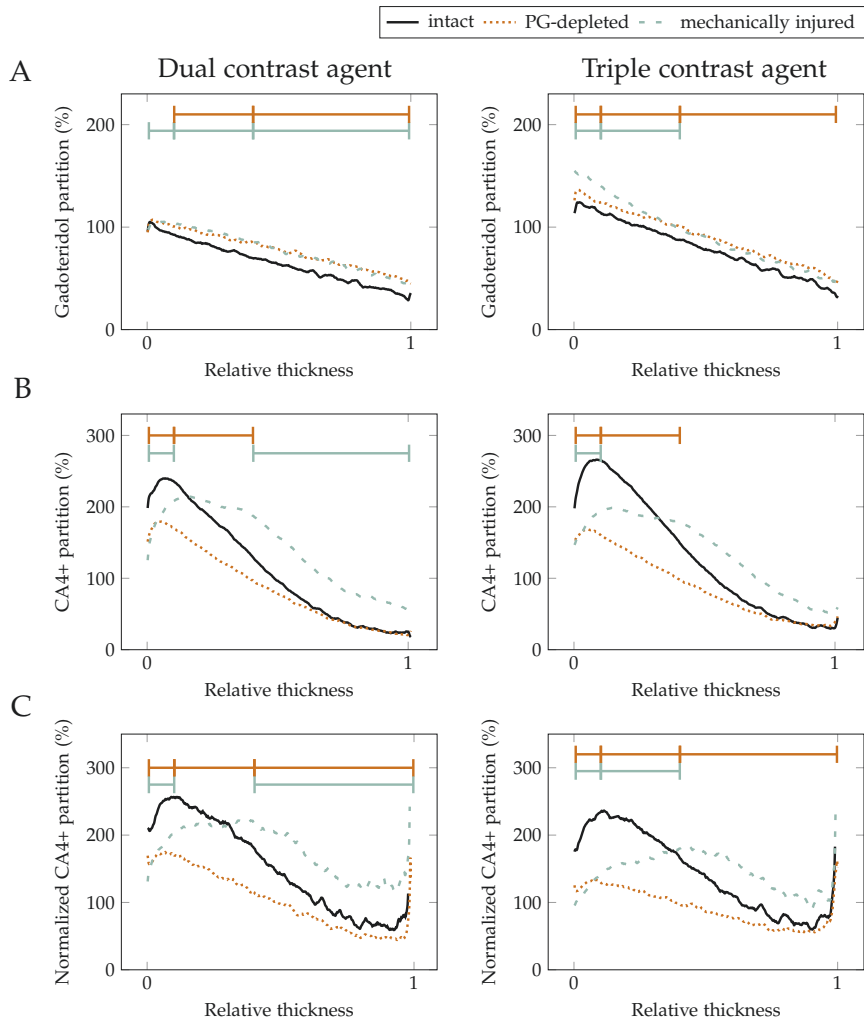
Figure 6.6: Mean depth-wise partitions of (A) gadoteridol, (B) CA4+, and (C) normalized CA4+ at 2 h after dual and triple contrast agent immersion. Statistical significant difference ($P < 0.05$) within the superficial, middle, and deep zones between proteoglycan (PG)-depleted samples (brown) or mechnanically injured samples (blue) and intact sample are presented with lines (⊢⊣) above the profiles with corresponding colors. Cartilage surface is denoted with 0 and cartilage-bone interface with 1.

6.4 DETECTION OF POST-TRAUMATIC OA USING QUANTITATIVE DUAL-ENERGY CT

In study **IV**, mean CA4+ partition was found significantly higher in experimental samples than in control samples at 30 min ($P = 0.004$) and 60 min ($P = 0.028$) after the contrast agent immersion as calculated for full cartilage thickness. On the contrary, the CA4+ partition in experimental samples was lower at 20 h ($P < 0.0001$). In superficial cartilage layer, a significantly higher CA4+ partition in experimental samples was found at 30 min ($P = 0.001$) and lower partition at 20 h ($P < 0.0001$) and 24 h ($P < 0.0001$). With gadoteridol, the mean partition for full cartilage thickness was lower in experimental samples compared with the control samples at 60 min ($P < 0.0001$) and at 120 min ($P = 0.002$). In superficial layer, gadoteridol partitions were lower in experimental samples at 30 min ($P = 0.003$), 60 min ($P < 0.0001$), and 120 min ($P < 0.0001$). At 20 h and 24 h, gadoteridol partition had no significant difference between the experimental and control samples. The mean partition maps of CA4+ and gadoteridol are presented in Figs. 6.7 and 6.8.

Spearman's rank correlations revealed significant ($P < 0.05$) positive correlation between the CA4+ partition and the reference parameters (OD, equilibrium moduli, and dynamic moduli) at 20 h and 24 h after the contrast agent immersion (Tab. 6.1). Significant ($P < 0.05$) negative correlation was also obtained at 30 min and 60 min imaging time points.

Figure 6.7: Representative partition maps of CA4+ for three experimental and three control samples. Partition maps for full thickness cartilage and superficial layer (50% of the total cartilage thickness) are presented. The locations of the lesions in the experimental samples are delineated with red lines. In control samples, the red lines are also drawn to the corresponding sites for clarity to demonstrate where the lesions would have been created.
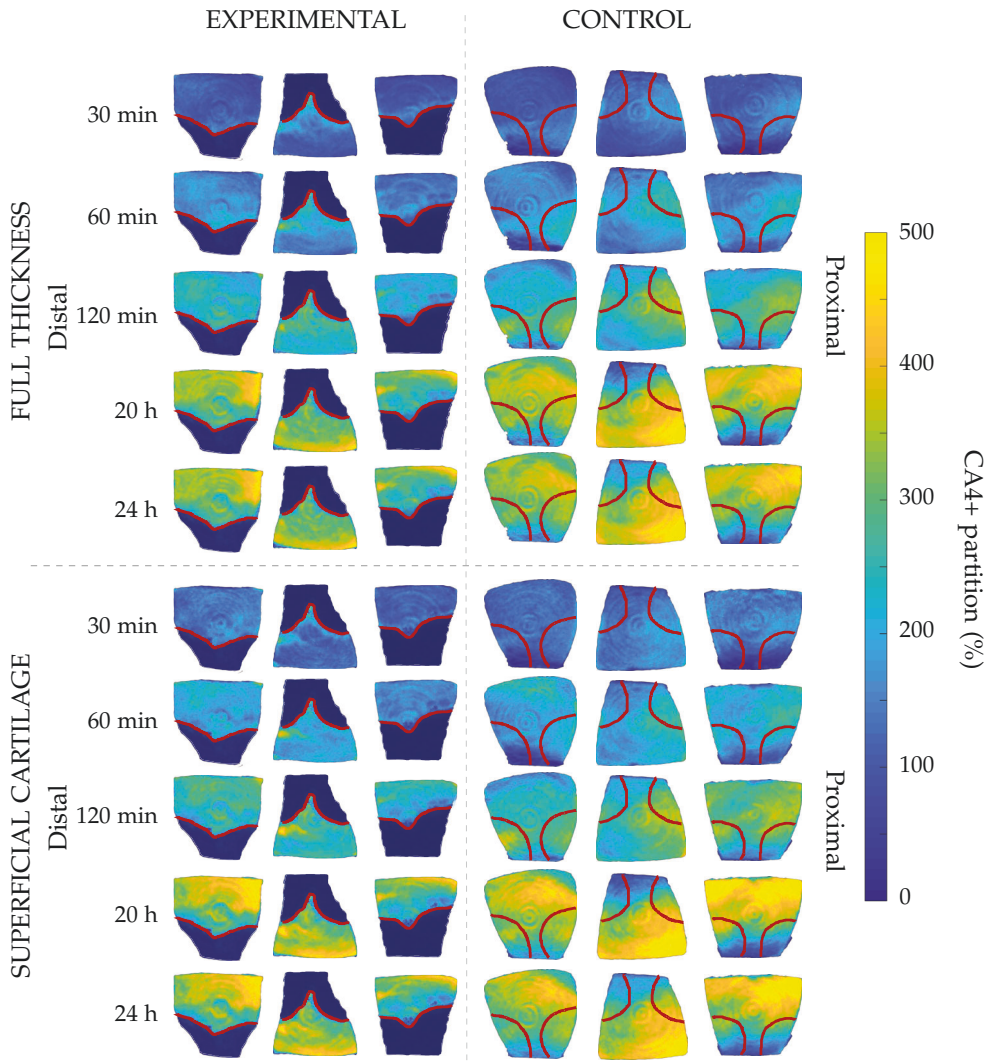
Figure 6.8: Representative partition maps of gadoteridol for three experimental and three control samples. Partition maps for full thickness cartilage and superficial layer (50% of the total cartilage thickness) are presented. The locations of the lesions in the experimental samples are delineated with red lines. In control samples, the red lines are also drawn to the corresponding sites for clarity to demonstrate where the lesions would have been created.
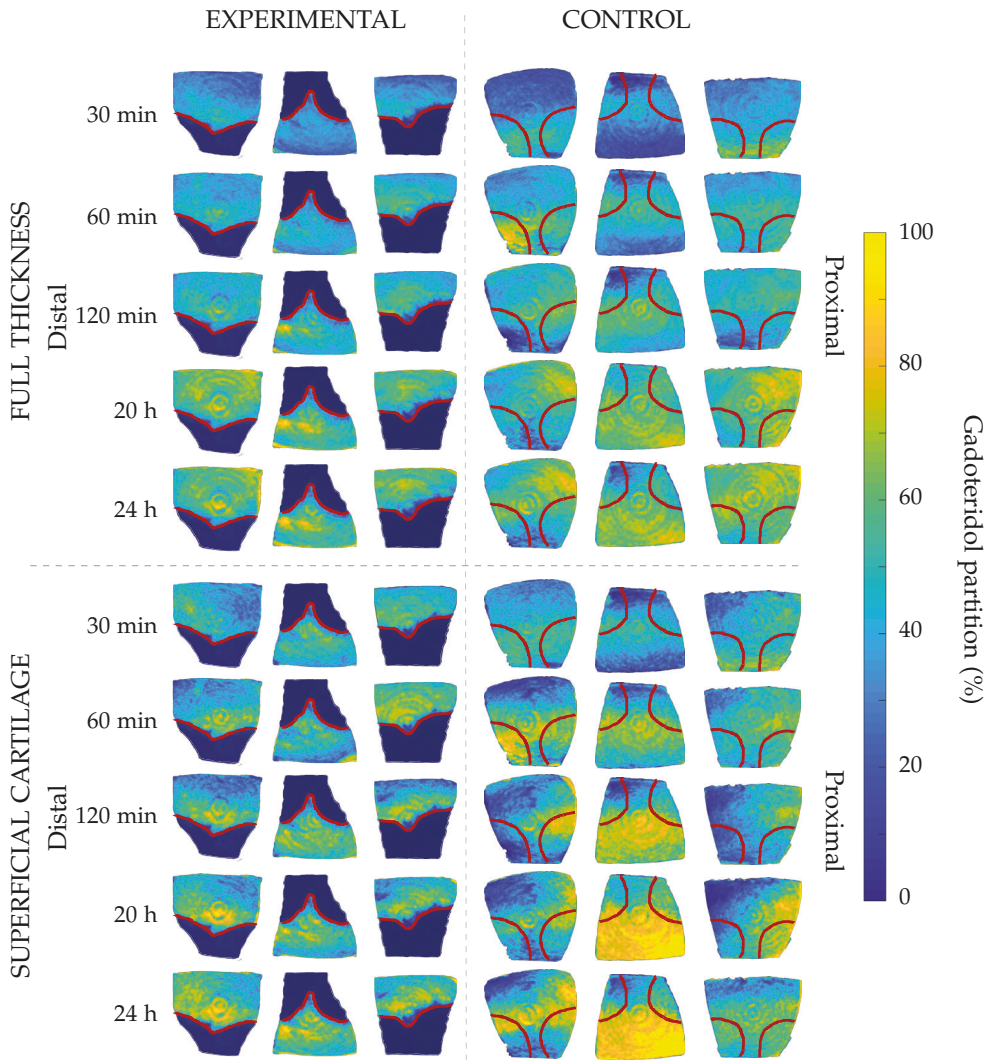
Table 6.1: Spearman's rank correlations of CA4+ partition and reference parameters (optical density, equilibrium, and dynamic moduli).

	Optical density		Equilibrium modulus		Dynamic modulus	
	Full cartilage thickness	**Superficial cartilage**	**Full cartilage thickness**	**Superficial cartilage**	**Full cartilage thickness**	**Superficial cartilage**
30 min	-0.148*	-0.304*	-0.137*	-0.289*	-0.078	-0.217*
60 min	-0.177*	-0.325*	-0.150*	-0.341*	-0.102	-0.281*
120 min	0.089	-0.014	0.101	-0.043	0.125	0.015*
20 h	0.693*	0.660*	0.635*	0.537*	0.610*	0.537*
24 h	0.627*	0.600*	0.553*	0.482*	0.550*	0.517*

* Correlation is significant at the $P < 0.05$ level

7 Discussion

For effective prevention and treatment of PTOA, early diagnosis is imperative. However, the lack of sensitive imaging techniques hinders the clinicians' opportunities to guide treatment before the degeneration of the cartilage is already widespread or severe. CECT is an emerging technique that enables cartilage imaging and assessment of the severity of the cartilage degeneration. As of today, it has been applied for quantification of PG content, equilibrium modulus, cartilage thickness in a variety of species, and coefficient of friction [16, 22, 23, 58, 123–125]. Nonetheless, since the conception of CECT of articular cartilage, the imaging has only been conducted using a single charged ($q = +/-1$) or non-charged ($q = 0$) contrast agent.

In this thesis, a triple contrast method was developed for the CECT diagnostics of cartilage degeneration. In study **I**, BiNPs were investigated in their potential to maintain a high contrast at the interface between synovial fluid and articular cartilage and provide visualization of superficial cartilage lesions. In study **II**, two contrast agents (CA4+ and gadoteridol) were combined to study whether QDECT would allow quantification of the contrast agent partitioning along with cartilage tissue and subsequent evaluation of PG and water contents. Study **III** combines QDECT and BiNP for simultaneous evaluation of cartilage composition and visualization of articulating surfaces. In study **IV**, the focus is shifted from the lesion site to its surrounding tissue, and QDECT is used to identify post-traumatic degeneration.

7.1 DUAL CONTRAST CT

In study **I**, the performance of the BiNPs to enhance the synovial fluid–cartilage interface was evaluated using two approaches. Firstly, the uptake values of ioxaglate and secondly, the segmented cartilage thickness from conventional ioxaglate-enhanced images and BiNP suspension-enhanced images with the thickness obtained from light microscopy images were compared. In conventional segmentation of the articulating surfaces, the diffusion of ioxaglate results in a loss of contrast at the cartilage surface, and thus, the superficial layer of the cartilage is often being falsely interpreted as synovial fluid. As a result, the uptake of ioxaglate would appear lower than actual uptake. Confirming the hypothesis, the uptake of ioxaglate was found higher in BiNP suspension-enhanced images than in the ioxaglate-enhanced images in all sample groups. Significant differences in segmented cartilage thickness and actual cartilage thickness were observed in both 0-minute and 45-minute ioxaglate-enhanced images, while no significant difference was found either in BiNP suspension-enhanced or dual contrast-enhanced images. These results indicate that BiNPs improve the visualization of articulating surface, thus enabling more accurate segmentation of the cartilage from both 0-minute and delayed images. As the superficial cartilage layer often shows the first signs of degeneration, the implementation

of the BiNPs could thus enable the detection of degeneration earlier than using the conventional methods.

For an accurate evaluation of cartilage degeneration based on ioxaglate uptake, it is important that BiNPs cannot penetrate the cartilage tissue. Thereby, X-ray attenuation values in the cartilage between 0- and 45-min BiNP suspension-enhanced images were examined and found similar, suggesting that BiNPs are indeed unable to penetrate the cartilage tissue.

Ioxaglate uptakes in PG-depleted and mechanically injured samples were higher than in intact samples. In mechanically injured samples, the uptake is higher as the surface lesions increase the area for diffusion but also because of the disruption of the collagen network, reducing the steric hindrance of contrast agent diffusion [126, 127]. In PG-depleted samples, the increased uptake is mainly due to decreased PG content, but also changes in structural and compositional properties of the tissue, such as collagen and water contents, have probably affected the diffusion of ioxaglate [18, 128].

Optimally, BiNPs enable free diffusion of ioxaglate molecules when mixed with ioxaglate as a dual contrast agent. However, the bulk ioxaglate values were higher in dual contrast agent-enhanced images than in ioxaglate-enhanced images. This increase in X-ray attenuation values is explained by the functioning of the microCT reconstruction algorithm that increases the X-ray attenuation values throughout the image in the presence of a highly attenuating contrast agent bath. The effect caused by this artefact was minimized by normalizing the images with the subchondral bone attenuation and by subtracting the 0-min image from the 45-min image having the same reconstruction-based artefact in their attenuation values. Due to this observation, the concentration of BiNPs in the study **III** was decreased.

In study **I**, the stability of the BiNP suspension in a high ion concentration was found weak, and consequently, the osmolalities of the BiNP suspension and dual contrast agent could not be adjusted to physiological osmolality. In a hypotonic bath, the swelling pressure of the cartilage increases and may lead to elevated water content in the tissue. However, since no significant increase in cartilage thickness was observed, the changes in cartilage diffusive properties and water content are expected to be minimal. In study **III**, the problem regarding the stability of the BiNPs in the presence of ions was solved by coating the BiNPs with PEG-silane.

Overall, the findings in study **I** indicate that the introduced dual contrast technique improves the feasibility of CECT by enabling accurate delineation of articulating surface and pathological surface alterations together with the simultaneous unveiling of degeneration from a single delayed CT image.

7.2 QUANTITATIVE DUAL-ENERGY CT

In study **II**, the depth-wise gadoteridol and CA4+ partition profiles were obtained from synchrotron microCT images using QDECT. The mechanically injured + PG-depleted samples were found to have significantly higher gadoteridol uptake when compared with the intact samples. No significant difference between the intact and PG-depleted samples was observed. The increase in gadoteridol uptake in mechanically injured + PG-depleted samples is most likely due to reduced articular cartilage steric hindrance caused by the mechanical impact on cartilage, affording

greater porosity for contrast agent diffusion. The diffusion is further increased as the surface area for diffusion in the mechanically injured + PG-depleted samples is increased because of the surface lesions.

The CA4+ uptake was significantly higher in the intact sample compared with the injured sample groups. This is in good agreement with the literature [13, 22, 108, 129, 130]. The uptake of CA4+ is proportionally related to the PG content of the cartilage tissue; thus, the uptake of CA4+ is lower in PG-depleted samples. The slightly higher CA4+ partitioning of the mechanically injured + PG-depleted samples compared with PG-depleted samples is likely due to decreased steric hindrance originating from the mechanical damage to the cartilage tissue since the water content analysis showed no difference between the two sample groups. Even though the CA4+ partition is proportionally related to the PG content, it is worth noting that the CA4+ distribution is not equivalent to depth-dependent PG content because the imaging is conducted during ongoing diffusion afar from the diffusion equilibrium.

The normalization of CA4+ partition with that of gadoteridol was performed to improve the sensitivity of cationic CA4+ at early diffusion time points. In degenerated cartilage, the uptake of CA4+ into tissue is decreased due to the loss of PG content. However, the diffusion of CA4+ is elevated at the same time due to an increase in tissue permeability and water content, as compared with the intact sample having the opposite effect on contrast agent diffusion. Thus, in early diffusion time points, distinguishing intact from degenerated cartilage is challenging [131]. The normalization is expected to improve the sensitivity of CA4+ to detect cartilage degeneration. The results, however, indicated that the normalization improved the detection of degeneration only moderately in study **II**. This moderate improvement migth be explained with the observation that no statistically significant difference in water content between the intact and injured sample groups was found [127, 132]. The normalization was hypothesized to remove the effect of varying CA4+ diffusion due to different water contents between intact and degenerated cartilage; thus, with no prominent differences in water content, the normalization with gadoteridol partition fail to produce the expected results.

To summarize the results obtained in study **II**, QDECT enabled simultaneous quantification of CA4+ and gadoteridol in cartilage tissue and thus subsequent evaluation of PG and water contents at clinically feasible imaging time points. With this, QDECT was able to differentiate PG-depleted and mechanically injured + PG-depleted samples from intact samples.

7.3   TRIPLE CONTRAST CT

High contrast between the contrast agent bath and articular cartilage was obtained when using BiNPs in triple contrast agent. The contrast was good even though the utilized concentration was substantially lower than in study **I**. Improved visualization of articulating surface significantly eased the cartilage segmentation in the triple contrast-enhanced images while in dual contrast-enhanced images (gadoteridol + CA4+) the delineation of the articulating surface was challenging. Interestingly, the surface lesions in mechanically injured samples were easily detectable as seen in Fig. 6.5.

The gadoteridol and CA4+ uptakes for dual and triple contrast agent were determined utilizing the segmentation obtained from triple contrast-enhanced images. The uptake of gadoteridol was higher in both PG-depleted and mechanically injured samples than in intact samples. This increase in gadoteridol uptake is related to reduced steric hindrance, affording easier penetration of the contrast agent molecules into cartilage. The reduced steric hindrance is caused by depletion of PGs, disruption of the collagen network, and increased water content. In the mechanically injured samples, the gadoteridol uptake is also increased owing to surface lesions that increase the surface area for diffusion of gadoteridol molecules.

The uptake of CA4+ in superficial and middle zones was higher in intact samples than in PG-depleted samples. In the deep zone, the CA4+ uptake into intact and PG-depleted samples are nearly similar. This is firstly due to short diffusion time - during 2 h of diffusion, only a small portion of the CA4+ molecules have reached the deep cartilage. Secondly, despite trypsin treatment, a small amount of PG still remains in deep cartilage (Fig. 6.5), increasing the uptake of CA4+. With normalization, the effect of increased water content is reduced, and therefore, the difference in CA4+ partitions between the PG-depleted and intact samples is increased. These findings are in agreement with the data in literature [22, 108, 129, 130].

In mechanically injured samples, the uptake of CA4+ was lower in the superficial zone, while in the deep zone, the CA4+ uptake was higher when compared with intact samples. In the superficial zone, the lower uptake results from contrast agent in surface lesions. During analysis, the cracks were removed in most parts but to ensure that no cartilage was removed, a small margin was used when applying the threshold. Thus, a small amount of contrast agent bath with contrast agents' partitions of exactly 100% was included, causing lower CA4+ partition than in reference samples at the surface. The higher uptake in deep zone can also be explained with surface lesions increasing the surface area for CA4+ diffusion similarly as for gadoteridol.

When comparing the gadoteridol and CA4+ profiles obtained between the dual and triple contrast agents, the mean gadoteridol and CA4+ partition profiles have similar shapes. However, the partitions of gadoteridol for triple contrast agent in the superficial and middle zones are slightly higher than those determined using the dual contrast agent with all the samples. Higher partitions of CA4+ in the superficial and middle zones of intact samples were observed. The increased partition values of Ca4+ in the superficial and middle zones might be reconstruction-based originating from a high change in attenuation level at the articulating surface when the triple contrast agent is used. Secondly, the difference may also rise from the samples. Adjacent samples were used for dual and triple contrast agent imaging, and thus, the samples may have had minor variations in the cartilage thickness, due to natural curvatures of the cartilage surfaces causing a minor difference in the contrast agent partitions. Since BiNPs are shown to be stable for 24 h and to have particle diameter (193 nm) much higher than the pore size of the cartilage (around 6 nm [27, 133]), the possibility of BiNPs to affect the increased partitions is negligible. Finally, higher gadoteridol partitions in triple contrast agent are reflected in the normalized CA4+ partitions. As the normalization is done by dividing the CA4+ partition with gadoteridol, the higher gadoteridol partition causes the normalized CA4+ partition to be lower in triple contrast agent than in dual contrast agent.

In study **III**, utilized monochromatic X-ray beam and high-resolution images provided by the synchrotron microCT allowed us to examine the full potential of the triple contrast agent without artefacts and limitations associated with conventional

CT systems, such as wide X-ray energy spectra and beam hardening. To conclude, the triple contrast method was shown for the first time to enable simultaneous quantification of PG and water contents, providing information on degenerative changes in articular cartilage, and segmentation of articulating surface and surface lesions 2 hours after contrast agent immersion.

7.4 DETECTION OF POST-TRAUMATIC OA USING QUANTITATIVE DUAL-ENERGY CT

In study IV, at early-diffusion time points, the partition of CA4+ was found higher in experimental samples than in control samples. In experimental samples, the post-traumatic changes decrease the steric hindrance that increases the diffusion rate of CA4+, thus increasing the CA4+ partition in the tissue. With gadoteridol, the partition was surprisingly lower in experimental samples at the 60 min and 120 min imaging time points. Similarly to CA4+, the post-traumatic-related changes should increase the gadoteridol uptake into the tissue. One explanation for this observation might be caused by interactions between the CA4+ and gadoteridol molecules. By examining the partition maps in Figs. 6.7 and 6.8, one can notice that in the areas of high CA4+ uptake, the uptake of gadoteridol seems to be lower, indicating that a repulsive interaction might take place between the two contrast agent molecules. Even though QDECT has been proven functional in previous test tube measurement [114], where CA4+ and gadoteridol concentrations were accurately measured, the results obtained here suggest that in a more demanding measurement set-up, the technique is subjected to the above-described challenges. The samples used in this study were bigger included more tissue around the measurement sites whereas the previous studies only had the cartilage with the measured lesions and a small amount of bone underneath. To fully understand the underlying reason why CA4+ partition in experimental samples in this study where higher, further investigation is needed.

At 20 h diffusion time point, a significantly lower CA4+ partition was found in full-thickness and superficial cartilage layers when experimental samples were compared with control samples. At 24 h diffusion time point, a lower CA4+ partition was observed only in the superficial layer. When the partitions of both contrast agents were compared at the late diffusion time points (20 h and 24 h) with the experimental samples, no apparent differences were observed, suggesting that the diffusion is at equilibrium or nearly approaching it. However, with control samples, the difference between the partition values at 20 h and 24 h imaging time points indicated that the diffusion equilibrium has not been reached. This incomplete diffusion explains why no statistically significant difference in CA4+ partitions between experimental and control samples was found at the 24 h imaging time point in full cartilage thickness.

Examination of gadoteridol partitions between the experimental and control samples at the late diffusion time points reveal that no difference is present, thus suggesting that no difference in water content exists between the two sample groups. Alternatively, the changes in water content can be so subtle that the limitation of the QDECT and conventional microCT may overshadow the changes. As mentioned above, the X-ray beam energy spectrum in conventional microCT is wide, exposing

the imaging to beam hardening and other artefacts. Imaging with a narrowed energy spectra or even the possibility for monochromatic imaging would improve the evaluation of water content in QDECT.

The present results indicated a positive correlation between the PG content and CA4+ partition at 20 h and 24 h imaging time points in both superficial cartilage and full-thickness cartilage. At early diffusion time points (30 min and 60 min), on the other hand, the correlations between PG content and CA4+ partition were negative and relatively weak. The linear correlations were similar for equilibrium and dynamic moduli, as indicated in Table 6.1. The correlations were positive in superficial and full cartilage layers at 20 h and 24 h imaging time points. At 30 min and 60 min imaging time points, the correlation was negative in superficial cartilage and full-thickness for equilibrium modulus and in the superficial layer for dynamic modulus. The negative correlations at early-diffusion time points are surprising since, in study III, the correlations were found positive. Literature has also previously reported positive correlations [23, 114]. The negative correlation in post-traumatic cartilage may originate from the reduced steric hindrance, which increases the uptake of CA4+ into the tissue. The diffusion is governed by the reduced steric hindrance on the onset of diffusion, but near diffusion equilibrium, the greater PG content dominates the CA4+ partitioning.

In summary, in study IV, the QDECT was studied for the first time in post-traumatic tissue around a lesion site and shown to enable quantification PG content at diffusion equilibrium. At 30 min and 60 min after contrast agent immersion, QDECT was able to differentiate post-traumatic tissue from healthy cartilage based on CA4+ partitioning within cartilage. However, in early diffusion time point, reliable evaluation of PG content was challenging.

7.5   LIMITATIONS

In all studies I–IV, the imaging was conducted using microCT scanners that involve longer scan times than clinical CT devices. In study I, the acquisition time was approximately 13 minutes, in studies II and III 2 minutes, and in study IV 3 minutes. The diffusion of contrast agents continues during the acquisitions, and thus, the obtained uptake is rather an average value over the acquisition time rather than a precise value at a certain time point. In studies II–IV, acquisitions with two energies were conducted consecutively. In consecutive imaging, minimizing the time between the acquisitions is important, since at the early-diffusion time, the diffusion rate of the contrast agent is at its highest, and the depth-wise partition is constantly changing. On the other hand, as the imaging set-ups were the same for each sample within the studies and as the samples were of similar thickness, we believe that even though the acquisition times were longer, they had no significant impact on the obtained results or conclusions.

The samples in studies I–IV went through a few freeze-thaw cycles that can alter the biomechanical properties of the cartilage tissue and diffusion kinematics of the contrast agents. Qu et al. concluded while studying the biochemical and biomechanical properties of the articular cartilage after a freeze-thaw cycle that only minor changes in the dynamic moduli could be observed while with other parameter no significant difference was seen [134]. Another limitation related to samples was a rel-

atively small sample population in each study. The number of sample in each study was selected based on previous papers on the topic [23, 109, 111, 116, 127, 130, 135]. Furthermore, as the sample groups were homogenous, the selected sample population is expected to suit the purpose of these proof-of-principle studies. In this light, we believe that these limitations had only minor effects on the results and thus allowed a reliable evaluation of the QDECT and triple contrast methods.

Before the clinical use, the safety of the contrast agents needs to be addressed. Gadoteridol has been in routine clinical use across a broad spectrum of indications. The rate of acute adverse reactions following exposure of gadoteridol at approved doses has been reported low (1.4% [136]) with reactions mostly limited to transient and self-resolving symptoms. With CA4+, the preliminary studies have reported that CA4+ can be used safely with articulating tissues [19,108]. The studies regarding the safety of BiNPs are still ongoing. The triple contrast technique requires the use of three contrast agents, but the applicable contrast agents are not limited to the contrast agent used in this thesis. CA4+ and gadoteridol can be changed to any positive and neutral contrast agents as long as their X-ray absorbing chemical elements are different. BiNPs can be replaced with any contrast agent that has a particle size large enough to ensure that it is unable to diffuse into cartilage tissue.

7.6 CLINICAL APPLICATION OF THE TRIPLE CONTRAST METHOD

To summarize, triple contrast-enhanced CT imaging quantitatively indicates PG and water contents in articular cartilage with simultaneous visualization of articulating surface. As a result, triple contrast-enhanced CT provides a clinically feasible technique for assessment of cartilage degeneration, and thus, may represents an important step in CECT diagnostics and monitoring of PTOA.

At present, CECT is a clinically available imaging technique. Nevertheless, despite its great potential in the detection of cartilage degeneration, the technique has been unable to reach wide use. Present CECT imaging of the knee includes two subsequent acquisitions using an anionic contrast agent [25]. The first arthrographic image is acquired immediately after the contrast agent administration, and a delayed image is acquired 30–60 minutes after the administration. The arthrographic image provides the possibility for accurate cartilage segmentation as the contrast agent has not yet completely blurred the contrast between the synovial fluid and cartilage. The delayed image is used for obtaining information on cartilage PG content based on anionic contrast agent diffusion. With triple contrast agent, only the delayed images with two energies are required to accomplish accurate segmentation of articulating cartilage but also to quantify the PG and water contents.

In the clinical triple contrast examination, the triple contrast agent would administered intra-articularly, and the patient is asked to move the joint to promote contrast agent distributing evenly within the joint capsule. Then, the delayed imaging would be performed after 30 min to 2 hours after contrast agent administration. In a living organism, active metabolism and perfusion results in contrast agent efflux from the joint. Thus, the optimal time for the delayed image should also be determined.

Emerging photon-counting CT technologies also provide interesting future prospects for triple contrast-enhanced CT imaging. A photon-counting CT device

employs a photon-counting detector (PCD) that enables the detection of both the photon and its energy.

In photon-counting imaging, the polychromatic spectrum can be divided into different energy bins, which allows the selection of optimal energy weighting. Triple contrast-enhanced imaging with PCD can be performed with one rotation, which simplifies the imaging protocol, reduces artefacts related to patient movement, and ensures imaging at the same contrast agent diffusion time point. Photon-counting CT provides the possibility for virtual monochromatic imaging in which CT images at different monochromatic X-ray beam energies could be synthesized from spectral-energy data [137]. Implementation of virtual monoenergetic imaging affords fewer beam-hardening, artefacts, lower image noise levels, lower radiation doses, and provides more quantitatively accurate attenuation measurements [138] – both traits that would improve the overall performance of the triple contrast method.

Before reaching clinical use, the triple contrast method requires further investigation. Measurements of the cadaveric human knee joint with a clinical CT device and biocompatibility studies of the BiNPs need to be conducted before clinical trials. Also, segmentation methods based on enhanced visualization of articulating surfaces due to BiNPs could be developed for optimal analysis of triple contrast-enhanced images. For instance, contrast agent partitioning within cartilage could be estimated from the CT images with advanced model fitting techniques developed for the analysis of cortical bone [139].

8 Summary and Conclusions

This thesis aimed to improve the CECT diagnostics in identifying the first signs of post-traumatic changes in articular cartilage. Accordingly, we developed BiNPs and introduced QDECT that finally led to the conception of a triple contrast method. To conclude, the findings of this thesis show that:

1. BiNPs, due to their size, are unable to diffuse into articular cartilage and are thus able to maintain a high contrast difference between the contrast agent bath and articular cartilage. High contrast at the articulating surface enables the visualization of lesions on the cartilage surface and accurate segmentation of cartilage tissue – both being previously challenging due to contrast agent diffusion-related loss of contrast at the articulating surface.

2. With two imaging energies selected based on element-specific absorption k-edge energies, the QDECT technique allows quantification of non-ionic, gadolinium-based and cationic, iodine-based contrast agents' partitioning within cartilage tissue at clinically feasible imaging time point. Based on the partitioning of the two contrast agents, subsequent evaluation of cartilage PG and water content is possible. Finally, normalization of the cationic contrast agent partition with that of the non-ionic contrast agent yields cationic contrast agent attenuation that has a significant correlation with the PG content of the tissue, thus enabling differentiation between intact and injured cartilage.

3. The triple contrast method combines the above-mentioned advantages of QDECT and the usage of BiNPs. The method excels in its capacity to be sensitive to PG depletion while simultaneously making possible the accurate segmentation of articulating surfaces and surface lesions.

4. At tissue surrounding the lesion, QDECT can identify post-traumatic changes at diffusion equilibrium based on quantification of PG and water contents. Further, at clinically feasible imaging time points (30 min and 60 min), QDECT can differentiate between post-traumatic and intact cartilage tissue.

5. Overall, the findings of this thesis may improve the diagnostics of different types of cartilage injuries, thus potentially providing clinicians more information on identifying more tailored treatment options and repair operations to prevent the onset and progression of PTOA.

BIBLIOGRAPHY

[1] D. D. Anderson, S. Chubinskaya, F. Guilak, J. A. Martin, T. R. Oegema, S. A. Olson, and J. A. Buckwalter, "Post-traumatic osteoarthritis: improved understanding and opportunities for early intervention," *Journal of Orthopaedic Research* **29**, 802–809 (2011).

[2] F. Guilak, A. Ratcliffe, N. Lane, M. P. Rosenwasser, and V. C. Mow, "Mechanical and biochemical changes in the superficial zone of articular cartilage in canine experimental osteoarthritis," *Journal of Orthopaedic Research* **12**, 474–484 (1994).

[3] J. Buckwalter and H. Mankin, "Articular cartilage: part ii," *Journal of bone and joint surgery* **79**, 612 (1997).

[4] X. Bi, X. Yang, M. P. Bostrom, and N. P. Camacho, "Fourier transform infrared imaging spectroscopy investigations in the pathogenesis and repair of cartilage," *Biochimica et Biophysica Acta (BBA)-Biomembranes* **1758**, 934–941 (2006).

[5] M. Heliövaara, P. Slätis, P. Paavolainen, et al., "Nivelrikon esiintyvyys ja kustannukset," *Duodecim* **124**, 1869–74 (2008).

[6] T. D. Brown, R. C. Johnston, C. L. Saltzman, J. L. Marsh, and J. A. Buckwalter, "Posttraumatic osteoarthritis: a first estimate of incidence, prevalence, and burden of disease," *Journal of Orthopaedic Trauma* **20**, 739–744 (2006).

[7] D. R. Dirschl, L. J. Marsh, J. A. Buckwalter, R. Gelberman, S. A. Olson, T. D. Brown, and A. Llinias, "Articular fractures," *Journal of the American Academy of Orthopaedic Surgeons* **12**, 416–423 (2004).

[8] S. A. Olson, B. D. Furman, V. B. Kraus, J. L. Huebner, and F. Guilak, "Therapeutic opportunities to prevent post-traumatic arthritis: lessons from the natural history of arthritis after articular fracture," *Journal of Orthopaedic Research* **33**, 1266–1277 (2015).

[9] X. Li, V. Pedoia, D. Kumar, J. Rivoire, C. Wyatt, D. Lansdown, K. Amano, N. Okazaki, D. Savic, M. F. Koff, et al., "Cartilage T1ρ and T2 relaxation times: longitudinal reproducibility and variations using different coils, MR systems and sites," *Osteoarthritis and cartilage* **23**, 2214–2223 (2015).

[10] T. M. Link, J. Neumann, and X. Li, "Prestructural cartilage assessment using MRI," *Journal of Magnetic Resonance Imaging* **45**, 949–965 (2017).

[11] B. A. Lakin, B. D. Snyder, and M. W. Grinstaff, "Assessing cartilage biomechanical properties: techniques for evaluating the functional performance of cartilage in health and disease," *Annual review of biomedical engineering* **19**, 27–55 (2017).

[12] J. Koivisto, T. Kiljunen, J. Wolff, and M. Kortesniemi, "Assessment of effective radiation dose of an extremity CBCT, MSCT and conventional X ray for knee area using MOSFET dosemeters," *Radiation protection dosimetry* **157**, 515–524 (2013).

[13] N. S. Joshi, P. N. Bansal, R. C. Stewart, B. D. Snyder, and M. W. Grinstaff, "Effect of contrast agent charge on visualization of articular cartilage using computed tomography: exploiting electrostatic interactions for improved sensitivity," *Journal of the American Chemical Society* **131**, 13234–13235 (2009).

[14] A. Kallioniemi, J. Jurvelin, M. Nieminen, M. Lammi, and J. Töyräs, "Contrast agent enhanced pQCT of articular cartilage," *Physics in Medicine & Biology* **52**, 1209 (2007).

[15] H. Lusic and M. W. Grinstaff, "X-ray-computed tomography contrast agents," *Chemical Reviews* **113**, 1641–1666 (2012).

[16] A. W. Palmer, R. E. Guldberg, and M. E. Levenston, "Analysis of cartilage matrix fixed charge density and three-dimensional morphology via contrast-enhanced microcomputed tomography," *Proceedings of the National Academy of Sciences* **103**, 19255–19260 (2006).

[17] T. Silvast, J. Jurvelin, M. Lammi, and J. Töyräs, "pQCT study on diffusion and equilibrium distribution of iodinated anionic contrast agent in human articular cartilage–associations to matrix composition and integrity," *Osteoarthritis and Cartilage* **17**, 26–32 (2009).

[18] T. S. Silvast, H. T. Kokkonen, J. S. Jurvelin, T. M. Quinn, M. T. Nieminen, and J. Töyräs, "Diffusion and near-equilibrium distribution of MRI and CT contrast agents in articular cartilage," *Physics in Medicine & Biology* **54**, 6823 (2009).

[19] R. C. Stewart, P. N. Bansal, V. Entezari, H. Lusic, R. M. Nazarian, B. D. Snyder, and M. W. Grinstaff, "Contrast-enhanced CT with a high-affinity cationic contrast agent for imaging ex vivo bovine, intact ex vivo rabbit, and in vivo rabbit cartilage," *Radiology* **266**, 141–150 (2013).

[20] J. A. Buckwalter, "Mechanical injuries of articular cartilage," *The Iowa Orthopaedic Journal* **12**, 50 (1992).

[21] P. M. Lin, C.-T. C. Chen, and P. A. Torzilli, "Increased stromelysin-1 (MMP-3), proteoglycan degradation (3B3-and 7D4) and collagen damage in cyclically load-injured articular cartilage," *Osteoarthritis and Cartilage* **12**, 485–496 (2004).

[22] P. Bansal, R. Stewart, V. Entezari, B. Snyder, and M. Grinstaff, "Contrast agent electrostatic attraction rather than repulsion to glycosaminoglycans affords a greater contrast uptake ratio and improved quantitative CT imaging in cartilage," *Osteoarthritis and cartilage* **19**, 970–976 (2011).

[23] B. Lakin, D. Grasso, S. Shah, R. Stewart, P. Bansal, J. Freedman, M. Grinstaff, and B. Snyder, "Cationic agent contrast-enhanced computed tomography imaging of cartilage correlates with the compressive modulus and coefficient of friction," *Osteoarthritis and cartilage* **21**, 60–68 (2013).

[24] H. T. Kokkonen, A. S. Aula, H. Kröger, J.-S. Suomalainen, E. Lammentausta, E. Mervaala, J. S. Jurvelin, and J. Töyräs, "Delayed computed tomography arthrography of human knee cartilage in vivo," *Cartilage* **3**, 334–341 (2012).

[25] K. A. Myller, M. J. Turunen, J. T. Honkanen, S. P. Väänänen, J. T. Iivarinen, J. Salo, J. S. Jurvelin, and J. Töyräs, "In vivo contrast-enhanced cone beam CT provides quantitative information on articular cartilage and subchondral bone," *Annals of biomedical engineering* **45**, 811–818 (2017).

[26] R. Stockwell, "The interrelationship of cell density and cartilage thickness in mammalian articular cartilage.," *Journal of Anatomy* **109**, 411 (1971).

[27] A. J. Sophia Fox, A. Bedi, and S. A. Rodeo, "The basic science of articular cartilage: structure, composition, and function," *Sports health* **1**, 461–468 (2009).

[28] V. C. Mow, A. Ratcliffe, and A. R. Poole, "Cartilage and diarthrodial joints as paradigms for hierarchical materials and structures," *Biomaterials* **13**, 67–97 (1992).

[29] J. Buckwalter and H. Mankin, "Articular cartilage: tissue design and chondrocyte-matrix interactions.," *Instructional Course Lectures* **47**, 477–486 (1997).

[30] J. Buckwalter and H. Mankin, "Articular Cartilage: Part I Tissue Design and Chondrocyte-Matrix Interactions," *JBJS* **79**, 600–611 (1997).

[31] V. C. Mow and R. Huiskes, *Basic orthopaedic biomechanics & mechano-biology* (Lippincott Williams & Wilkins, 2005).

[32] V. C. Mow, "Structure and function of articular cartilage and meniscus," *Basic orthopaedic biomechanics* 31–58 (1997).

[33] M. Huber, S. Trattnig, and F. Lintner, "Anatomy, biochemistry, and physiology of articular cartilage," *Investigative Radiology* **35**, 573–580 (2000).

[34] M. Venn and A. Maroudas, "Chemical composition and swelling of normal and osteoarthrotic femoral head cartilage. I. Chemical composition.," *Annals of the Rheumatic Diseases* **36**, 121–129 (1977).

[35] J. A. Buckwalter, "Articular cartilage: injuries and potential for healing," *Journal of Orthopaedic & Sports Physical Therapy* **28**, 192–202 (1998).

[36] I. L. JONES, S.-E. LARSSON, and R. LEMPERG, "The glycosaminoglycans of human articular cartilage: concentration and distribution in different layers in the adult individual.," *Clinical Orthopaedics and Related Research* **127**, 257–264 (1977).

[37] A. Maroudas, "Physicochemical properties of cartilage in the light of ion exchange theory," *Biophysical Journal* **8**, 575 (1968).

[38] V. C. Mow, C. C. Wang, and C. T. Hung, "The extracellular matrix, interstitial fluid and ions as a mechanical signal transducer in articular cartilage," *Osteoarthritis and Cartilage* **7**, 41–58 (1999).

[39] R. Stockwell, "The cell density of human articular and costal cartilage.," *Journal of anatomy* **101**, 753 (1967).

[40] H. Muir, "The chondrocyte, architect of cartilage. Biomechanics, structure, function and molecular biology of cartilage matrix macromolecules," *Bioessays* **17**, 1039–1048 (1995).

[41] A. J. S. Fox, A. Bedi, and S. A. Rodeo, "The basic science of articular cartilage: structure, composition, and function," *Sports Health: A Multidisciplinary Approach* **1**, 461–468 (2009).

[42] Y. Xia, J. Moody, H. Alhadlaq, N. Burton-Wurster, and G. Lust, "Characteristics of topographical heterogeneity of articular cartilage over the joint surface of a humeral head," *Osteoarthritis and Cartilage* **10**, 370–380 (2002).

[43] M. Mozafari, J. Rajadas, and D. Kaplan, *Nanoengineered biomaterials for regenerative medicine* (Elsevier, 2018).

[44] R. Bank, M. Bayliss, F. Lafeber, A. Maroudas, and J. Tekoppele, "Ageing and zonal variation in post-translational modification of collagen in normal human articular cartilage," *Biochemical Journal* **330**, 345–351 (1998).

[45] D. Eyre, "Collagen of articular cartilage," *Arthritis Research* **4**, 30–35 (2002).

[46] W. Hayes and L. Mockros, "Viscoelastic properties of human articular cartilage.," *Journal of applied physiology* **31**, 562–568 (1971).

[47] V. Mow, "Fundamentals of articular cartilage and meniscus biomechanics," *Articular cartilage and knee joint function* 1–18 (1990).

[48] V. Mow, G. Ateshian, and A. Ratcliffe, "Anatomic form and biomechanical properties of articular cartilage of the knee joint," in *Biology and Biomechanics of the Traumatized Synovial Joint: the Knee as a Model, edited by Finerman GAM and Noyes FR. AAOS Symposium, Rosemont, IL* (1992).

[49] V. Mow and M. Rosenwasser, "Articular cartilage: biomechanics," *Injury and repair of the musculoskeletal soft tissues* **1**, 427–463 (1988).

[50] V. C. Mow, M. H. Holmes, and W. M. Lai, "Fluid transport and mechanical properties of articular cartilage: a review," *Journal of biomechanics* **17**, 377–394 (1984).

[51] M. Laasanen, J. Töyräs, R. Korhonen, J. Rieppo, S. Saarakkala, M. Nieminen, J. Hirvonen, and J. Jurvelin, "Biomechanical properties of knee articular cartilage," *Biorheology* **40**, 133–140 (2003).

[52] J. J. Irrgang, L. Snyder-Mackler, R. S. Wainner, F. H. Fu, and C. D. HARNER, "Development of a patient-reported measure of function of the knee," *JBJS* **80**, 1132–45 (1998).

[53] G. Jay, J. Torres, M. Warman, M. Laderer, and K. Breuer, "The role of lubricin in the mechanical behavior of synovial fluid," *Proceedings of the National Academy of Sciences* **104**, 6194–6199 (2007).

[54] G. A. Ateshian, "The role of interstitial fluid pressurization in articular cartilage lubrication," *Journal of Biomechanics* **42**, 1163–1176 (2009).

[55] W. W. Curl, J. Krome, E. S. Gordon, J. Rushing, B. P. Smith, and G. G. Poehling, "Cartilage injuries: a review of 31,516 knee arthroscopies," *Arthroscopy: The Journal of Arthroscopic & Related Surgery* **13**, 456–460 (1997).

[56] T. Wei, N. Kulkarni, Q. Zeng, L. Helvering, X. Lin, F. Lawrence, L. Hale, M. Chambers, C. Lin, A. Harvey, et al., "Analysis of early changes in the articular cartilage transcriptisome in the rat meniscal tear model of osteoarthritis: pathway comparisons with the rat anterior cruciate transection model and with human osteoarthritic cartilage," *Osteoarthritis and Cartilage* **18**, 992–1000 (2010).

[57] J. Borrelli Jr, Y. Zhu, M. Burns, L. Sandell, and M. J. Silva, "Cartilage tolerates single impact loads of as much as half the joint fracture threshold.," *Clinical Orthopaedics and Related Research* **426**, 266–273 (2004).

[58] T. Silvast, J. Jurvelin, A. Aula, M. Lammi, and J. Töyräs, "Contrast agent-enhanced computed tomography of articular cartilage: association with tissue composition and properties," *Acta Radiologica* **50**, 78–85 (2009).

[59] J. A. Buckwalter and T. D. Brown, "Joint injury, repair, and remodeling: roles in post-traumatic osteoarthritis," *Clinical Orthopaedics and Related Research®* **423**, 7–16 (2004).

[60] H. A. Wieland, M. Michaelis, B. J. Kirschbaum, and K. A. Rudolphi, "Osteoarthritis – an untreatable disease?," *Nature Reviews Drug discovery* **4**, 331–344 (2005).

[61] A. Thambyah, "A hypothesis matrix for studying biomechanical factors associated with the initiation and progression of posttraumatic osteoarthritis," *Medical Hypotheses* **64**, 1157–1161 (2005).

[62] J. A. Buckwalter and D. T. Felson, "Post-traumatic arthritis: definitions and burden of disease," in *Post-Traumatic Arthritis* (Springer, 2015), pp. 7–15.

[63] D. D. Anderson, C. Van Hofwegen, J. L. Marsh, and T. D. Brown, "Is elevated contact stress predictive of post-traumatic osteoarthritis for imprecisely reduced tibial plafond fractures?," *Journal of Orthopaedic Research* **29**, 33–39 (2011).

[64] J. L. Marsh, T. McKinley, D. Dirschl, A. Pick, G. Haft, D. D. Anderson, and T. Brown, "The sequential recovery of health status after tibial plafond fractures," *Journal of orthopaedic trauma* **24**, 499 (2010).

[65] J. Borrelli Jr, P. A. Torzilli, R. Grigiene, and D. L. Helfet, "Effect of impact load on articular cartilage: development of an intra-articular fracture model," *Journal of orthopaedic trauma* **11**, 319–326 (1997).

[66] D. D. D'lima, S. Hashimoto, P. C. Chen, M. K. Lotz, and C. W. Colwell Jr, "Prevention of chondrocyte apoptosis," *JBJS* **83**, 25–26 (2001).

[67] J. A. Martin, D. McCabe, M. Walter, J. A. Buckwalter, and T. O. McKinley, "N-acetylcysteine inhibits post-impact chondrocyte death in osteochondral explants," *The Journal of Bone and Joint Surgery. American volume.* **91**, 1890 (2009).

[68] E. L. Cain and W. G. Clancy, "Treatment algorithm for osteochondral injuries of the knee," *Clinics in Sports Medicine* **20**, 321–342 (2001).

[69] G. Spahn, H. M. Klinger, and G. O. Hofmann, "How valid is the arthroscopic diagnosis of cartilage lesions? Results of an opinion survey among highly experienced arthroscopic surgeons," *Archives of orthopaedic and trauma surgery* **129**, 1117–1121 (2009).

[70] M. Prakash, A. Joukainen, J. K. Sarin, L. Rieppo, I. O. Afara, and J. Töyräs, "Near-infrared spectroscopy based arthroscopic evaluation of human knee joint cartilage, through automated selection of an anatomically specific regression model," in *Optical Tomography and Spectroscopy* (Optical Society of America, 2018), pp. OF4D–3.

[71] P. Puhakka, J. Ylärinne, M. Lammi, S. Saarakkala, V. Tiitu, H. Kröger, T. Virén, J. Jurvelin, and J. Töyräs, "Dependence of light attenuation and backscattering on collagen concentration and chondrocyte density in agarose scaffolds," *Physics in Medicine & Biology* **59**, 6537 (2014).

[72] E. Kaleva, T. Virén, S. Saarakkala, J. Sahlman, J. Sirola, J. Puhakka, T. Paatela, H. Kröger, I. Kiviranta, J. S. Jurvelin, et al., "Arthroscopic ultrasound assessment of articular cartilage in the human knee joint: A potential diagnostic method," *Cartilage* **2**, 246–253 (2011).

[73] D. Burstein and M. Gray, "New MRI techniques for imaging cartilage," *JBJS* **85**, 70–77 (2003).

[74] M. L. Gray, D. Burstein, and Y. Xia, "Biochemical (and functional) imaging of articular cartilage," in *Seminars in musculoskeletal radiology*, Vol. 5 (Copyright© 2001 by Thieme Medical Publishers, Inc., 333 Seventh Avenue, New . . . , 2001), pp. 329–344.

[75] M. L. Gray, D. Burstein, Y.-J. Kim, and A. Maroudas, "Magnetic resonance imaging of cartilage glycosaminoglycan: basic principles, imaging technique, and clinical applications," *Journal of Orthopaedic Research* **26**, 281–291 (2008).

[76] J. Rautiainen, M. J. Nissi, E.-N. Salo, V. Tiitu, M. A. Finnilä, O.-M. Aho, S. Saarakkala, P. Lehenkari, J. Ellermann, and M. T. Nieminen, "Multiparametric MRI assessment of human articular cartilage degeneration: correlation with quantitative histology and mechanical properties," *Magnetic resonance in medicine* **74**, 249–259 (2015).

[77] J.-A. Choi and G. E. Gold, "MR imaging of articular cartilage physiology," *Magnetic Resonance Imaging Clinics* **19**, 249–282 (2011).

[78] D. Burstein, J. Velyvis, K. T. Scott, K. W. Stock, Y.-J. Kim, D. Jaramillo, R. D. Boutin, and M. L. Gray, "Protocol issues for delayed Gd (DTPA) 2—enhanced MRI (dGEMRIC) for clinical evaluation of articular cartilage," *Magnetic Resonance in Medicine: An Official Journal of the International Society for Magnetic Resonance in Medicine* **45**, 36–41 (2001).

[79] D. R. Dirschl and G. L. Adams, "A critical assessment of factors influencing reliability in the classification of fractures, using fractures of the tibial plafond as a model," *Journal of orthopaedic trauma* **11**, 471–476 (1997).

[80] P. I. Sallay, R. A. Pedowitz, W. J. Mallon, R. M. Vandemark, J. D. Dalton, and K. P. Speer, "Reliability and reproducibility of radiographic interpretation of proximal humeral fracture pathoanatomy," *Journal of shoulder and elbow surgery* **6**, 60–69 (1997).

[81] J. Doornberg, A. Lindenhovius, P. Kloen, C. N. Van Dijk, D. Zurakowski, and D. Ring, "Two and three-dimensional computed tomography for the classification and management of distal humeral fractures: evaluation of reliability and diagnostic accuracy," *JBJS* **88**, 1795–1801 (2006).

[82] T. E. Trumble, R. Culp, D. Hanel, W. Geissler, and R. Berger, "Intra-articular fractures of the distal aspect of the radius.," *Instructional course lectures* **48**, 465–480 (1999).

[83] T. E. McAlindon, R. Bannuru, M. Sullivan, N. Arden, F. Berenbaum, S. Bierma-Zeinstra, G. Hawker, Y. Henrotin, D. Hunter, H. Kawaguchi, et al., "OARSI guidelines for the non-surgical management of knee osteoarthritis," *Osteoarthritis and cartilage* **22**, 363–388 (2014).

[84] K. Pridie, "A method of resurfacing osteoarthritic knee joints," *The Journal of Bone & Joint Surgery. British Volume* **41**, 618–619 (1959).

[85] M. Brittberg, A. Lindahl, A. Nilsson, C. Ohlsson, O. Isaksson, and L. Peterson, "Treatment of deep cartilage defects in the knee with autologous chondrocyte transplantation," *New England Journal of Medicine* **331**, 889–895 (1994).

[86] L. Hangody and P. Füles, "Autologous osteochondral mosaicplasty for the treatment of full-thickness defects of weight-bearing joints," *J Bone Joint Surg Am* **85**, 25–32 (2003).

[87] G. L. Zeng, *Medical image reconstruction: a conceptual tutorial.* (Springer, 2010).

[88] J.-B. Thibault, K. D. Sauer, C. A. Bouman, and J. Hsieh, "A three-dimensional statistical approach to improved image quality for multislice helical CT," *Medical physics* **34**, 4526–4544 (2007).

[89] F. Mueck, M. Körner, M. Scherr, L. Geyer, Z. Deak, U. Linsenmaier, M. Reiser, and S. Wirth, "Upgrade to iterative image reconstruction (IR) in abdominal MDCT imaging: a clinical study for detailed parameter optimization beyond vendor recommendations using the adaptive statistical iterative reconstruction environment (ASIR)," in *RöFo-Fortschritte auf dem Gebiet der Röntgenstrahlen und der bildgebenden Verfahren*, Vol. 184 (© Georg Thieme Verlag KG, 2012), pp. 229–238.

[90] J. Leipsic, T. M. Labounty, B. Heilbron, J. K. Min, G. J. Mancini, F. Y. Lin, C. Taylor, A. Dunning, and J. P. Earls, "Adaptive statistical iterative reconstruction: assessment of image noise and image quality in coronary CT angiography," *American Journal of Roentgenology* **195**, 649–654 (2010).

[91] B. L. McClennan, "Preston M. Hickey memorial lecture. Ionic and nonionic iodinated contrast media: evolution and strategies for use.," *AJR. American Journal of Roentgenology* **155**, 225–233 (1990).

[92] J. Singh and A. Daftary, "Iodinated contrast media and their adverse reactions," *Journal of Nuclear Medicine Technology* **36**, 69–74 (2008).

[93] K. J. Murphy, J. A. Brunberg, and R. H. Cohan, "Adverse reactions to gadolinium contrast media: a review of 36 cases.," *AJR. American journal of roentgenology* **167**, 847–849 (1996).

[94] L. E. Cole, R. D. Ross, J. M. Tilley, T. Vargo-Gogola, and R. K. Roeder, "Gold nanoparticles as contrast agents in x-ray imaging and computed tomography," *Nanomedicine* **10**, 321–341 (2015).

[95] H. Pietsch, "CT contrast agents," in *Small Animal Imaging* (Springer, 2011), pp. 141–149.

[96] G. G. Briand and N. Burford, "Bismuth compounds and preparations with biological or medicinal relevance," *Chemical Reviews* **99**, 2601–2658 (1999).

[97] P. Nelson, *Biological physics* (WH Freeman New York, 2003).

[98] E. L. Cussler, *Diffusion: mass transfer in fluid systems* (Cambridge University Press, 2009).

[99] F. G. Donnan, "The theory of membrane equilibria.," *Chemical Reviews* **1**, 73–90 (1924).

[100] A. Bashir, M. L. Gray, and D. Burstein, "Gd-DTPA2- as a measure of cartilage degradation," *Magnetic Resonance in Medicine* **36**, 665–673 (1996).

[101] K. Kulmala, R. Korhonen, P. Julkunen, J. Jurvelin, T. Quinn, H. Kröger, and J. Töyräs, "Diffusion coefficients of articular cartilage for different CT and MRI contrast agents," *Medical engineering & physics* **32**, 878–882 (2010).

[102] E.-N. Salo, M. Nissi, K. Kulmala, V. Tiitu, J. Töyräs, and M. Nieminen, "Diffusion of Gd-DTPA 2- into articular cartilage," *Osteoarthritis and Cartilage* **20**, 117–126 (2012).

[103] P. A. Torzilli, J. M. Arduino, J. D. Gregory, and M. Bansal, "Effect of proteoglycan removal on solute mobility in articular cartilage," *Journal of Biomechanics* **30**, 895–902 (1997).

[104] E. Nimer, R. Schneiderman, and A. Maroudas, "Diffusion and partition of solutes in cartilage under static load," *Biophysical Chemistry* **106**, 125–146 (2003).

[105] C. J. Skipp and H. V. Tyrrell, "Diffusion in viscous solvents. Part 2.—Planar and spherical molecules in propane-1, 2-diol at 15, 25 and 35° C," *Journal of the Chemical Society, Faraday Transactions 1: Physical Chemistry in Condensed Phases* **71**, 1744–1753 (1975).

[106] H. J. Tyrrell and P. J. Watkiss, "Diffusion in viscous solvents. Part 3.—Inter-diffusion coefficients for planar and spherical solutes in 2-methylpentane 2, 4-diol, and their relationship to diffusion coefficients derived from luminescence measurements," *Journal of the Chemical Society, Faraday Transactions 1: Physical Chemistry in Condensed Phases* **75**, 1417–1432 (1979).

[107] T. Chan, H. Li, and K. Li, "Effects of shapes of solute molecules on diffusion: A study of dependences on solute size, solvent, and temperature," *The Journal of Physical Chemistry B* **119**, 15718–15728 (2015).

[108] R. C. Stewart, A. N. Patwa, H. Lusic, J. D. Freedman, M. Wathier, B. D. Snyder, A. Guermazi, and M. W. Grinstaff, "Synthesis and preclinical characterization of a cationic iodinated imaging contrast agent (CA4+) and its use for quantitative computed tomography of ex vivo human hip cartilage," *Journal of medicinal chemistry* **60**, 5543–5555 (2017).

[109] P. Bansal, N. S. Joshi, V. Entezari, M. Grinstaff, and B. D. Snyder, "Contrast enhanced computed tomography can predict the glycosaminoglycan content and biomechanical properties of articular cartilage," *Osteoarthritis and cartilage* **18**, 184–191 (2010).

[110] R. C. Evans and T. M. Quinn, "Solute diffusivity correlates with mechanical properties and matrix density of compressed articular cartilage," *Archives of biochemistry and biophysics* **442**, 1–10 (2005).

[111] H. Kokkonen, J. Mäkelä, K. Kulmala, L. Rieppo, J. Jurvelin, V. Tiitu, H. Karjalainen, R. Korhonen, V. Kovanen, and J. Töyräs, "Computed tomography detects changes in contrast agent diffusion after collagen cross-linking typical to natural aging of articular cartilage," *Osteoarthritis and cartilage* **19**, 1190–1198 (2011).

[112] K. Kulmala, H. Karjalainen, H. Kokkonen, V. Tiitu, V. Kovanen, M. Lammi, J. Jurvelin, R. Korhonen, and J. Töyräs, "Diffusion of ionic and non-ionic contrast agents in articular cartilage with increased cross-linking—contribution of steric and electrostatic effects," *Medical engineering & physics* **35**, 1415–1420 (2013).

[113] H. T. Kokkonen, J.-S. Suomalainen, A. Joukainen, H. Kröger, J. Sirola, J. S. Jurvelin, J. Salo, and J. Töyräs, "In vivo diagnostics of human knee cartilage lesions using delayed CBCT arthrography," *Journal of orthopaedic research* **32**, 403–412 (2014).

[114] A. Bhattarai, J. T. Honkanen, K. A. Myller, M. Prakash, M. Korhonen, A. E. Saukko, T. Virén, A. Joukainen, A. N. Patwa, H. Kröger, et al., "Quantitative Dual Contrast CT Technique for Evaluation of Articular Cartilage Properties," *Annals of biomedical engineering* **46**, 1038–1046 (2018).

[115] I. Danad, Z. A. Fayad, M. J. Willemink, and J. K. Min, "New applications of cardiac computed tomography: dual-energy, spectral, and molecular CT imaging," *JACC: Cardiovascular Imaging* **8**, 710–723 (2015).

[116] H. R. Moody, C. P. Brown, J. Bowden, R. W. Crawford, D. McElwain, and A. Oloyede, "In vitro degradation of articular cartilage: does trypsin treatment produce consistent results?," *Journal of anatomy* **209**, 259–267 (2006).

[117] J. Buckwalter and H. Mankin, "Articular cartilage repair and transplantation," *Arthritis & Rheumatism: Official Journal of the American College of Rheumatology* **41**, 1331–1342 (1998).

[118] I. Mancini, F. Bragance, H. Brommer, J. Visser, J. Malda, and P. van Weeren, "Objective gait analysis as a tool to improve longitudinal monitoring of long-term large animal studies into cartilage repair," in *13th World Congress of ICRS, Sorrento, Italy* (2016).

[119] J. Visser, F. P. Melchels, J. E. Jeon, E. M. Van Bussel, L. S. Kimpton, H. M. Byrne, W. J. Dhert, P. D. Dalton, D. W. Hutmacher, and J. Malda, "Reinforcement of hydrogels using three-dimensionally printed microfibres," *Nature communications* **6**, 1–10 (2015).

[120] G. Lovric, R. Mokso, C. M. Schlepütz, and M. Stampanoni, "A multi-purpose imaging endstation for high-resolution micrometer-scaled sub-second tomography," *Physica Medica* **32**, 1771–1778 (2016).

[121] F. Marone and M. Stampanoni, "Regridding reconstruction algorithm for real-time tomographic imaging," *Journal of synchrotron radiation* **19**, 1029–1037 (2012).

[122] W. Hayes, L. M. Keer, G. Herrmann, and L. Mockros, "A mathematical analysis for indentation tests of articular cartilage," *Journal of biomechanics* **5**, 541–551 (1972).

[123] L. Xie, A. S. Lin, R. E. Guldberg, and M. E. Levenston, "Nondestructive assessment of sGAG content and distribution in normal and degraded rat articular cartilage via EPIC-μCT," *Osteoarthritis and Cartilage* **18**, 65–72 (2010).

[124] I. Haugen, B. Slatkowsky-Christensen, P. Bøyesen, D. van der Heijde, and T. Kvien, "Cross-sectional and longitudinal associations between radiographic features and measures of pain and physical function in hand osteoarthritis," *Osteoarthritis and Cartilage* **21**, 1191–1198 (2013).

[125] K. A. Kulmala, H. Pulkkinen, L. Rieppo, V. Tiitu, I. Kiviranta, A. Brünott, H. Brommer, R. van Weeren, P. Brama, M. Mikkola, et al., "Contrast-enhanced micro–computed tomography in evaluation of spontaneous repair of equine cartilage," *Cartilage* **3**, 235–244 (2012).

[126] B. Ewers, V. Jayaraman, R. Banglmaier, and R. C. Haut, "Rate of blunt impact loading affects changes in retropatellar cartilage and underlying bone in the rabbit patella," *Journal of biomechanics* **35**, 747–755 (2002).

[127] H. Kokkonen, J. Jurvelin, V. Tiitu, and J. Töyräs, "Detection of mechanical injury of articular cartilage using contrast enhanced computed tomography," *Osteoarthritis and cartilage* **19**, 295–301 (2011).

[128] T. Piscaer, J. Waarsing, N. Kops, P. Pavljasevic, J. Verhaar, G. Van Osch, and H. Weinans, "In vivo imaging of cartilage degeneration using μCT-arthrography," *Osteoarthritis and cartilage* **16**, 1011–1017 (2008).

[129] B. A. Lakin, D. J. Grasso, R. C. Stewart, J. D. Freedman, B. D. Snyder, and M. W. Grinstaff, "Contrast enhanced CT attenuation correlates with the GAG content of bovine meniscus," *Journal of orthopaedic research* **31**, 1765–1771 (2013).

[130] J. T. Honkanen, M. J. Turunen, J. D. Freedman, S. Saarakkala, M. W. Grinstaff, J. H. Ylärinne, J. S. Jurvelin, and J. Töyräs, "Cationic contrast agent diffusion differs between cartilage and meniscus," *Annals of biomedical engineering* **44**, 2913–2921 (2016).

[131] S. S. Karhula, M. A. Finnilä, J. D. Freedman, S. Kauppinen, M. Valkealahti, P. Lehenkari, K. P. Pritzker, H. J. Nieminen, B. D. Snyder, M. W. Grinstaff, et al., "Micro-scale distribution of CA4+ in ex vivo human articular cartilage detected with contrast-enhanced micro-computed tomography imaging," *Frontiers in Physics* **5**, 38 (2017).

[132] J. Rieppo, J. Töyräs, M. T. Nieminen, V. Kovanen, M. M. Hyttinen, R. K. Korhonen, J. S. Jurvelin, and H. J. Helminen, "Structure-function relationships in enzymatically modified articular cartilage," *Cells Tissues Organs* **175**, 121–132 (2003).

[133] F. C. Linn and L. Sokoloff, "Movement and composition of interstitial fluid of cartilage," *Arthritis & Rheumatism: Official Journal of the American College of Rheumatology* **8**, 481–494 (1965).

[134] C. Qu, M. Hirviniemi, V. Tiitu, J. S. Jurvelin, J. Töyräs, and M. J. Lammi, "Effects of freeze–thaw cycle with and without proteolysis inhibitors and cryopreservant on the biochemical and biomechanical properties of articular cartilage," *Cartilage* **5**, 97–106 (2014).

[135] J. Honkanen, M. Turunen, V. Tiitu, J. Jurvelin, and J. Töyräs, "Transport of iodine is different in cartilage and meniscus," *Annals of biomedical engineering* **44**, 2114–2122 (2016).

[136] "ProHance FDA product Description," `https://www.accessdata.fda.gov/drugsatfda_docs/label/2017/020131s027lbl.pdf` (2017), Accessed: 2020-09-13.

[137] L. Yu, S. Leng, and C. H. McCollough, "Dual-energy CT–based monochromatic imaging," *American journal of Roentgenology* **199**, S9–S15 (2012).

[138] M. J. Willemink, M. Persson, A. Pourmorteza, N. J. Pelc, and D. Fleischmann, "Photon-counting CT: technical principles and clinical prospects," *Radiology* **289**, 293–312 (2018).

[139] R. A. Pearson, *Automated modelling of cortical bone from clinical CT*, PhD thesis (University of Cambridge, 2017).

Paper **I**

Saukko, A. E., Honkanen, J. T., Xu, W., Väänänen, S. P.,
Jurvelin, J. S., Lehto, V. P., & Töyräs, J.
"Dual contrast CT method enables diagnostics of cartilage
injuries and degeneration using a single CT image"

Dual Contrast CT Method Enables Diagnostics of Cartilage Injuries and Degeneration Using a Single CT Image

Annina E. A. Saukko [ORCID],[1,2] Juuso T. J. Honkanen,[1,2] Wujun Xu,[1] Sami P. Väänänen [ORCID],[1,3] Jukka S. Jurvelin,[1] Vesa-Pekka Lehto [ORCID],[1] and Juha Töyräs [ORCID],[1,2]

[1]Department of Applied Physics, University of Eastern Finland, POB 1627, 70211 Kuopio, Finland; [2]Diagnostic Imaging Center, Kuopio University Hospital, POB 100, 70029 Kuopio, Finland; and [3]Department of Orthopaedics, Traumatology and Hand Surgery, Kuopio University Hospital, POB 100, 70029 Kuopio, Finland

Associate Editor Sean S. Kohles oversaw the review of this article.

Abstract—Cartilage injuries may be detected using contrast-enhanced computed tomography (CECT) by observing variations in distribution of anionic contrast agent within cartilage. Currently, clinical CECT enables detection of injuries and related post-traumatic degeneration based on two subsequent CT scans. The first scan allows segmentation of articular surfaces and lesions while the latter scan allows evaluation of tissue properties. Segmentation of articular surfaces from the latter scan is difficult since the contrast agent diffusion diminishes the image contrast at surfaces. We hypothesize that this can be overcome by mixing anionic contrast agent (ioxaglate) with bismuth oxide nanoparticles (BINPs) too large to diffuse into cartilage, inducing a high contrast at the surfaces. Here, a dual contrast method employing this mixture is evaluated by determining the depth-wise X-ray attenuation profiles in intact, enzymatically degraded, and mechanically injured osteochondral samples ($n = 3 \times 10$) using a microCT immediately and at 45 min after immersion in contrast agent. BiNPs were unable to diffuse into cartilage, producing high contrast at articular surfaces. Ioxaglate enabled the detection of enzymatic and mechanical degeneration. In conclusion, the dual contrast method allowed detection of injuries and degeneration simultaneously with accurate cartilage segmentation using a single scan conducted at 45 min after contrast agent administration.

Keywords—Computed tomography, Double contrast agent, Bismuth oxide nanoparticles.

Address correspondence to Annina E. A. Saukko, Department of Applied Physics, University of Eastern Finland, POB 1627, 70211 Kuopio, Finland. Electronic mails: annina.saukko@uef.fi, juuso.honkanen@uef.fi, wujun.xu@uef.fi, sami.vaananen@uef.fi, jukka.jurvelin@uef.fi, vplehto@uef.fi, juha.toyras@uef.fi

INTRODUCTION

Acute articular cartilage damage, resulting from a sudden accidental impact, e.g., a fall or sports accident, is a relatively common injury; twelve knee injuries per one thousand inhabitants occur annually in Europe causing significant healthcare burden.[26] Cartilage damage can cause joint pain, swelling, limited mobility, and ultimately initiate development of post-traumatic osteoarthritis (PTOA).[5] PTOA is a joint disease characterized by gradual erosion of cartilage covering the ends of articulating joints. Early diagnostics of cartilage injury is important for successful prevention of PTOA by means of surgical and pharmaceutical interventions.[1,23] Current diagnostic techniques, including magnetic resonance imaging (MRI), clinical examination, X-ray imaging without contrast agent, and arthroscopic examination, lack the sensitivity to detect acute cartilage injuries and early PTOA changes in the surrounding tissue. They can only detect more advanced tissue changes that are known to be irreversible.[4] For these reasons, diagnostic methods should be improved to detect initial cartilage changes to enable the early treatment for prevention of PTOA.

Contrast-enhanced computed tomography (CECT) is an imaging technique utilizing contrast agents to detect articular cartilage degeneration and injuries.[17,32,36] Recently, clinical CECT imaging of a knee joint has been introduced.[14,17,22] Increased water content, superficial collagen disruption and proteoglycan (PG) loss are the first signs of cartilage degeneration.[6,18] These changes increase tissue permeability and thus also the diffusion of contrast agents into cartilage at the injury site.[29] In addition to detection of tissue injury, contrast agents can enhance visualization

of articular cartilage, as the natural image contrast at this interface is almost non-existent due to similar X-ray attenuation in the synovial fluid and cartilage.

Recently, CECT was successfully applied for *in vivo* imaging of human articular cartilage.[14,17] Current CECT technique is based on two subsequent CT scans of the joint. The first scan (arthrography) is conducted immediately and the latter scan (delayed arthrography) 45 min after the contrast agent administration. The arthrographic image is required for accurate segmentation of articulating tissues and sensitive detection of cartilage lesions. The delayed arthrography image is used to evaluate the internal tissue degeneration at the lesion site and the surrounding tissue by observing alterations in the distribution of anionic contrast agent within cartilage. However, accurate segmentation of the cartilage tissue from the delayed arthrographic image is difficult as diffusion of anionic contrast agent induces loss of image contrast at the cartilage-synovial fluid interface. The optimal time point for delayed arthrographic imaging is at 45 min since the maximum concentration of contrast agent in human knee cartilage is empirically determined to be at 30–60 min post administration.[14] In a living human knee, diffusion equilibrium is impossible to achieve without multiple intra-articular injections due to excretion of the contrast agent. Nevertheless, previous studies have shown that the cartilage injuries can be detected already before the diffusion equilibrium is reached, i.e., before the contrast agents have had the time to diffuse through the full thickness of the tissue.[14,16,27,29] CECT of the knee joint has been preliminarily found to be suitable for clinical application,[22] but it is not yet in wide clinical use.

Utilization of nanoparticles (NPs) as X-ray contrast agents have raised interest during the last decade.[7,24] NPs have several advantages over the most commonly used iodinated contrast agents. The main advantage of NPs includes the possibility to modify their composition, shape, size, and NPs surface to improve their functionality. Therefore, their size can be adjusted such that they do not penetrate into porous material. Attaching bioconjugates to NPs owing a large surface area, is a second advantage since then their targeting properties can be enhanced, thus enabling improved delivery of heavy atoms to the targeted region.[10,24] Also, nanometer-sized, metal-based contrast agents with high atomic numbers produce stronger photoelectric X-ray attenuation compared with iodinated contrast agents with usually significantly smaller molecular sizes and lower atomic numbers. Further, well-stabilized NPs enable long blood circulation times when administered into living organisms.[19] In this respect, NPs are expected to have high potential in the future.

In this laboratory study, we present a new dual contrast CT method to improve the early diagnostics of articular cartilage injuries and detection of tissue changes related to the initiation of PTOA. This method employs a dual contrast agent which is a mixture of an iodinated contrast agent (ioxaglate) and a bismuth(III) oxide NP (Bi_2O_3-NP, later abbreviated as BiNP) suspension. In the dual contrast method, ioxaglate allows the assessment of the tissue quality as anionic ioxaglate distributes inversely to cartilage fixed charge density induced by negatively charged PGs.[12,30]

We hypothesize that BiNPs in the mixture ensure, without interfering in the diffusion of ioxaglate, a high contrast at articular surface even at 45 min after the contrast agent administration as BiNPs are unable to diffuse into cartilage due to their physical size. Thus, we suggest that introduction of BiNPs into contrast agent mixture improves the detection of articular cartilage surfaces. Distribution of ioxaglate reveals degeneration of the tissue at the delayed arthrographic image leaving the arthrography image unnecessary. This would make the clinical application logistically more feasible, halve the patient radiation dose, and eliminate the need for often laborious co-registration of the image stacks.

The aim of this study is to evaluate the potential of the dual contrast method in detection of different types of articular cartilage injuries in laboratory settings. Most importantly, we examined the ability of the dual contrast method to enable segmentation of cartilage surface and lesions from the delayed arthrographic image. To this end, intact, mechanically injured and enzymatically degraded bovine cartilage samples were imaged utilizing a microCT scanner. Moreover, X-ray attenuation along the cartilage depth was determined. Additionally, the PG distribution in cartilage was measured using digital densitometry (DD) of Safranin-O stained sections and compared with the microCT measurements.

MATERIALS AND METHODS

Contrast Agent Preparation and Characterization

In this study, three contrast agents were used: (1) ioxaglate solution (48 mg I/ml, $M = 1269$ g/mol, ioxaglate, Hexabrix, Mallinckrodt Inc., USA), (2) BiNP suspension (Bi_2O_3 nanopowder, Sigma-Aldrich, USA), and (3) a mixture of both contrast agents, i.e., the dual contrast agent. The ioxaglate solution was adjusted to be isotonic (~308 mOsm/kg) with phosphate-buffered saline (PBS) that was supplemented with proteolytic inhibitors [5 mM ethylenediaminetetraacetic acid (EDTA, VWR International, France) and 5 mM ben-

zamidine hydrochloride hydrate (Sigma-Aldrich Inc., USA)] to prevent general degradation of proteins in tissue. BiNP suspension was prepared by ball-milling bismuth(III) oxide nanopowder in water at a speed of 800 rpm for 4 h (Planetary Micro Mill, Pulverisette 7, Fritsch GmbH, Germany). Then, the suspension was stabilized by coating the BiNPs with polyethylene glycol (PEG, $M = 12,000$ g/mol, Alfa Aesar, USA) by adding the PEG to the BiNP suspension and stirring the suspension for 1 h. Free PEG was not removed from the solution in order to increase the osmolality of the BiNP solution. The final concentrations were 100 mg/ml for bismuth(III) oxide and 25 mg/ml for PEG. The size distribution, zeta potential, and polydispersity index (PdI) were measured using a Malvern Zetasizer Nano ZS instrument (Malvern Instruments Ltd., UK). The size distribution of BiNP suspension was 260 ± 80 nm (mean $\pm$ SD) and PdI 0.171. The zeta potential distribution of BiNPs with PEG coating polymer was measured to be 59 ± 9 mV. The pH was adjusted to 7.4 by using acetic acid (Sigma-Aldrich, USA), and the osmolality was measured to be 65 mOsm/kg. Dual contrast agent was prepared by mixing BiNP suspension and ioxaglate. The final concentrations of BiNP suspension and ioxaglate in the dual contrast agent were equal to those applied separately. The osmolality of dual contrast agent was 114 mOsm/kg when measured with a freeze-point osmometer (Halbmikro-osmometer, GWB, Knauer & Co GmbH, Germany). Osmolalities of BiNP suspension and dual contrast agent solution were accepted to be hypotonic.

Sample Preparation

Intact knee joints ($N = 10$) from skeletally mature bovines were obtained from a local butcher (Savo-Karjalan liha Oy, Finland) and, thus, no ethical permission for tissue collection was needed. First, patellae were carefully dissected from the surrounding tissues, wrapped in PBS-soaked gauze, and stored at -20 °C. Prior to the measurements, patellae were thawed at room temperature. Subsequently, a large osteochondral disc ($d = 2.65$ cm) was extracted from the upper lateral quadrant of the patella and three adjacent osteochondral plugs ($n = 30$ in total, $d = 7$ mm) were prepared from the disc.[15] After the sample preparation, one of the osteochondral plugs was enzymatically degraded and one mechanically injured. The third osteochondral plug was used as an intact reference sample.

Early-state OA, involving PG loss, is often mimicked by treating cartilage with degradative enzymes.[9,28] In this study, the osteochondral samples were degraded enzymatically by immersing them in a trypsin solution (0.5 mg/ml, Sigma-Aldrich, USA) for 15 h at 37.5 °C in an incubator to achieve nearly complete depletion of the PGs.[21] Subsequently, the samples were immersed in PBS for 2 h at 7 °C to wash out the trypsin and to stop the enzymatic degradation.

A mechanical injury was induced using a custom-made drop tower.[15] A stainless steel impactor (500 g) with a polished face was dropped on the sample from the height of 20 cm. The magnitude of the impact was selected based on a previous study[15] to create minor cracks on the articular surface. To prevent any creep deformation, the impactor was lifted from the sample immediately after the impact. Furthermore, the samples were allowed to recover while immersed in PBS for 2 h after the injury.

MicroCT Imaging

To study the contrast agent diffusion and distribution within the cartilage, the samples were imaged using a microCT scanner (Skyscan 1172, SkyScan, Belgium). Prior to microCT imaging, the side and the bottom of each osteochondral sample were sealed carefully with cyanoacrylate to allow the contrast agent to diffuse only through the articular surface. The samples were imaged immediately after immersing them into contrast agent and second time at 45 min after the immersion in contrast agent. Imaging time points were selected to correspond clinically relevant time points.[14] Between the imaging sessions, the samples were immersed in contrast agent. The contrast agent bath (volume 3 ml/sample) was agitated between the imaging sessions. The voxel size was 15.98 μm $\times$ 15.98 μm $\times$ 15.98 μm and the tube voltage 100 kV. Intact, enzymatically degraded, and mechanically injured samples were imaged using all three contrast agents separately. The order of contrast agents, in which the samples were imaged, was randomly varied between the samples. After each imaging session, contrast agents were washed out by immersing the samples in PBS (~308 mOsm/kg, 100 ml) for 2 h at 7 °C between the changes of contrast agents. In our preliminary measurements, the washout time was found to be sufficient to fully remove contrast agent from the tissue. Since we ultimately aim to develop this method for *in vivo* use and to minimize the X-ray dose for the subject, no imaging without contrast agents was conducted.

Image Analysis

X-ray attenuation profiles through the osteochondral samples were calculated using MATLAB (R2014a, MathWorks, Inc., USA). The cartilage surface and the cartilage-bone interface were delineated

BMES
BIOMEDICAL ENGINEERING SOCIETY™
www.bmes.org

from the microCT image stacks by selecting manually approximately 100 evenly distributed points from both interfaces. The natural curvatures of articular surface and cartilage-bone interface were removed, i.e., straightened, before the determination of contrast agent depth wise distribution profiles to ensure that the cartilage samples were co-aligned and that the defined region of interest (ROI) included only cartilage. First, planes were fitted on both surfaces by minimizing the Euclidean distance between the plane and points, and the manual points were projected on these planes. Thereafter, the planes were aligned horizontally to allow cubic ROI; first, the sum normal vector of the planes was aligned vertically by rotating both planes together around their common center point and then normal vectors of each plane were aligned vertically and by rotating each plane separately. Finally, the distance between the planes was normalized to 100 pixels (1.598 mm) which closely preserved the original voxel size. The original microCT images were warped to common aligned and normalized shape using thin-plate spline (TPS)[3,34] mapping between the original curvy shape of cartilage and horizontally aligned shape. Here, TPS generates the map by moving each point from its original location exactly to the horizontally aligned location. The deformation elsewhere in the space is defined based on these point movements such that energy required for the deformation is minimized. Next, a $200 \times 200 \times 140$ pixels sized ROI was selected at the center of each sample. Perpendicular to the surfaces (i.e., through the cartilage thickness), ROI was selected to extend 20 pixels outside of the cartilage to include subchondral bone and contrast agent on top of the articular surface. Subsequently, pixels parallel to the surface planes were averaged to obtain the mean vertical X-ray attenuation profile from subchondral bone through cartilage, articular surface, and contrast agent bath (Fig. 1). When the same sample was imaged with different contrast agents, the variation in attenuation values between the scans was corrected according to mean X-ray attenuation value of the subchondral bone. Finally, the attenuation values were normalized with the greatest attenuation value observed during the whole measurement series.

To analyze the bulk attenuation differences in cartilage between the 0- and 45-min images, the average X-ray attenuation value in native cartilage was determined in 0-min image at deep cartilage and subtracted from both 0- and 45-min images. Only the deep cartilage was included to ensure that no contrast agent affected the X-ray attenuation value of native cartilage tissue. Diffusion of the ioxaglate dissipated the contrast at cartilage surface. Therefore, to obtain the real cartilage thickness for the analysis, the cartilage-bone interface and cartilage surface from the 0-min BiNP-

enhanced image of the same sample were registered together with the ioxaglate-enhanced images. The attenuation profiles for ioxaglate-enhanced images were evaluated using two different approaches: firstly, based on segmentation from image enhanced with ioxaglate and secondly, based on registered segmentation from BiNP suspension-enhanced, 0-minute image. Reconstruction-based artefacts and depth-related variation in native tissue were removed from X-ray attenuation profiles along the cartilage thickness. This was done by subtracting the X-ray attenuation profile of cartilage (obtained from intact 0-min image) from the 45-min attenuation profile. This was done separately for each sample. The X-ray attenuation values were then normalized to the scale ranging from 0 to 1. Since microCT used in this study yields data in 16-bit gray scale values instead of standard 12-bit HU images, the results are presented in arbitrary units (AU).

Histological Analysis

Prior to histological analysis, the samples were fixed in 10% formalin and dehydrated in ascending series of ethanol. Next, the samples were decalcified in EDTA, embedded in paraffin and cut into 3 μm thick sections. After sectioning, the paraffin was removed and the sections were stained with Safranin-O to reveal the spatial PG distribution in the tissue. The PG distribution in cartilage was measured using quantitative DD (Fig. 2).[25] DD measurements were conducted using a light microscope (Nikon Microphot-FXA, Nikon Co., Japan) equipped with a monochromatic light source and a 12-bit CCD camera (ORCA-ER, Hamamatsu Photonics K.K., Japan). Prior to measurements, the system was calibrated with neutral density filters (Schott, Germany) covering optical density (OD) range from 0 to 2.6. Then, depth-wise PG content profiles were determined for three sections per sample and averaged. The stained sections were also imaged with a light microscope (Leica MZ75, Leica Microsystems Ltd., Switzerland) fitted with a CCD camera (Nikon digital sight DS-Fi2, Nikon Co., Japan) to determine the cartilage thickness.

Statistical Analysis

The significance of the differences in parameter values was calculated utilizing Wilcoxon signed-rank test. The statistical dependence between the bulk OD and the attenuation values were determined using Spearman's rank correlation. The statistical analysis was performed using SPSS software package (v. 24.0 SPSS Inc., IBM Company, USA). Here, nonparametric test was chosen due to relatively small number of

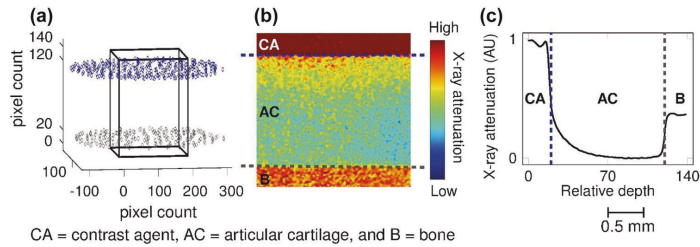CA = contrast agent, AC = articular cartilage, and B = bone

FIGURE 1. MicroCT image analysis of dual contrast-enhanced images. Analysis was performed similarly also for ioxaglate and BiNP suspension-enhanced images. (a) Articular surface (blue) and cartilage-bone interface (grey) were determined by manually selecting points on both interfaces. Then, the natural curvatures of articular surface and cartilage-bone interface were straightened and the cartilage thickness was normalized to 100 pixels which closely preserved the original voxel size and allowed straight-forward comparison between the samples. Next, the region of interest (ROI, delineated with black box) was selected to be 200 × 200 × 140 pixels so that the ROI was extended outside the cartilage to include subchondral bone beneath and contrast agent on top of the articular surface. (b) Pixels parallel to the surfaces were averaged in horizontal direction to obtain the mean 2D contrast agent distribution within cartilage. (c) Mean X-ray attenuation profile was obtained by averaging the 3D ROI parallel to the surfaces (i.e., both horizontal directions). The cartilage-contrast agent bath interface is delineated with a blue dashed line and the subchondral bone-cartilage interface with a gray dashed line.
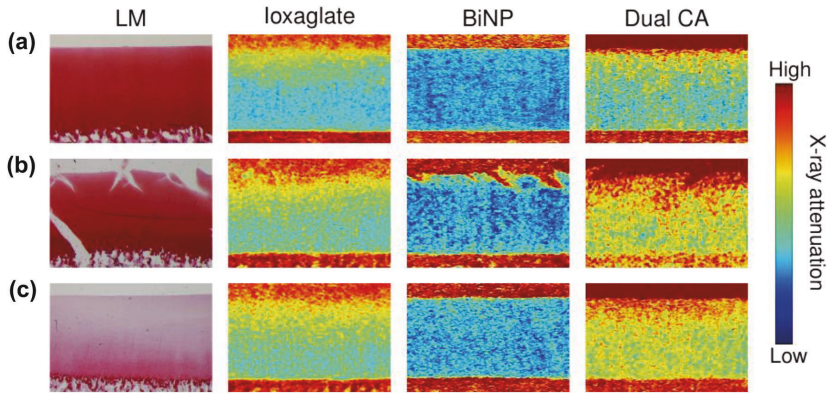
FIGURE 2. Safranin-O stained histological sections of the (a) intact, (b) mechanically injured, and (c) enzymatically degraded samples imaged with a light microscope (LM) and corresponding ioxaglate, BiNP suspension, and dual contrast agent microCT images acquired 45 min post administration. The cartilage surface lesions can be detected from the dual contrast-enhanced computed tomography image. Furthermore, degeneration of the mechanically injured and enzymatically degraded cartilage can be identified as higher X-ray attenuation (i.e., ioxaglate diffusion) of cartilage when compared with that of intact cartilage.

samples. This was done as small sample groups do not contain enough information to make reliable assumption about the normality of the distribution of the data.

RESULTS

The BiNPs were unable to diffuse into healthy, enzymatically degraded, or mechanically injured cartilage layer even 45 min after contrast agent administration. This enables accurate segmentation of cartilage and detection of cracks in the articular surface (Table 1; Fig. 3). The cartilage surface was segmented from ioxaglate-enhanced images in two ways: directly from ioxaglate-enhanced images and by using segmentation from BiNP suspension enhanced images of the same sample which was registered to the ioxaglate-enhanced image based on bone surface. The bulk X-ray attenuation values were observed to be significantly higher when the segmentation based on BiNP suspension was used. The X-ray attenuation values increased as follows in 0-min images: intact $+66.1\%$, $p = 0.013$; mechanically injured $+89.3\%$,

$p = 0.005$; and enzymatically degraded $+92.7\%$, $p = 0.005$ and in 45-min images: intact $+15.2\%$, $p = 0.013$; mechanically injured $+35.4\%$, $p = 0.005$; and enzymatically degraded $+25.1\%$, $p = 0.005$. The ioxaglate uptake at 45 min was greater into mechanically injured ($+86.6\%$, $p = 0.005$) and enzymatically degraded ($+60.0\%$, $p = 0.005$) injured samples than into the intact samples. Also when mixed with BiNPs (i.e., dual contrast agent), ioxaglate uptake showed increase in mechanically injured ($+113.1\%$, $p = 0.013$) and enzymatically degraded ($+70.3\%$, $p = 0.013$) samples in 45-min images compared with intact samples (Fig. 4).

Cartilage thicknesses segmented from BiNP suspension-enhanced images were similar to thicknesses obtained from histological sections with light microscopy. For 0-min images, the segmented cartilage thickness was 0.6% less and for 45-min image 0.7% less than the actual cartilage thickness. The segmented cartilage thicknesses from ioxaglate-enhanced images were 7.0 and 9.3% less in 0-min and in 45-min time points, respectively, than the actual cartilage thickness obtained with light microscopy. With dual contrast agent, the thickness was 2.3% less in both 0-min and in 45-min time points. The differences between the thicknesses obtained from CT images and from histological sections were statistically significant only for ioxaglate-enhanced images at both time points ($p < 0.05$ for all sample groups). When compared with the reference samples (Table 1), the PG content was significantly lower in mechanically injured ($p = 0.009$) and enzymatically injured samples ($p = 0.0005$).

DISCUSSION

In this laboratory study, we introduce a new dual contrast agent that can enhance the CT diagnostics of acute cartilage injuries. In particular, we study the validity of implementing BiNPs into iodinated clinical CT contrast agent to enable simultaneous evaluation of tissue integrity and accurate segmentation of cartilage layer. Previously, CECT imaging of joints has been conducted using single charged contrast agent (e.g., ioxaglate) diffusing into tissue inversely proportionally to PG concentration. This method can be used to evaluate cartilage integrity using two subsequent imaging sessions at 0 and 45 min post administration. In that technique, cartilage tissue properties and initiation of PTOA can be evaluated from the 45-min (i.e., delayed) image while the 0-min image is required to locate the articular surfaces and for detection of lesions in the cartilage surface. In this study, we have shown that by mixing BiNPs with anionic contrast agent, the articular surface can be segmented more accurately

from the delayed image, thus simplifying the diagnostics of articular cartilage degeneration. In this context, the 0-minute image is no longer needed in diagnostics of fresh cartilage injuries.

In all sample groups, the ioxaglate induced X-ray attenuation in cartilage was stronger when cartilage segmentation was based on the BiNP suspension-enhanced images instead of conventional ioxaglate-enhanced images. This is because in conventional segmentation the superficial layer of the cartilage was falsely interpreted as synovial fluid and segmented out due to high concentration of diffused ioxaglate contrast agent. This indicates that the use and analysis of the conventional ioxaglate-enhanced images may not be optimal. Indeed, cartilage thicknesses reveal that the cartilage surface in ioxaglate-enhanced images is segmented much lower than the actual cartilage surface due to loss of contrast at the surface. Thus, implementation of BiNPs could solve uncertainties related to correct segmentation of cartilage layer from CT images.

Similar X-ray attenuation values between 0- and 45-min images (Table 1; Fig. 3) reveal that BiNPs are unable to penetrate into cartilage, thereby maintaining the distinctiveness of articular cartilage surface. The thickness values obtained from histological sections and ioxaglate-enhanced images are expected to have good correspondence with 0-minute images but poor with 45-minute images. However, the thickness values obtained from BiNP suspension and dual contrast agent images at both time points are expected to be similar with the thickness values obtained from histological section. Since our results supported our hypothesis, we can conclude that BiNPs are unable to diffuse into cartilage, thus enabling improved segmentation of the cartilage surface compared with that using ioxaglate. Accurate segmentation of the cartilage surface is important as superficial cartilage layer often shows the first signs of degeneration.

Ioxaglate diffusion in mechanically injured and enzymatically degraded samples was greater compared to that in the intact samples (Fig. 3).[2,15] In mechanically injured samples, higher attenuation values were partially due to contrast agent located in cracks on the cartilage surface after mechanical damage. Additionally, in mechanically injured samples, the permeability of the articular surface for ioxaglate is higher due to increased surface area for ioxaglate diffusion caused by cracks but also due to the disruption of the collagen network reducing the steric hindrance of contrast agent diffusion.[8,15] In enzymatically degraded samples, the greater penetration of anionic ioxaglate is mainly due to extensive PG loss in the tissue.[12] However, in addition to PG loss (e.g., decreased fixed negative charge density), also other structural and compositional properties of the tissue, such as collagen and

TABLE 1. X-ray attenuation values (mean ± SD), optical densities, and cartilage thickness for intact, mechanically injured, and enzymatically degraded bovine samples ($n = 10$ for each group).

	X-ray attenuation (AU)		Optical		Thickness (mm)[b]	
	0 min	45 min	Density (−)	LM	0 min	45 min
Ioxaglate						
Intact	0.10 ± 0.07/0.14 ± 0.07[a]	0.29 ± 0.14/0.33 ± 0.13[a]	1.63 ± 0.18	2.28 ± 0.65	2.17 ± 0.59	2.17 ± 0.58
Mechanically injured	0.17 ± 0.07/0.27 ± 0.08[a]	0.42 ± 0.12/0.55 ± 0.12[a]	1.30 ± 0.16	2.20 ± 0.61	2.00 ± 0.62	1.91 ± 0.62
Enzymatically degraded	0.10 ± 0.06/0.17 ± 0.08[a]	0.40 ± 0.16/0.49 ± 0.18[a]	0.42 ± 0.25	2.30 ± 0.55	2.14 ± 0.51	2.08 ± 0.52
BiNP suspension						
Intact	0.05 ± 0.04	0.05 ± 0.08			2.24 ± 0.63	2.24 ± 0.61
Mechanically injured	0.18 ± 0.12	0.18 ± 0.09			2.21 ± 0.63	2.20 ± 0.60
Enzymatically degraded	0.03 ± 0.07	0.03 ± 0.08			2.28 ± 0.51	2.28 ± 0.51
Dual contrast agent						
Intact	0.28 ± 0.10	0.44 ± 0.20			2.23 ± 0.64	2.23 ± 0.63
Mechanically damaged	0.51 ± 0.12	0.73 ± 0.16			2.17 ± 0.64	2.17 ± 0.62
Enzymatically degraded	0.29 ± 0.08	0.62 ± 0.21			2.23 ± 0.51	2.23 ± 0.52

AU arbitrary unit.

[a]X-ray attenuation based on visual segmentation/actual cartilage thickness based on BiNP enhancement.

[b]The thickness values are obtained from histological sections using a light microscope (LM) and from.

0- and 45-min microCT images using ioxaglate, BiNP suspension, and dual contrast agent.
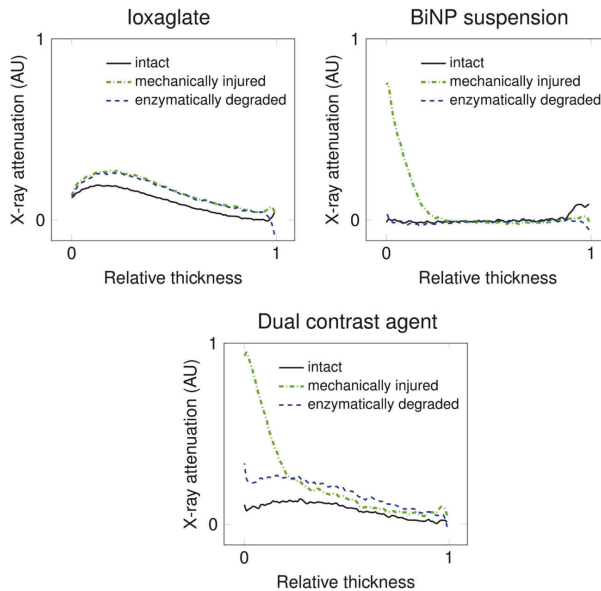
FIGURE 3. Mean depth-wise contrast agent X-ray attenuation difference (AU = Arbitrary unit) between 0-min intact and 45-min intact, mechanically injured, and enzymatically degraded bovine articular cartilage samples ($n = 10$/group) imaged using ioxaglate, BiNP suspension, and dual contrast agent. The horizontal axis presents the relative distance from articular surface (0) to the cartilage-bone interface (1).

water contents, have probably affected the diffusion of ioxaglate.[27,30]

The X-ray attenuation values in BINP suspension and dual contrast agent-enhanced images were greater than those of ioxaglate-enhanced images (Table 1). This was caused by microCT reconstruction algorithm increasing the attenuation of the X-ray attenuation throughout the image when highly attenuating con-
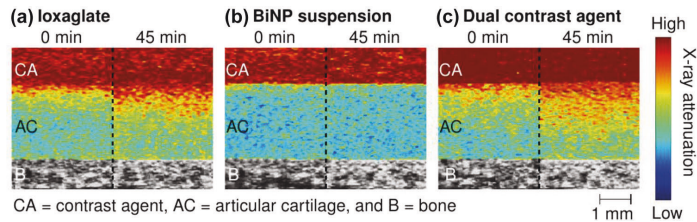
FIGURE 4. MicroCT images of a representative enzymatically degraded osteochondral sample at 0-min and 45-min time points using (a) ioxaglate, (b) BiNP suspension, and (c) dual contrast agent enhancement. Ioxaglate diffusion reveals the state of the cartilage degeneration while BiNP suspension creates a high contrast at the articular surface. Thus, detection of articular cartilage surface and degeneration of the tissue can be observed simultaneously in the delayed arthrographic image (45 min) when using the dual contrast agent.

trast agent bath was present. This artifact was removed when calculating the bulk attenuation values by normalizing the images with subchondral bone attenuation and by subtracting the 0-min image from 45-min image having the same reconstruction-based artifact in their attenuation values. In the future studies, we will decrease the concentration of BiNP in dual contrast agents. In this study, however, high BiNP concentration was selected to demonstrate that with high contrast, the segmentation of the cartilage surface can be done reliably along to evaluation of cartilage degeneration.

The histology-based technique to measure cartilage thickness has certain limitations. Firstly, the area used in thickness analysis includes only a small number of points along the surface while the thickness calculated based on CT images covers nearly the entire sample. This may cause some error especially with samples having spatial variations in cartilage thickness. Additionally, fixation-associated shrinkage can decrease the thickness measured from the sections. However, we expect this shrinkage to have only minor effect on the results.

At this development stage of the dual contrast method, we used microCT rather than a clinical CT scanner even though we are ultimately aiming for clinically applicable method. On the other hand, usage of microCT enabled the evaluation of this method in more detail due to its high resolution. With clinical full-body and cone-beam CT scanners in the future studies, the lower spatial resolution may also bring some challenges along. Nevertheless, these are expected to be solvable as the previous *in vivo and ex vivo* CECT studies have been successful.[14,17,32] The future aim, however, is to test the dual contrast method with a clinical CT scanner and develop the technique towards clinical use.

In this study, anionic contrast agent was preferred over cationic contrast agent. Cationic contrast agents have better sensitivity for PG depletion at diffusion equilibrium as compared to conventional contrast agents.[31,33] However, simultaneous increase in water content (increased diffusion) and decrease in PG content (decreased diffusion), both characteristic to cartilage degeneration, induces opposite effects on diffusion of cationic contrast agents at early time points. This can complicate the use of positive contrast agents at clinically feasible timeframes.

With microCT, the acquisition times are usually longer than with clinical CT devices. In our study, the acquisition time was approximately 13 min and during that time samples were immersed in contrast agents, enabling the diffusion still to occur. For this reason, the bulk X-ray attenuation value is rather an average value over the acquisition time rather than the precise value at a time point. Nevertheless, we believe that this had no significant impact on the results or conclusions as the imaging settings were the same for all the samples. In clinical examination after the administration of the contrast agent, the patient actively moves the joint to promote the contrast agent to distribute evenly within the joint capsule. Consequently, the immediate imaging at the 0-minute time point is not possible even in clinical settings. In this light, the dual contrast method gains advantage over the conventional CECT diagnostics of articular cartilage degeneration as in dual contrast method the delayed arthrographic image provides all the necessary information.

Bismuth and its salts are generally considered to have low toxicity.[20] In addition, bismuth-based compounds can readily be prepared in NPs and are also one of the least expensive high atomic number (Z) elements. However, biological applications and excretion of BiNPs requires further investigation.[37] Especially,

understanding the effect of NP size and shape distribution[13,38] along with their surface properties is essential.[35] As NPs are generally unstable owing to their high surface energy, they are usually coated with an organic, stabilizing polymer. For this reason, PEG was used to modify the BiNP surfaces to achieve long-term colloidal stability and to decrease the electrostatic attraction between ioxaglate and BiNPs. PEG is commonly used and known to reduce cytotoxicity and lengthen the circulation times of NPs by reducing the non-specific binding of proteins.[11] The hydrodynamic effect caused by free PEG molecules is expected to be minor. Further, NPs are expected not to alter the diffusion of the ioxaglate molecules but this is something that should be further verified in the future studies. PEG was also observed to provide the best stability over polyvinylpyrrolidone (PVP) and polyvinylalcohol (PVA) according to our preliminary tests.

Since the stability of the present NP suspension was extremely sensitive to high ion concentrations, we were unable to adjust the osmolalities of BiNP suspension and dual contrast agent to the physiological osmolality. Mechanical properties of cartilage are significantly controlled by osmotic swelling pressure. In a hypotonic bath, swelling pressure increases potentially elevating the cartilage water content. Since cartilage thickness did not increase significantly, we believe, the changes in cartilage diffusive properties and water content were limited. However, in the future, we aim to develop an isotonic version of the dual contrast agent. A further limitation was the use of freezing point osmometer designed for measuring the osmolality of solution containing small soluble molecules. Low concentrations of NPs are not expected to affect the measured osmolality; however, since the concentration of NPs in our solutions was relatively high, we anticipate NPs to cause some inaccuracy. In BiNP suspension, the osmolality is mainly due to free PEG molecules in the solution.

In conclusion, the introduced dual contrast technique improves the feasibility of CECT and can provide valuable diagnostic information (e.g., enables accurate delineation of pathological surface alterations), and requires only the acquisition of the single delayed image. The dual contrast method can detect cartilage degenerations produced by enzymes as well as damages caused by a mechanical impact. Potentially, the dual contrast CT method may help to more effectively select patient-specific surgical treatment options and prevention of PTOA. Moreover, the method relieves some logistical pressures regarding image acquisition and will cut the patient radiation dose to half as compared with the current method used in CECT diagnostics of the knee joint.

CONFLICT OF INTEREST

Authors declare no conflicts of interest.

REFERENCES

[1]Anderson, D. D., S. Chubinskaya, F. Guilak, J. A. Martin, T. R. Oegema, S. A. Olson, and J. A. Buckwalter. Posttraumatic osteoarthritis: improved understanding and opportunities for early intervention. *J. Orthop. Res.* 29:802–809, 2011.

[2]Bansal, P. N., N. S. Joshi, V. Entezari, M. W. Grinstaff, and B. D. Snyder. Contrast Enhanced Computed Tomography can predict the glycosaminoglycan content and biomechanical properties of articular cartilage. *Osteoarthr. Cartil.* 18:184–191, 2010.

[3]Bookstein, F. L. Random walk and the existence of evolutionary rates. *Paleobiology* 13:446–464, 1987.

[4]Braun, H. J., and G. E. Gold. Diagnosis of osteoarthritis: imaging. *Bone* 51:278–288, 2012.

[5]Brown, T. D., R. C. Johnston, C. L. Saltzman, J. L. Marsh, and J. A. Buckwalter. Posttraumatic osteoarthritis: a first estimate of incidence, prevalence, and burden of disease. *J. Orthop. Trauma* 20:739–744, 2006.

[6]Buckwalter, J. A. Mechanical injuries of articular cartilage. *Iowa Orthop. J.* 12:50, 1992.

[7]De La Vega, J. C., and U. O. Häfeli. Utilization of nanoparticles as X-ray contrast agents for diagnostic imaging applications. *Contrast Media Mol. Imaging* 10:81–95, 2015.

[8]Ewers, B., V. Jayaraman, R. Banglmaier, and R. C. Haut. Rate of blunt impact loading affects changes in retropatellar cartilage and underlying bone in the rabbit patella. *J. Biomech.* 35:747–755, 2002.

[9]Harris, E. D., H. G. Parker, E. L. Radin, and S. M. Krane. Effects of proteolytic enzymes on structural and mechanical properties of cartilage. *Arthritis Rheumatol.* 15:497–503, 1972.

[10]Javier, D. J., N. Nitin, M. Levy, A. Ellington, and R. Richards-Kortum. Aptamer-targeted gold nanoparticles as molecular-specific contrast agents for reflectance imaging. *Bioconjugate Chem.* 2008. doi:10.1021/BC8001248.

[11]Jokerst, J., V. T. Lobovkina, R. N. Zare, and S. S. Gambhir. Nanoparticle PEGylation for imaging and therapy. *Nanomedicine* 6:715–728, 2011.

[12]Kallioniemi, A. S., J. S. Jurvelin, M. T. Nieminen, M. J. Lammi, and J. Töyräs. Contrast agent enhanced pQCT of articular cartilage. *Phys. Med. Biol.* 52:1209–1219, 2007.

[13]Karlsson, H. L., J. Gustafsson, P. Cronholm, and L. Möller. Size-dependent toxicity of metal oxide particles—a comparison between nano- and micrometer size. *Toxicol. Lett.* 188:112–118, 2009.

[14]Kokkonen, H. T., A. S. Aula, H. Kröger, J.-S. Suomalainen, E. Lammentausta, E. Mervaala, J. S. Jurvelin, and J. Töyräs. Delayed computed tomography arthrography of human knee cartilage *in vivo*. *Cartilage* 3:334–341, 2012.

[15]Kokkonen, H. T., J. S. Jurvelin, V. Tiitu, and J. Töyräs. Detection of mechanical injury of articular cartilage using contrast enhanced computed tomography. *Osteoarthr. Cartil.* 19:295–301, 2011.

[16]Kokkonen, H. T., J. Mäkelä, K. A. M. Kulmala, L. Rieppo, J. S. Jurvelin, V. Tiitu, H. M. Karjalainen, R. K. Korhonen, V. Kovanen, and J. Töyräs. Computed tomography detects changes in contrast agent diffusion after collagen cross-linking typical to natural aging of articular cartilage. *Osteoarthr. Cartil.* 19:1190–1198, 2011.

[17]Kokkonen, H. T., J.-S. Suomalainen, A. Joukainen, H. Kröger, J. Sirola, J. S. Jurvelin, J. Salo, and J. Töyräs. In vivo diagnostics of human knee cartilage lesions using delayed CBCT arthrography. *J. Orthop. Res.* 32:403–412, 2014.

[18]Lin, P. M., C.-T. C. Chen, and P. A. Torzilli. Increased stromelysin-1 (MMP-3), proteoglycan degradation (3B3- and 7D4) and collagen damage in cyclically load-injured articular cartilage. *Osteoarthr. Cartil.* 12:485–496, 2004.

[19]Liu, X. H., L. Zhong, S. Huang, S. X. Mao, T. Zhu, and J. Y. Huang. Size-dependent fracture of silicon nanoparticles during lithiation. *ACS Nano* 6:1522–1531, 2012.

[20]Mohan, R. S. In your element: green bismuth. *Nat. Chem.* 2:336, 2010.

[21]Moody, H. R., C. P. Brown, J. C. Bowden, R. W. Crawford, D. L. S. McElwain, and A. O. Oloyede. In vitro degradation of articular cartilage: does trypsin treatment produce consistent results? *J. Anat.* 209:259–267, 2006.

[22]Myller, K. A. H., M. J. Turunen, J. T. J. Honkanen, S. P. Väänänen, J. T. Iivarinen, J. Salo, J. S. Jurvelin, and J. Töyräs. In vivo contrast-enhanced cone beam CT provides quantitative information on articular cartilage and subchondral bone. *Ann. Biomed. Eng.* 45:811–818, 2017.

[23]Olson, S. A., B. D. Furman, V. B. Kraus, J. L. Huebner, and F. Guilak. Therapeutic opportunities to prevent post-traumatic arthritis: lessons from the natural history of arthritis after articular fracture. *J. Orthop. Res.* 33:1266–1277, 2015.

[24]Pan, D., E. Roessl, J.-P. Schlomka, S. D. Caruthers, A. Senpan, M. J. Scott, J. S. Allen, H. Zhang, G. Hu, P. J. Gaffney, E. T. Choi, V. Rasche, S. A. Wickline, R. Proksa, and G. M. Lanza. Computed tomography in color: NanoK-enhanced spectral CT molecular imaging. *Angew. Chem.* 122:9829–9833, 2010.

[25]Panula, H. E., M. M. Hyttinen, J. P. Arokoski, T. K. Långsjö, A. Pelttari, I. Kiviranta, and H. J. Helminen. Articular cartilage superficial zone collagen birefringence reduced and cartilage thickness increased before surface fibrillation in experimental osteoarthritis. *Ann. Rheum. Dis.* 57:237–245, 1998.

[26]Peat, G., C. Bergknut, R. Frobell, A. Jöud, and M. Englund. Population-wide incidence estimates for soft tissue knee injuries presenting to healthcare in southern Sweden: data from the Skåne Healthcare Register. *Arthritis Res. Ther.* 16:R162, 2014.

[27]Piscaer, T. M., J. H. Waarsing, N. Kops, P. Pavljasevic, J. A. N. Verhaar, G. J. V. M. van Osch, and H. Weinans. In vivo imaging of cartilage degeneration using μCT-arthrography. *Osteoarthr. Cartil.* 16:1011–1017, 2008.

[28]Rieppo, J., J. Töyräs, M. T. Nieminen, V. Kovanen, M. M. Hyttinen, R. K. Korhonen, J. S. Jurvelin, and H. J. Helminen. Structure-function relationships in enzymatically modified articular cartilage. *Cells Tissues Organs* 175:121–132, 2003.

[29]Silvast, T. S., J. S. Jurvelin, A. S. Aula, M. J. Lammi, and J. Töyräs. Contrast agent-enhanced computed tomography of articular cartilage: association with tissue composition and properties. *Acta Radiol.* 50:78–85, 2009.

[30]Silvast, T. S., H. T. Kokkonen, J. S. Jurvelin, T. M. Quinn, M. T. Nieminen, and J. Töyräs. Diffusion and near-equilibrium distribution of MRI and CT contrast agents in articular cartilage. *Phys. Med. Biol.* 54:6823–6836, 2009.

[31]Stewart, R. C., P. N. Bansal, V. Entezari, H. Lusic, R. M. Nazarian, B. D. Snyder, and M. W. Grinstaff. Contrast-enhanced CT with a high-affinity cationic contrast agent for imaging ex vivo bovine, intact ex vivo rabbit, and in vivo rabbit cartilage. *Radiology* 266:141–150, 2013.

[32]Stewart, R. C., J. T. J. Honkanen, H. T. Kokkonen, V. Tiitu, S. Saarakkala, A. Joukainen, B. D. Snyder, J. S. Jurvelin, M. W. Grinstaff, and J. Töyräs. Contrast-enhanced computed tomography enables quantitative evaluation of tissue properties at intrajoint regions in cadaveric knee cartilage. *Cartilage* 2016. doi:10.1177/1947603516 665443.

[33]Stewart, R. C., A. N. Patwa, H. Lusic, J. D. Freedman, M. Wathier, B. D. Snyder, A. Guermazi, and M. W. Grinstaff. Synthesis and preclinical characterization of a cationic iodinated imaging contrast agent (CA4+) and its use for quantitative computed tomography of ex vivo human hip cartilage. *J. Med. Chem.* 60:5543–5555, 2017.

[34]Väänänen, S. P., J. S. Jurvelin, and H. Isaksson. Estimation of 3D shape, internal density and mechanics of proximal femur by combining bone mineral density images with shape and density templates. *Biomech. Model. Mechanobiol.* 11:791–800, 2012.

[35]Verma, A., and F. Stellacci. Effect of surface properties on nanoparticle-cell interactions. *Small* 6:12–21, 2010.

[36]Yoo, H. J., S. H. Hong, J.-Y. Choi, I. J. Lee, S. J. Kim, J.-A. Choi, and H. S. Kang. Contrast-enhanced CT of articular cartilage: experimental study for quantification of glycosaminoglycan content in articular cartilage. *Radiology* 261:805–812, 2011.

[37]Zhang, X.-D., D. Wu, X. Shen, J. Chen, Y.-M. Sun, P.-X. Liu, and X.-J. Liang. Size-dependent radiosensitization of PEG-coated gold nanoparticles for cancer radiation therapy. *Biomaterials* 33:6408–6419, 2012.

[38]Zhang, X.-D., D. Wu, X. Shen, P.-X. Liu, N. Yang, B. Zhao, H. Zhang, Y.-M. Sun, L.-A. Zhang, and F.-Y. Fan. Size-dependent in vivo toxicity of peg-coated gold nanoparticles. *Int. J. Nanomed.* 6:2071–2081, 2011.

Paper **II**

SCIENTIFIC REP⚙RTS

OPEN

Simultaneous Quantitation of Cationic and Non-ionic Contrast Agents in Articular Cartilage Using Synchrotron MicroCT Imaging

Annina E. A. Saukko [1], Mikael J. Turunen [1], Miitu K. M. Honkanen [1,2], Goran Lovric [3,4], Virpi Tiitu [5], Juuso T. J. Honkanen [1,6], Mark W. Grinstaff [7], Jukka S. Jurvelin [1] & Juha Töyräs [1,2,8]

Early diagnosis of acute cartilage injuries enables monitoring of disease progression and improved treatment option planning to prevent post-traumatic osteoarthritis. In contrast-enhanced computed tomography (CECT), the changes in cationic agent diffusion within the tissue reflect cartilage degeneration. The diffusion in degenerated cartilage depends on proteoglycan (PG) content and water content, but each having an opposite effect on diffusion, thus compromising the diagnostic sensitivity. To overcome this limitation, we propose the simultaneous imaging of cationic (sensitive to PG and water contents) and non-ionic (sensitive to water content) agents. In this study, quantitative dual-energy CT (QDECT) imaging of two agents is reported for the first time at clinically feasible imaging time points. Furthermore, this is the first time synchrotron microCT with monochromatic X-rays is employed in cartilage CECT. Imaging was conducted at 1 and 2 h post contrast agent immersion. Intact, PG-depleted, and mechanically injured + PG-depleted cartilage samples ($n = 33$) were imaged in a mixture of cationic (iodine-based CA4+) and non-ionic (gadolinium-based gadoteridol) agents. Concurrent evaluation of CA4+ and gadoteridol partitions in cartilage is accomplished using QDECT. Subsequent normalization of the CA4+ partition with that of the gadoteridol affords CA4+ attenuations that significantly correlate with PG content – a key marker of OA.

Post-traumatic osteoarthritis (PTOA) typically develops after acute traumas, such as sport injuries or sudden impacts, for example, during vehicle accidents or falls. Cartilage damage, subchondral bone contusions, torn ligaments or meniscal tears are characteristic tissue features after acute joint injuries. Furthermore, abnormal joint function after injuries may create excessive tissue stresses and strains that lead to progressive loss of joint cartilage and subsequent osteoarthritis (OA). Recent findings suggest that the early detection of original tissue injury enables surgical and pharmaceutical interventions to prevent or slow down the development of PTOA[1,2]. In this context, techniques which enable sensitive detection of lesions and early post-traumatic degeneration of surrounding cartilage tissue are of interest and needed. Magnetic resonance imaging (MRI) is used to identify cartilage tissue properties, such as PG content, collagen orientation, and water content[3,4]. As MRI exhibits excellent soft tissue contrast, it is an important clinical tool in cartilage imaging. However, MRI provides relatively low spatial resolution of the tissue and requires relatively long *in vivo* image acquisition times[4,5].

As an alternative, contrast-enhanced computed tomography (CECT) provides high-resolution images of cartilage with short scan times at approximately half the cost of MRI. CECT also allows the early detection of

[1]Department of Applied Physics, University of Eastern Finland, POB 1627, FI-70211, Kuopio, Finland. [2]Diagnostic Imaging Center, Kuopio University Hospital, POB 100, FI-70029, Kuopio, Finland. [3]Centre d'Imagerie BioMédicale, École Polytechnique Fédérale de Lausanne, Lausanne, 1015, Switzerland. [4]Swiss Light Source, Paul Scherrer Institute, 5234, Villigen, Switzerland. [5]Institute of Biomedicine, Anatomy, University of Eastern Finland, POB 1627, FI-70211, Kuopio, Finland. [6]Center of Oncology, Kuopio University Hospital, POB 100, FI-70029, Kuopio, Finland. [7]Departments of Biomedical Engineering, Chemistry, and Medicine, Boston University, 590 Commonwealth Ave., Boston, MA 02215, USA. [8]School of Information Technology and Electrical Engineering, The University of Queensland, Brisbane, QLD 4072, Australia. Correspondence and requests for materials should be addressed to A.E.A.S. (email: annina.saukko@uef.fi)

tissue changes after an acute injury. Although CECT has been recently introduced in clinics, it is not yet widely used[6–10]. In CECT, contrast agents enhance the visualization of the cartilage tissue, as well as the cartilage-bone and synovial fluid-cartilage interfaces. Although the natural difference in the X-ray absorption at the synovial fluid-cartilage interfaces is nearly non-existent, CECT enables separation of these tissues and their boundaries. Further, degenerative cartilage changes are detected by examining the uptake and partitioning of mobile, ionic contrast agents in tissue[11–16]. The early degenerative changes (i.e., decrease in cartilage fixed charge density (FCD) via loss of PGs, increase in cartilage water content, and disruption of superficial collagen network[17,18]) alter the uptake of the contrast agent into cartilage tissue[19].

Typically, CECT relies on two subsequent CT scans conducted immediately and at delayed time point, e.g. approximately 45 minutes after the intra-articular injection of the contrast agent[6–8]. The first scan (arthrography) is needed for identification of articulating surfaces and surface lesions while the second scan (delayed arthrography) allows the evaluation of internal integrity of the cartilage and assessment of PTOA. A previous study showed that the optimal time point for delayed imaging is 30–60 minutes after administration of the anionic contrast agent in order to achieve maximum contrast agent concentration in cartilage[6].

Anionic, iodine-based molecules are the most commonly used contrast agents in knee CECT[7,8,16]. Owing to their negative charge, anionic contrast agents distribute by diffusion into cartilage, inversely proportionally to the spatial distribution of the negatively charged PGs[20,21]. Recent findings show that cationic contrast agents are more sensitive to detect changes in PG content at diffusion equilibrium than the conventional anionic contrast agents[22–24]. However, a limitation with cationic contrast agents is that their diffusion into degenerated cartilage tissue is controlled by two factors with opposite effects. The loss of PGs decreases the uptake (less attraction) while increased water content and reduced steric hindrance enhance the diffusion of cationic agents into cartilage, impairing diagnostic sensitivity of CECT especially at early imaging time points.

A novel approach to improve the capability of CECT is to apply a quantitative dual-energy CT (QDECT) technique[25]. This technique employs the use of a mixture of two contrast agents: 1) a cationic, iodinated contrast agent (CA4+)[14,22]; and 2) a non-ionic, gadolinium-based contrast agent (gadoteridol). In the dual contrast agent approach, CA4+ possesses a high affinity for the negative charge of PGs and distributes into cartilage proportionally to PG content. Gadoteridol, on the other hand, distributes into cartilage in relation to water content and steric hindrance of the tissue (i.e., physical diffusion barrier caused by collagen network architecture and PGs in the matrix), and is unaffected by the negative charge of PGs. Thus, the diagnostic value of CA4+ in clinical applications with a typical diffusion time frame of 30–60 minutes may be improved by normalizing the uptake of CA4+ with that of gadoteridol. Here, the normalization is achieved by dividing the CA4+ uptake in cartilage with that of gadoteridol.

With QDECT, the uptake of CA4+ and gadoteridol within cartilage are measured simultaneously by imaging with two different X-ray energies which represents a significant advantage over conventional CECT technique. Specifically, QDECT relies on element specific absorption k-edge energies of 33.2 and 50.3 keV for iodine and gadolinium, respectively. In this context, the QDECT technique allows the simultaneous quantification of interstitial water and PG contents based on CA4+ and gadoteridol distributions within tissue, thus enabling better diagnostic sensitivity for tissue degradation and osteoarthritic stage. The current technique also enables early detection of acute cartilage injuries by simultaneously providing information on the composition of cartilage, which is not currently possible with the standard techniques such as CT and MRI. Thus, QDECT provides an important alternative for MRI and CT imaging in cases where more specific information is needed in order to select the best treatment option after acute cartilage injury.

One of the limitations of conventional microCT and clinical CT scanners is that they lack imaging with monochromatic energies and this inevitably leads to beam hardening artifacts. Beam hardening reduces the accuracy of current CT technique. In beam hardening, the average photon energy in the X-ray beam is increased due to selective attenuation of lower energy photons, shifting the energy distribution of the X-ray beam away from the k-edge of iodine and towards that of gadolinium, resulting in a higher proportion of the higher energies exceeding the k-edge of gadolinium. This shift reduces the attenuation caused by iodine, while minimally affecting the attenuation by gadolinium[26]. In addition, when high resolution is required, conventional microCT instruments also require long imaging times. This limitation hinders the diagnostic sensitivity of the QDECT techniques due to continued diffusion of the contrast agents.

In the present study, synchrotron microCT is used as it provides imaging with monochromatic energies contemporally offering fast tomographic imaging with high resolution[27]. Specifically, QDECT is evaluated using intact, PG-depleted, and mechanically injured + PG-depleted samples. The first aim addresses the hypothesis that the uptake of cationic, iodine-based and non-ionic, gadolinium-based contrast agents can be determined simultaneously at clinically feasible diffusion time points (at 1 and 2 h after immersion). Further, we hypothesize that the differences between the intact, PG-depleted, and mechanically injured + PG-depleted samples can be quantitatively determined. The second aim addresses the hypothesis that the use of monochromatic X-ray energies provides sensitive QDECT diagnostics without the limitations commonly encountered with conventional CT scanners. We characterize the effect of mechanical impact, known to reduce steric hindrance on contrast agent diffusion[28]. As the first study to investigate simultaneously the diffusion of two different contrast agents into cartilage using separate monochromatic X-ray energies and the fact that dual-energy CT scanners are becoming more common in hospitals, these results provide a basis for a future quantitative diagnostic method for cartilage health and injury.

Materials and Methods

Sample preparation. Intact, skeletally mature bovine knee joints ($N = 11$) were obtained and patellae were carefully dissected. Three adjacent osteochondral plugs ($n = 33$, $d = 4\,mm$) were extracted from the upper lateral quadrant of each patellae. The samples were kept moist by using phosphate buffered saline (PBS) during the extraction process[29–33]. The number of samples was selected based on our previous papers[29–33] and the number was maximized to capitalize on the beamtime allocated to us by Paul Scherrer Institute (PSI). No ethical permission or approval for the experimental protocol and tissue collection were needed as the samples were obtained from a local grocery store (Prisma, Kuopio, Finland). After detaching the samples, the adjacent osteochondral plugs from the same patellae were divided into three groups: 1) intact, 2) PG-depleted, and 3) mechanically injured + PG-depleted. Preparation of PG depleted osteochondral plugs were prepared by enzymatic (trypsin) degradation. Degradation was performed by immersing the samples in PBS supplemented with trypsin (0.5 mg/ml, Sigma-Aldrich, MO, USA) for 15 h at 37.5 °C in an incubator[34]. After 15 h, the process was suppressed and the trypsin was washed out by immersing the samples in PBS for 2 h at 7 °C. With enzymatic degradation, early-stage OA, which is characterized by loss of PGs, is simulated using these enzymatically degraded plugs[35,36].

After the enzymatic degradation, the samples from the group 3 were injured mechanically using a custom-made drop tower. Mechanical impact on cartilage is known to reduce steric hindrance of articular cartilage and thus increase the uptake of contrast agent[28,32]. To mechanically damage the cartilage, a 500 g stainless steel impactor with a polished face was dropped on the sample from the height of 6.7 cm. The magnitude of impact was $P = 0.387\,kgm/s$ as used in previous studies[29,32]. The impactor was lifted immediately after the impact to prevent any cartilage creep deformation, after which the samples were kept immersed in PBS for 1 h to allow recovery from the impact. The procedure creates minor cracks on the surface of the cartilage[29,32]. Subsequently, the samples were immersed in PBS and frozen at −20 °C until thawing prior to synchrotron microCT imaging. All experimental protocols were carried out in accordance with the guidelines and regulations.

Synchrotron microCT imaging. The dual contrast method was examined by utilizing a third-generation synchrotron-based X-ray source (X02DA TOMCAT beamline of the Swiss Light Source, PSI, Villigen, Switzerland)[37]. With this synchrotron-based microCT technique, the X-ray beams are produced by a 2.9 T super-bending magnet on a 2.4 GeV storage ring (operated in top-up mode and 400 mA ring current). Monochromatic X-ray energies with an approximate energy bandwidth of 2–3% are tuned by using a double-multilayer monochromator (DMM) and ensure maximum difference between CA4+ and gadoteridol X-ray attenuation during imaging, thereby allowing high accuracy detection of contrast agent partitions within cartilage. The osteochondral samples, contrast agent calibration series, and a set of contrast agent mixtures described in more detail later were imaged by coupling a 1:1 magnifying visible light optics with a 300 μm thick scintillator (LuAg) in combination with a scientific CMOS detector (pco.Edge 4.2). Two X-ray energies (25 keV and 37 keV) with a field of view (FOV) of 17.07 mm × 17.07 mm × 2.75 mm and a minimal time difference (~5 min 20 s) between the scans were utilized with an effective pixel size of 6.5 × 6.5 μm². The samples were placed at a distance of 26.3 m away from the X-ray source while the detector was placed downstream as close as possible (<5 mm) to the samples in order to avoid edge-enhancement artifacts caused by Fresnel diffraction. Thus, only the bordering pixels of the air-to-sample interface were affected by Fresnel diffraction and these pixels were not used for the subsequent analysis[38,39]. The acquisition times for each tomographic scan were approximately 128 seconds. The reconstruction was performed using a highly optimized algorithm based on Fourier methods[40]. Off-beam sample alignment was used to minimize the radiation exposure to the samples during the alignment procedures[41]. The single-projection entrance doses (i.e., skin doses), with cartilage tissue modelled as water, were measured with a calibrated passivated implanted planar silicon (PIPS) diode32 and yielded 2.7 Gy and 1.1 Gy for the two energies (25 keV and 37 keV), respectively.

First, the calibration series of solutions with varying iodine (CA4+) and gadolinium (gadoteridol) concentrations in distilled water were imaged using both energies to determine the mass attenuation coefficients of the contrast agent compounds. In the solutions, the iodine concentration was 0.5, 1, 1.5, 2, 2.5, 3, 5, 10, 15, 20 mg I/mL and the gadolinium concentration 1, 2, 3, 4, 5, 7.5, 10, 12.5, 15 mg Gd/mL. In order to validate this method, four different mixtures of iodine- and gadolinium-based contrast agents in distilled water were imaged after the calibration series. The compositions of the mixtures were 1) 20 mg I/mL and 5 mg Gd/mL, 2) 10 mg I/mL and 10 mg Gd/mL, 3) 5 mg I/mL and 20 mg Gd/mL, and 4) 3 mg I/mL and 3 mg Gd/mL.

Prior to imaging, the side and the bottom of each osteochondral plug were sealed carefully using cyanoacrylate (Loctite, Henkel Norden AB, Dusseldorf, Germany). Thereby, the contrast agent diffusion was possible only through the articulating surface. To determine the X-ray attenuation profile in native cartilage the osteochondral samples were imaged in air with both energies before the contrast agent immersion. Then, the samples were immersed in isotonic (~308 mOsm/kg) mixture of iodinated, cationic contrast agent (CA4+, $q = +4$, $M = 1499.87\,g/mol$) and gadolinium-based, electrically neutral contrast agent (gadoteridol, $q = 0$, $M = 558.69\,g/mol$, ProHance™, Bracco Diagnostic Inc., Monroe Twp., NJ, USA) diluted in PBS. In the mixture, the iodine and gadolinium concentrations were 5 mg I/ml and 10 mg Gd/ml. Further, proteolytic inhibitors [5 mM ethylenediaminetetraacetic acid (EDTA, VWR International, France) and 5 mM benzamidine hydrochloride hydrate (Sigma-Aldrich Inc., St Louis, MO, USA)] were added to prevent general protein degradation in tissue. The samples were kept immersed in 3 ml of the contrast agent mixture for 2 h at 7 °C and imaged in air at 1 and 2 h time points with both energies. After the microCT imaging, the samples were immersed in a 60 ml bath of PBS for 6 h at 7 °C to wash out the contrast agent from the cartilage tissue and subsequently frozen until histological analysis.

Image analysis. The concentrations of iodine and gadolinium in the mixtures and partitions within cartilage can be solved using Beer-Lambert law and Bragg's rule[42]:

$$I_E = I_{0,E} e^{-\alpha_E} \tag{1}$$

$$\alpha_E = \mu_{I,E} C_I + \mu_{Gd,E} C_{Gd}, \tag{2}$$

where I_E and $I_{0,E}$ are the intensities of the transmitted and incident X-ray beams of energy E, α_E the attenuation coefficient, $\mu_{I,E}$ and $\mu_{Gd,E}$ the mass attenuation coefficients, and C_I and C_{Gd} the concentrations of iodine (I) and gadolinium (Gd). Thus, the concentrations C_I and C_{Gd} can be solved from the following equations (in the case X-ray energies 25 keV and 37 keV are used):

$$C_I = \frac{\alpha_{37keV} \mu_{Gd,25keV} - \alpha_{25keV} \mu_{Gd,37keV}}{\mu_{I,37keV} \mu_{Gd,25keV} - \mu_{I,25keV} \mu_{Gd,37keV}} \tag{3}$$

$$C_{Gd} = \frac{\alpha_{25keV} \mu_{I,37keV} - \alpha_{37keV} \mu_{I,25keV}}{\mu_{I,37keV} \mu_{Gd,25keV} - \mu_{I,25keV} \mu_{Gd,37keV}}. \tag{4}$$

The articulating surface and bone-cartilage interface were first delineated manually from the CT image stacks using a segmentation software (Seg3D v2.4, The University of Utah, Salt Lake City, UT, USA). Then, the CA4+ and gadoteridol partition profiles through the cartilage layer were calculated using a custom-made MATLAB (R2014a, MathWorks, Inc., USA) script as described in more detail in Saukko et al.[29]. The volume of interest (VOI) was selected to be 2275 µm × 2275 µm × cartilage thickness and was delineated from the CT image stack to closely preserve the initial volume of cartilage. Next, the mean vertical X-ray attenuation profiles from the subchondral bone through to the articular surface were obtained by averaging the pixels in the horizontal direction in the VOI for native cartilage as well as for the samples imaged at the 1 h and 2 h time points. From the X-ray attenuation profiles, the concentrations of CA4+ (iodine, C_I) and gadoteridol (gadolinium, C_{Gd}) in cartilage were calculated (Eqs 3 and 4). Equations 3 and 4 require data on attenuation caused by iodine and gadolinium. Consequently, the attenuation as a result of cartilage tissue and water present in the VOI was eliminated from the 1 h and 2 h X-ray attenuation profiles. This was accomplished by subtracting the X-ray attenuation profile of native cartilage tissue from the attenuation profiles recorded on each time point, after which Eqs 2 and 3 were used to calculate the concentrations of iodine and gadolinium in the cartilage.

Partitions of CA4+ and gadoteridol were determined by dividing the obtained contrast agent concentration inside the cartilage with the contrast agent concentration in the immersion bath. Finally, the CA4+ partition was normalized by dividing the CA4+ partition in cartilage with the gadoteridol partition. This was performed to minimize the effects on uptake of cationic contrast agent, as caused by a difference in water content and steric hindrance. The normalization was assumed to improve the diagnostic sensitivity of cationic contrast agent for cartilage PG content. Further, CA4+ and gadoteridol concentration maps of the cartilage were calculated by averaging the image slices in the VOI in the horizontal direction. After obtaining the average X-ray attenuation in the cartilage tissue and water from the baseline image stack, their effect was removed by subtracting the baseline image stack from the 1 and 2 h images similarly as was done when calculating the X-ray attenuation profiles. Then, the CA4+ and gadoteridol distributions were calculated for each pixel in the image (Eqs 3 and 4). Finally, the CA4+ and gadoteridol distributions within the cartilage samples were averaged to obtain the average distributions of the contrast agents.

Histological analysis. After synchrotron microCT imaging, the frozen samples were thawed and cut in half. The first half was fixed in 10% formalin and then dehydrated in ascending series of ethanol for the reference histological analysis. After dehydration, the samples were decalcified in EDTA and embedded in paraffin in order to cut 3 µm thick sections. Then, the paraffin was removed, and Safranin-O staining was performed to study the spatial FCD (i.e. PG) distribution in the cartilage. After staining, quantitative digital densitometry measurements were conducted to study the optical density (OD, e.g., PG distribution) in cartilage using a light microscope (Nikon Microphot-FXA, Nikon Co., Japan) equipped with a monochromatic light source and a 12-bit CCD camera (ORCA-ER, Hamamatsu Photonics K.K., Japan). System was calibrated using neutral density filters (Schott, Germany) covering OD range from 0 to 2.6. Histological images of Safranin-O stained sections were also imaged with a light microscope (Leica MZ75, Leica Microsystems Ltd., Switzerland) fitted with a CCD camera (Nikon digital sight DS-Fi2, Nikon Co., Japan). The depth-wise PG content within each cartilage sample was determined as an average of three sections. From the second half, water content was determined by calculating the difference between the wet weight and dry weight after freeze-dying the samples for 20 h.

Statistical analysis. Relation between the known and measured iodine and gadolinium concentrations in the contrast agent mixtures was studied using Pearson's correlation. As our study had relatively small number of samples and since Shapiro-Wilk test showed that the data was not from a normally distributed population, a nonparametric test was chosen. Therefore, significance of the differences in parameter values between the intact and injured samples were calculated utilizing Wilcoxon signed-rank test. The statistical significance of dependence between the contrast agent partitions in superficial cartilage layer (20% of the cartilage thickness) and optical density was determined. All statistical analyses were conducted using SPSS software (v. 24.0 SPSS Inc., IBM Company, USA). $P < 0.05$ was the limit for statistical significance.

	Known concentration (mg I/ml)/(mg Gd/ml)	Measured concentration (mg I/ml)/(mg Gd/ml)	Error (%)
Mixture 1	20/5	19.64/5.14	1.8/2.8
Mixture 2	10/10	10.09/9.92	0.9/0.8
Mixture 3	5/20	4.88/19.61	2.4/2.0
Mixture 4	3/3	2.84/3.22	5.3/7.3

Table 1. Known and measured iodine and gadolinium concentrations in the contrast agent mixtures.
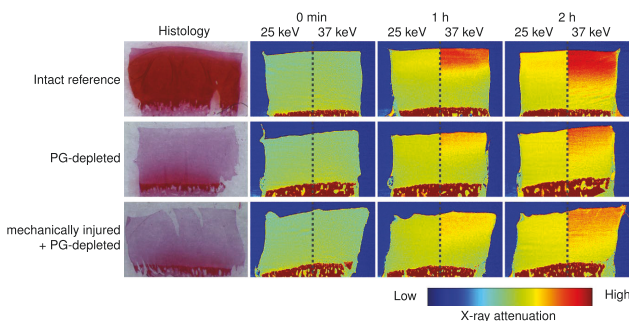

Figure 1. Safranin-O stained histological section and synchrotron microCT images (average of 21 consecutive 6.5 μm thick slices) of representative intact, proteoglycan (PG) depleted, and mechanically injured + PG-depleted samples, as acquired with both photon energies (25 keV and 37 keV energies) prior to the contrast agent immersion and 1 and 2 h after the immersion. These synchrotron microCT images highlight the changes in X-ray attenuation at two photon energies during diffusion of contrast agent into articular cartilage. Based on these images, the depth-wise partitions of gadoteridol and CA4+ is solved using the Beer-Lambert law and Bragg's rule.

Results

Measured iodine and gadolinium concentrations in the contrast agent mixtures correlated linearly with the known concentrations ($R^2 = 0.99$, $P < 0.001$, Table 1), the average error being 2.89%. Synchrotron microCT images, obtained with the two energies, showing changes in X-ray attenuation during contrast agent diffusion together with corresponding histological images are presented in Fig. 1. The uptake of non-ionic gadoteridol into mechanically injured + PG-depleted samples was significantly higher than into intact reference samples at both imaging time points ($P < 0.008$, Fig. 2). No significant difference in gadoteridol uptake was observed between the intact reference and PG-depleted samples. The uptake of cationic agent (CA4+), as a function of cartilage depth, was significantly higher in the intact samples than in damaged samples (Fig. 2B). After normalization of the CA4+ partition with the gadoteridol partition, cartilage degradation and injury were more effectively detected. The detection of these features was significantly improved, especially, for the mechanically injured samples, as indicated by the statistically significant differences present in the deeper cartilage depth as shown in Fig. 2. No statistically significant changes in water contents between the sample groups were observed in water content analysis. Concentration maps of CA4+ and gadoteridol are shown in Fig. 3. The PG content (i.e., OD of Safranin-O stained sections) was significantly lower in PG-depleted ($P = 0.008$) and mechanically injured + PG-depleted samples ($P = 0.008$) than in intact samples (Figs 1 and 2D). Correlations between OD and CA4+ partition values were determined for the superficial cartilage layer (20% of the cartilage thickness); the obtained Spearman's rhos ($P < 0.001$) for non-normalized CA4+ partitions after 1 and 2 h were $\rho = 0.683$ and $\rho = 0.738$, respectively. For normalized CA4+ partitions the spearman's rhos after 1 and 2 h were $\rho = 0.734$ and $\rho = 0.662$.

Discussion

In this synchrotron-based microCT study, the QDECT technique is evaluated along with a dual contrast agent solution consisting of a mixture of the cationic, iodinated contrast agent (CA4+) and the non-ionic, gadolinium-based contrast agent (gadoteridol). The application of cationic contrast agents for imaging soon after the contrast agent administration is challenging as the diffusion of cationic contrast agent into cartilage is governed by the composition and structure of cartilage extracellular matrix. In degenerated cartilage, reduced PG content decreases the diffusion of the cationic agent while weakened steric hindrance and elevated water content increase agent diffusion resulting in opposite effects on the diffusion[43]. In this study, we demonstrate that by using QDECT, with a mixture of cationic and non-ionic contrast agents, cartilage PG content and changes in water content and steric hindrance can be evaluated simultaneously. In addition, mechanical impact was found to increase the uptake of
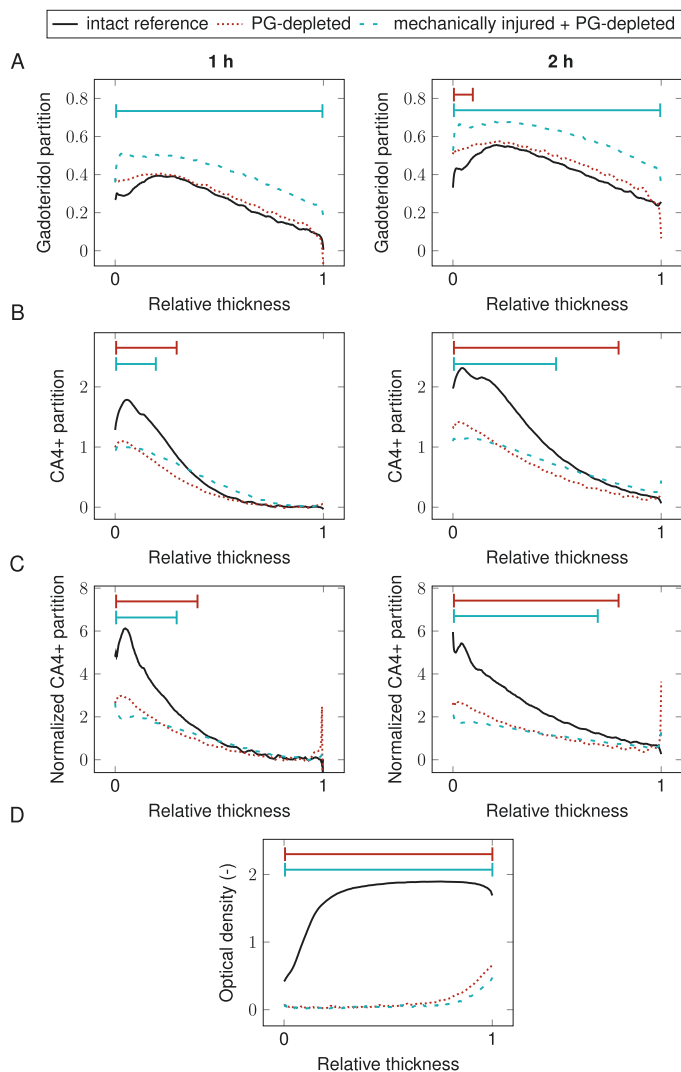
Figure 2. Mean depth-wise partitions of (**A**) gadoteridol, (**B**) CA4+, and (**C**) normalized CA4+ in cartilage after 1 h and 2 h immersion in contrast agent mixture. (**D**) optical density profile through cartilage thickness. ⊢——⊣ represents the statistically significant ($P < 0.05$) difference between intact and damaged samples. 0 denotes the cartilage surface and 1 cartilage-bone interface.

non-charged gadoteridol into cartilage. Furthermore, the use of monochromatic X-ray energies eliminates the problems arising from the use of continuous X-ray spectrum.

The results show, known CA4+ and gadoteridol concentrations in the contrast agent mixtures corre-late linearly with the measured concentrations ($R^2 = 0.99$, $P < 0.001$), indicating that CA4+ and gadoteridol
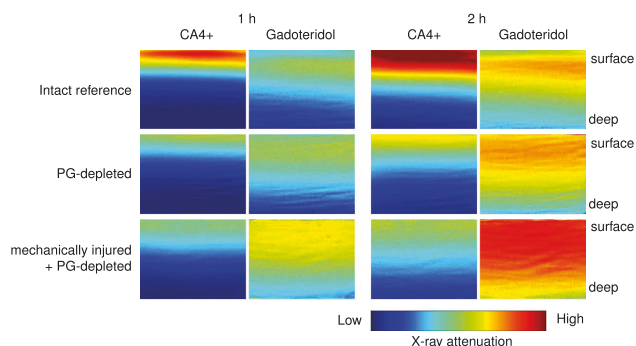
Figure 3. CA4+ and gadoteridol distribution within cartilage (cartilage surface on the top edge of the image and cartilage-bone interface on the bottom edge) at 1 and 2 h after contrast agent immersion for intact, proteoglycan (PG) depleted, and mechanically injured + PG-depleted samples. CA4+ distributes into cartilage proportionally to PG content while gadoteridol distributes related to water content and steric hindrance of the tissue.

concentrations in aqueous solution can be measured accurately using QDECT. Depth-wise contrast agent partition profiles, acquired with synchrotron microCT (Fig. 2), illustrate the highest gadoteridol uptake is observed with mechanically injured, PG-depleted samples. This increase in gadoteridol uptake is attributed to reduced articular cartilage steric hindrance due to mechanical impact[28,32] affording greater porosity and increased surface area, owing to the cracks on the cartilage surface.

The uptake of CA4+ was found to be significantly higher in intact samples than in injured samples. This result is consistent with previous observations[22,23,31,44] that showed that the cationic CA4+ uptake is proportionally related to the cartilage PG content[14,22], and intact cartilage has higher PG content compared to injured samples. When comparing the PG-depleted samples with the mechanically injured + PG-depleted samples, the latter group shows slightly higher CA4+ uptake than the PG-depleted samples. This is likely due to reduced steric hindrance caused by the mechanical damage as water content showed no significant changes in water content measurements. This result indicates that reduced steric hindrance affects the diagnostic potential of CA4+.

At early time points of diffusion, CA4+ is unable to distinguish intact (e.g., high PG content) from degenerated cartilage (e.g., mechanical injured), as similar uptake ratios are observed[43]. We hypothesized that the sensitivity of cationic CA4+ in early time points could be improved by normalizing the CA4+ partition with that of gadoteridol, a non-ionic contrast agent. The present results show that normalizing the CA4+ partition with that of gadoteridol increases the capability of CA4+ to differentiate injured and intact tissue. This normalization procedure improves the diagnostic sensitivity of CA4+ to detect PG content, however, only moderately since the enzymatic degradation and mechanical impact had no statistical significant effect on tissue water content[32,36]. In arthritic cartilage, the water content is increased by approximately 10%[45,46]. Thus, the normalization of CA4+ attenuation can increase its diagnostic sensitivity of arthritic cartilage.

To obtain optimal results, the acquisitions of the imaging data are conducted as consecutively as possible using the two energies. At early time points after contrast agent immersion, the diffusion rate is at its highest and the depth-wise partition is constantly changing. Thus, conducting these acquisitions as consecutively as possible is of utmost importance. The time difference between the starting points of 25 keV and 37 keV acquisitions was approximately 5 min 20 s, and the acquisition took approximately 128 seconds. During this time, diffusion continues to occur within the cartilage. Thus, as the obtained attenuation profiles with two energies are not obtained exactly at the same time point, the X-ray attenuation profiles represent an average value over the scan time rather than a precise value. Nevertheless, these issues minimally impacted the results or conclusions as the imaging settings were similar for all the samples and the samples were of similar thickness.

Compared with MRI, the drawback of QDECT is the application of ionizing radiation. However, the patient doses used in routine knee imaging are small (27–48 μSv effective dose) and even lower (13 μSv effective dose) with modern orthopedic cone beam CT scanners[47]. A further limitation of the current CECT technique is the requirement of two scans (arthrographic scan and delayed scan). In a clinical setting, performing two scans is time consuming doubling the radiation dose and being logistically challenging. Fortunately, as dual-energy CT scanners have become more widespread, imaging with two energies is now conducted simultaneously, supporting the application of the QDECT.

In this paper, we describe a proof-of-principle approach to study the potential of QDECT for cartilage diagnostics at clinically feasible imaging time points. Future studies will focus on minimizing the problems arising from the continuous X-ray energy spectra applied in clinical devices and exploring the technique in a true clinical setting for *in vivo* diagnostics. Additionally, as photon counting detector (PCD) systems with energy

discrimination capabilities have evolved rapidly during the last 10 years, the potential of QDECT together with PCD utilizing two energy thresholds should be examined.

In conclusion, QDECT allows simultaneous and quantitative evaluation of cationic and non-ionic contrast agent uptake within cartilage at early imaging time points. The shortcoming related to CA4+ diffusion is minimized by normalizing its uptake with that of a non-ionic contrast agent. Further, by utilizing monochromatic energies the problems related to continuous X-ray spectra (mainly beam hardening) are avoided. The present dual contrast method provides valuable information on early tissue changes in cartilage related to PTOA. Specifically, the uptake of cationic agent (CA4+) was significantly lower ($P < 0.05$) in both injured sample group compared with the intact samples, confirming reduced PG content. Moreover, after normalizing the CA4+ partition with that of gadoteridol (e.g., reducing the effect of reduced steric hindrance and increased water content on contrast agent diffusion), the detection of cartilage degradation and injury was significantly improved. Although, the number of samples was relatively low ($n = 11$/group, resulting in total of $N = 33$ samples), the results were found statistically significant with the current number of samples. Potentially, QDECT will allow enhanced diagnostics of the disease, improved planning of surgical treatment options, and better strategies for preventing OA after a traumatic injury.

Data Availability
All data are available from the corresponding author upon reasonable request.

References
1. Anderson, D. D. *et al*. Post-traumatic osteoarthritis: Improved understanding and opportunities for early intervention. *J. Orthop. Res.* **29**, 802–809 (2011).
2. Olson, S. A., Furman, B. D., Kraus, V. B., Huebner, J. L. & Guilak, F. Therapeutic opportunities to prevent post-traumatic arthritis: Lessons from the natural history of arthritis after articular fracture. *J. Orthop. Res.* **33**, 1266–1277 (2015).
3. Li, X. *et al*. Cartilage T1ρ and T2 relaxation times: longitudinal reproducibility and variations using different coils, MR systems and sites. *Osteoarthr. Cartil* **23**, 2214–2223 (2015).
4. Link, T. M., Neumann, J. & Li, X. Prestructural cartilage assessment using MRI. *J. Magn. Reson. Imaging* **45**, 949–965 (2017).
5. Lakin, B. A., Snyder, B. D. & Grinstaff, M. W. Assessing Cartilage Biomechanical Properties: Techniques for Evaluating the Functional Performance of Cartilage in Health and Disease. *Annu. Rev. Biomed. Eng.* **19**, 27–55 (2017).
6. Kokkonen, H. T. *et al*. Delayed Computed Tomography Arthrography of Human Knee Cartilage *In Vivo*. *Cartilage* **3**, 334–341 (2012).
7. Kokkonen, H. T. *et al*. *In vivo* diagnostics of human knee cartilage lesions using delayed CBCT arthrography. *J. Orthop. Res.* **32**, 403–412 (2014).
8. Myller, K. A. H. *et al*. *In Vivo* Contrast-Enhanced Cone Beam CT Provides Quantitative Information on Articular Cartilage and Subchondral Bone. *Ann. Biomed. Eng.* **45**, 811–818 (2017).
9. Yoo, H. J. *et al*. Contrast-enhanced CT of Articular Cartilage: Experimental Study for Quantification of Glycosaminoglycan Content in Articular Cartilage. *Radiology* **261**, 805–812 (2011).
10. Stewart, R. C. *et al*. Contrast-Enhanced Computed Tomography Enables Quantitative Evaluation of Tissue Properties at Intrajoint Regions in Cadaveric Knee *Cartilage*. *Cartilage* (2016).
11. Silvast, T. S. *et al*. Diffusion and near-equilibrium distribution of MRI and CT contrast agents in articular cartilage. *Phys. Med. Biol.* **54**, 6823–6836 (2009).
12. Kallioniemi, A. S., Jurvelin, J. S., Nieminen, M. T., Lammi, M. J. & Töyräs, J. Contrast agent enhanced pQCT of articular cartilage. *Phys. Med. Biol.* **52**, 1209–1219 (2007).
13. Stewart, R. C. *et al*. Contrast-enhanced CT with a High-Affinity Cationic Contrast Agent for Imaging *ex Vivo* Bovine, Intact *ex Vivo* Rabbit, and *in Vivo* Rabbit Cartilage. *Radiology* **266**, 141–150 (2013).
14. Joshi, N. S., Bansal, P. N., Stewart, R. C., Snyder, B. D. & Grinstaff, M. W. Effect of Contrast Agent Charge on Visualization of Articular Cartilage Using Computed Tomography: Exploiting Electrostatic Interactions for Improved Sensitivity. *J. Am. Chem. Soc.* **131**, 13234–13235 (2009).
15. Palmer, A. W., Guldberg, R. E. & Levenston, M. E. Analysis of cartilage matrix fixed charge density and three-dimensional morphology via contrast-enhanced microcomputed tomography. *Proc. Natl. Acad. Sci. USA* **103**, 19255–60 (2006).
16. Lusic, H. & Grinstaff, M. W. X-ray-Computed Tomography Contrast Agents. *Chem. Rev.* **113**, 1641–1666 (2013).
17. Lin, P. M., Chen, C.-T. C. & Torzilli, P. A. Increased stromelysin-1 (MMP-3), proteoglycan degradation (3B3- and 7D4) and collagen damage in cyclically load-injured articular cartilage. *Osteoarthr. Cartil.* **12**, 485–496 (2004).
18. Buckwalter, J. A. Mechanical Injuries of Articular Cartilage. *Iowa Orthop. J.* **12**, 50 (1992).
19. Silvast, T. S., Jurvelin, J. S., Aula, A. S., Lammi, M. J. & Töyräs, J. Contrast Agent-Enhanced Computed Tomography of Articular Cartilage: Association with Tissue Composition and Properties. *Acta radiol.* **50**, 78–85 (2009).
20. Silvast, T. S., Jurvelin, J. S., Lammi, M. J. & Töyräs, J. pQCT study on diffusion and equilibrium distribution of iodinated anionic contrast agent in human articular cartilage – associations to matrix composition and integrity. *Osteoarthr. Cartil.* **17**, 26–32 (2009).
21. Bashir, A., Gray, M. L., Boutin, R. D. & Burstein, D. Glycosaminoglycan in articular cartilage: *in vivo* assessment with delayed Gd(DTPA)(2-)-enhanced MR imaging. *Radiology* **205**, 551–8 (1997).
22. Bansal, P. N., Stewart, R. C., Entezari, V., Snyder, B. D. & Grinstaff, M. W. Contrast agent electrostatic attraction rather than repulsion to glycosaminoglycans affords a greater contrast uptake ratio and improved quantitative CT imaging in cartilage. *Osteoarthr. Cartil.* **19**, 970–976 (2011).
23. Lakin, B. A. *et al*. Contrast enhanced CT attenuation correlates with the GAG content of bovine meniscus. *J. Orthop. Res.* **31**, 1765–1771 (2013).
24. Lakin, B. A. *et al*. Cationic agent contrast-enhanced computed tomography imaging of cartilage correlates with the compressive modulus and coefficient of friction. *Osteoarthr. Cartil.* **21**, 60–68 (2013).
25. Bhattarai, A. *et al*. Quantitative Dual Contrast CT Technique for Evaluation of Articular Cartilage Properties. *Ann. Biomed. Eng.* **46**, 1–9 (2018).
26. Galper, M. W. *et al*. Effect of computed tomography scanning parameters on gold nanoparticle and iodine contrast. *Invest. Radiol.* **47**, 475–81 (2012).
27. Stampanoni, M. *et al*. Tomographic Hard X-ray Phase Contrast Micro- and Nano-imaging at TOMCAT. In 13–17 (2010).
28. Ewers, B., Jayaraman, V., Banglmaier, R. & Haut, R. C. Rate of blunt impact loading affects changes in retropatellar cartilage and underlying bone in the rabbit patella. *J. Biomech.* **35**, 747–755 (2002).
29. Saukko, A. E. A. *et al*. Dual Contrast CT Method Enables Diagnostics of Cartilage Injuries and Degeneration Using a Single CT Image. *Ann. Biomed. Eng.* **45**, 2857–2866 (2017).

30. Honkanen, J. T. J., Turunen, M. J., Tiitu, V., Jurvelin, J. S. & Töyräs, J. Transport of Iodine Is Different in Cartilage and Meniscus. *Ann. Biomed. Eng.* **44**, 2114–2122 (2016).
31. Honkanen, J. T. J. *et al.* Cationic Contrast Agent Diffusion Differs Between Cartilage and Meniscus. *Ann. Biomed. Eng.* **44**, 2913–2921 (2016).
32. Kokkonen, H. T., Jurvelin, J. S., Tiitu, V. & Töyräs, J. Detection of mechanical injury of articular cartilage using contrast enhanced computed tomography. *Osteoarthr. Cartil.* **19**, 295–301 (2011).
33. Kokkonen, H. T. *et al.* Computed tomography detects changes in contrast agent diffusion after collagen cross-linking typical to natural aging of articular cartilage. *Osteoarthr. Cartil.* **19**, 1190–1198 (2011).
34. Moody, H. R. *et al. In vitro* degradation of articular cartilage: does trypsin treatment produce consistent results? *J. Anat.* **209**, 259–267 (2006).
35. Harris, E. D., Parker, H. G., Radin, E. L. & Krane, S. M. Effects of proteolytic enzymes on structural and mechanical properties of cartilage. *Arthritis Rheum.* **15**, 497–503 (1972).
36. Rieppo, J. *et al.* Structure-function relationships in enzymatically modified articular cartilage. *Cells. Tissues. Organs* **175**, 121–32 (2003).
37. Stampanoni, M. *et al.* TOMCAT: A beamline for TOmographic Microscopy and Coherent rAdiology experimenTs. In *AIP Conference Proceedings* **879**, 848–851 (AIP, 2007).
38. Margaritondo, G. & Tromba, G. Coherence-based edge diffraction sharpening of x-ray images: A simple model. *J. Appl. Phys.* **85**, 3406 (1999).
39. Monnin, P. *et al.* Quantitative characterization of edge enhancement in phase contrast x-ray imaging. *Med. Phys.* **31**, 1372–1383 (2004).
40. Marone, F. & Stampanoni, M. Regridding reconstruction algorithm for real-time tomographic imaging. *J. Synchrotron Radiat.* **19**, 1029–1037 (2012).
41. Lovric, G., Mokso, R., Schlepütz, C. M. & Stampanoni, M. A multi-purpose imaging endstation for high-resolution micrometer-scaled sub-second tomography. *Phys. Medica* **32**, 1771–1778 (2016).
42. Rangacharyulu, C. *Physics of nuclear radiations: concepts, techniques and applications.* (CRC Press, 2013).
43. Karhula, S. S. *et al.* Micro-Scale Distribution of CA4+ in *Ex vivo* Human Articular Cartilage Detected with Contrast-Enhanced Micro-Computed Tomography Imaging. *Front. Phys.* **5** (2017).
44. Stewart, R. C. *et al.* Synthesis and Preclinical Characterization of a Cationic Iodinated Imaging Contrast Agent (CA4+) and Its Use for Quantitative Computed Tomography of *Ex Vivo* Human Hip Cartilage. *J. Med. Chem.* **60**, 5543–5555 (2017).
45. Mankin, H. J. & Thrasher, A. Z. Water content and binding in normal and osteoarthritic human cartilage. *J. Bone Joint Surg. Am.* **57**, 76–80 (1975).
46. Guilak, F., Ratcliffe, A., Lane, N., Rosenwasser, M. P. & Mow, V. C. Mechanical and biochemical changes in the superficial zone of articular cartilage in canine experimental osteoarthritis. *J. Orthop. Res.* **12**, 474–484 (1994).
47. Koivisto, J., Kiljunen, T., Wolff, J. & Kortesniemi, M. Assessment of effective radiation dose of an extremity CBCT, MSCT and conventional X ray for knee area using MOSFET dosemeters. *Radiat. Prot. Dosimetry* **157**, 515–524 (2013).

Acknowledgements

Author Contributions

The conception and design of the study was done by A.E.A. Saukko, M.J. Turunen, M.K.M. Honkanen, J.T.J. Honkanen, M. Grinstaff, J.S. Jurvelin, and J. Töyräs. A.E.A. Saukko, M.K.M. Honkanen, M.J. Turunen, and G. Lovric participated in data acquisition. Digital densitometry measurements were conducted by V. Tiitu. A.E.A. Saukko analysed the data and data interpretation was done by A.E.A. Saukko, M.J. Turunen, M.K.M. Honkanen, J.T.J. Honkanen, and J. Töyräs. A.E.A. Saukko, M. Grinstaff, and J. Töyräs drafted the manuscript. All the authors critically reviewed and approved the final manuscript.

Additional Information

Competing Interests: The authors declare no competing interests.

Publisher's note: Springer Nature remains neutral with regard to jurisdictional claims in published maps and institutional affiliations.

Paper **III**

BMES BIOMEDICAL ENGINEERING SOCIETY

Original Article

Triple Contrast CT Method Enables Simultaneous Evaluation of Articular Cartilage Composition and Segmentation

MIITU K. M. HONKANEN [iD],[1,2] ANNINA E. A. SAUKKO [iD],[1,3] MIKAEL J. TURUNEN [iD],[1,4] WUJUN XU [iD],[1] GORAN LOVRIC [iD],[5,6] JUUSO T. J. HONKANEN [iD],[7] MARK W. GRINSTAFF [iD],[8] VESA-PEKKA LEHTO [iD],[1] and JUHA TÖYRÄS [iD][1,2,9]

[1]Department of Applied Physics, University of Eastern Finland, P.O. Box 1627, 70211 Kuopio, Finland; [2]Diagnostic Imaging Center, Kuopio University Hospital, Kuopio, Finland; [3]Department of Medical Physics, Turku University Hospital, Turku, Finland; [4]SIB-labs, University of Eastern Finland, Kuopio, Finland; [5]Centre d'Imagerie BioMédicale, École Polytechnique Fédérale de Lausanne, Lausanne, Switzerland; [6]Swiss Light Source, Paul Scherrer Institute, Villigen, Switzerland; [7]Center of Oncology, Kuopio University Hospital, Kuopio, Finland; [8]Departments of Biomedical Engineering, Chemistry, and Medicine, Boston University, Boston, MA, USA; and [9]School of Information Technology and Electrical Engineering, The University of Queensland, Brisbane, Australia

Associate Editor Sean S. Kohles oversaw the review of this article.

Abstract—Early degenerative changes of articular cartilage are detected using contrast-enhanced computed tomography (CT) with a cationic contrast agent (CA). However, cationic CA diffusion into degenerated cartilage decreases with proteoglycan depletion and increases with elevated water content, thus hampering tissue evaluation at early diffusion time points. Furthermore, the contrast at synovial fluid-cartilage interface diminishes as a function of diffusion time hindering accurate cartilage segmentation. For the first time, we employ quantitative dual-energy CT (QDECT) imaging utilizing a mixture of three CAs (cationic CA4+ and non-ionic gadoteridol which are sensitive to proteoglycan and water contents, respectively, and bismuth nanoparticles which highlight the cartilage surface) to simultaneously segment the articulating surfaces and determine of the cartilage condition. Intact healthy, proteoglycan-depleted, and mechanically injured bovine cartilage samples ($n = 27$) were halved and imaged with synchrotron microCT 2-h post immersion in triple CA or in dual CA (CA4+ and gadoteridol). CA4+ and gadoteridol partitions were determined using QDECT, and pairwise evaluation of these partitions was conducted for samples immersed in dual and triple CAs. In conclusion, the triple CA method is sensitive

to proteoglycan depletion while maintaining sufficient contrast at the articular surface to enable detection of cartilage lesions caused by mechanical impact.

Keywords—Triple contrast agent, Dual contrast agent, Computed tomography, Contrast-enhanced computed tomography, Post-traumatic osteoarthritis, Synchrotron microCT.

INTRODUCTION

Osteoarthritis (OA) arises due to prolonged use, over use, or injury of an articulating joint with a breakdown of cartilage and sclerosis of subchondral bone causing pain, joint stiffness, swelling, and mobility loss.[1,4,32,35] Post-traumatic osteoarthritis (PTOA) is one form of OA caused by an acute injury of a knee joint resulting from a sport accident, a fall, or any other source of physical trauma, and it primarily affects younger individuals.[1] However, by identifying OA early on, the progression of the damage or injury can be slowed down or even prevented using surgical and pharmaceutical interventions.[1,41] Thus, methods for early diagnosis of cartilage injuries are needed. Magnetic resonance imaging (MRI) is an important tool in diagnosis of cartilage degeneration and PTOA. It is sensitive to the water content in cartilage tissue, the 3D architecture of the collagen network, and also to proteoglycan (PG) content.[27,30] However, MRI

suffers from its relatively long *in vivo* imaging acquisition times, high costs, and being unsuitable for imaging patients with implanted medical devices that are incompatible with MRI.[26,30]

Contrast-enhanced computed tomography (CECT) allows imaging with high-resolution, short scan times and, thus, with less motion artifacts at approximately half the cost of MRI, providing an alternative imaging method to evaluate the cartilage condition. Even though CECT exploits ionizing radiation for extremity imaging, the doses involved in clinical cone-beam CT (CBCT) instruments are low with effective doses below 50 μSv.[20] CECT utilizes contrast agents that enhance the contrast at synovial fluid-cartilage interface where the natural contrast is nearly non-existent due to similar X-ray absorptions. In addition to providing the contrast between cartilage and synovial fluid, contrast agents reveal degenerative changes in cartilage.[16,17,34,42,47,48,53] The uptake and diffused partition of contrast agents are altered in degenerated cartilage tissue due to degeneration-related changes including (1) decreased cartilage fixed charge density (FCD) *via* loss of PGs, (2) increased water content, and (3) disruption of the superficial collagen network.[7,28] Therefore, CECT could be used along with MRI to detect internal articular cartilage and meniscus[11,24] degeneration after acute injury. In addition, CECT allows simultaneous assessment of the bony structures of the joint.[39,55]

Anionic or non-ionic contrast agents are traditionally used in CECT imaging but a recently introduced cationic contrast agent (CA4 +) shows superior sensitivity at diffusion equilibrium to detect tissue PG content.[2,24,25] Despite this, the widespread use of CA4 + is hindered due to suboptimal performance at imaging times during early diffusion (0–2 h from contrast agent administration).[18,22] The distribution of cationic contrast agents with articular cartilage is proportional to PG content as the negative fixed charge carried by PG molecules attracts the positively charged contrast agents. However, especially in the early stage of diffusion, the diffusion of cationic contrast agent is also controlled by degeneration-related factors having opposite effects; the loss of PGs decreases the diffusion of cationic contrast agent while increase in water content and decrease in steric hindrance (i.e., physical diffusion barrier of the tissue caused by collagen network architecture and PGs in the matrix) increase the diffusion. This shortcoming can be overcome using a quantitative dual-energy CT technique (QDECT).[5]

QDECT utilizes a mixture of a cationic, iodinated contrast agent (e.g., CA4 +)[2,16] and a non-ionic, gadolinium-based contrast agent (e.g., gadoteridol). As mentioned above, CA4 + possesses a high affinity for PGs. Gadoteridol, on the other hand, as an un-charged molecule distributes into cartilage according to water content and steric hindrance. Thus, by normalizing (e.g., dividing) the cationic contrast agent partition in the cartilage with that of the non-ionic contrast agent, the effects of water content and steric hindrance on the diffusion of the cationic contrast agent can be limited.[5,12,46] Simultaneous determination of the uptake of the both contrast agents within cartilage requires imaging with two X-ray energies. In QDECT, these energies are selected based on element specific absorption k-edge energies of iodine (33.2 keV) and gadolinium (50.3 keV).

Current CECT of a knee joint requires two subsequent CT scans acquired immediately (arthrography) and 30 min to 2 h (delayed arthrography) after the intra-articular injection of contrast agent.[22,23,39] The first scan enables accurate segmentation of articulating surface and lesions while the latter scan provides information on internal changes in cartilage tissue and properties related to the initiation of PTOA by examining the diffusion of the contrast agent in the tissue. The two scans are required since the segmentation of articulating surface and delineation of lesions is difficult from the latter scan owing to diffusion-related loss of image contrast at the synovial fluid-cartilage interface. In addition, no interpretation of the cartilage tissue properties is made from the first scan as the contrast agent has not had sufficient time to diffuse into cartilage. Acquiring two images is logistically burdensome and doubles the radiation dose to a patient. Our recent findings have shown that bismuth nanoparticles (BiNP) can be utilized to overcome this problem of requiring two CT scans.[45] Due to their size, BiNPs are too large to diffuse into the cartilage tissue, and, thus, remain at the synovial space.[45] Using the QDECT with BiNPs and ioxaglate, only the delayed arthrography is required since both the segmentation and evaluation of the cartilage condition can be done simultaneously.

In this study, we introduce for the first time a triple contrast agent composed of three contrast agents: (1) cationic, iodine-based CA4 +, (2) non-ionic, gadolinium-based gadoteridol, and (3) BiNP suspension. Using the triple contrast agent, we hypothesize that the PG and interstitial water contents in articular cartilage will be simultaneously and quantitatively assessed based on CA4 + and gadoteridol distributions within tissue (Fig. 1). Further, we hypothesize that accurate segmentation of the articulating surface from the delayed CT arthrography images will be facile as BiNPs maintain good contrast between the articulating surface and immersion bath. To address these hypotheses, intact healthy, proteoglycan-depleted, and mechanically injured cartilage samples are evaluated using synchrotron microCT as it provides fast tomographic

Immediately after
contrast agent
administration

Healthy intact cartilage
delayed imaging

Degenerated cartilage
delayed imaging

NP Bi₂O₃
nano-
particles   ● CA4+   ◀ Gadoteridol   ⠿⠿ Proteoglycan
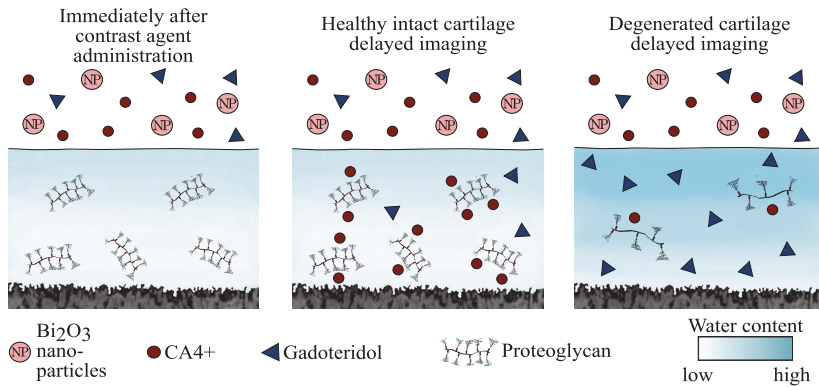
Water content

low   high

FIGURE 1.   The uptake of cationic contrast agent (CA4+) is proportional to the fixed charge density conferred by proteoglycans (PGs). Healthy cartilage has a high PG content, and thus the uptake of cationic contrast agent (CA4+) is also high. In degenerated cartilage the uptake of cationic contrast agent into cartilage matrix is limited due to decreased PG content. On the other hand, as the tissue degenerates, the tissue water content increases and steric hindrance decreases allowing more contrast agent molecules (both CA4+ and gadoteridol) to penetrate the tissue. Bismuth nanoparticles (average diameter of 194 nm) are too large to be able to diffuse into either healthy or degenerated cartilage, thus maintaining the contrast at the articulating surface at all diffusion time points.

imaging with monochromatic X-ray spectra and high resolution.[51]

MATERIALS AND METHODS

Intact bovine patellae ($N = 9$) were dissected from skeletally mature stifle joints obtained from a local butcher (Savo-Karjalan liha Oy, Finland) and stored in -20 °C wrapped in phosphate buffered saline (PBS) soaked gauze in a zip lock bag until sample preparation (a detailed flowchart of the sampling and experiments are presented in Fig. 2). Prior to the sample preparation, the patellae were thawed in a bath of PBS in room temperature, and three adjacent osteochondral plugs ($n = 27$, $d = 7$ mm) were extracted from the upper lateral quadrant of the patellae. Osteochondral plugs were trimmed to include 1 mm of bone underneath the cartilage.[8] The osteochondral plugs were divided into three sample groups: (1) intact, (2) PG-depleted, and (3) mechanically injured. The latter two served as models of cartilage degeneration and acute injury, respectively. Early-stage OA involving PG-loss can be mimicked by treating the cartilage with proteolytic enzymes.[3,6,10,29,38,44,45] Nearly complete PG-depletion in sample group 2 was achieved by immersing the samples in PBS supplemented with trypsin (0.5 mg/mL, Sigma-Aldrich, MO, USA) for 15 h at 37.5 °C, 5% CO_2 atmosphere in an incubator.[38,45] Subsequently, trypsin-treated samples were immersed in PBS for 2 h at 7 °C to suppress the

degradation process. To mimic disruption of the cartilage surface (related to PTOA) and cartilage lesion after the physical trauma caused by impact, a mechanical injury was induced to cartilage.[15] This damage was accomplished using a custom-made drop tower with a stainless-steel impactor (500 g) having a flat polished face.[21,45] The impactor was dropped on the sample from the height of 20 cm[21,45] creating cracks with varying depth and size on the articular surface. After the impact, the impactor was immediately lifted from the articular surface, and the samples were allowed to recover in PBS for 2 h to prevent creep deformation. Then, the samples were imaged with a double contrast agent (mixture of ioxaglate and BiNPs) as described in our previous study,[45] and the contrast agent was subsequently washed out (by immersing the samples in PBS for 2 h) and the samples were frozen (-20 °C) in a zip lock bag as immersed in fresh PBS. Prior to the measurements for this study, the samples were thawed and halved (Fig. 2). The first half was used in digital densitometry (DD) measurements to determine the optical density of Safranin-O stained sections (i.e., the PG content) of the sample while the second half was halved again for pairwise evaluation of dual and triple contrast agents. The sides and the bottom of the quarter osteochondral samples intended for synchrotron microCT imaging were carefully sealed with cyanoacrylate (Loctite, Henkel Norden AB, Dusseldorf, Germany) and stored at -20 °C until the measurements. The quarter samples were measured at synchrotron microCT beamline (X02DA

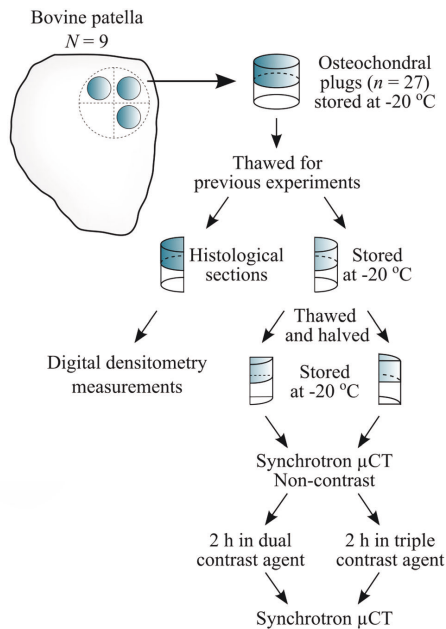**BMES** BIOMEDICAL
ENGINEERING
SOCIETY

Bovine patella
$N = 9$

FIGURE 2. Workflow of the sample preparation and processing protocol. The samples were thawed for previous experiments described in Saukko *et al.*[45] Bovine osteochondral samples were immersed in dual (mixture of CA4+ and gadoteridol) or in triple (mixture of CA4+, gadoteridol and bismuth nanoparticles) contrast agents for 2 h before the synchrotron microCT (μCT) measurements.

TOMCAT beamline of the Swiss Light Source, Paul Scherrer Institut (PSI), Villigen, Switzerland.[50]

BiNPs were prepared by ball-milling (Planetary Micro Mill, Pulverisette 7, Fritsch GmbH, Germany) bismuth(III) oxide powder in two standard milling bowls each containing 10 g of powder, 70 g of 1 mm milling balls, and 40 mL of distilled water. The bismuth oxide powder was milled in 10 min cycles at a speed of 700 rpm with a cooling time of 15 min in between each milling round resulting in a total milling time of 2 h. After milling, 0.5 kDa PEG-silane (2-[Methoxy(polyethyleneoxy)9-12propyl]trimethoxysilane, tech-90, Fluorochem, Old Glossop, UK) was added to the milled NP solution to improve the stability with the mass ratio of PEG-silane to BiNP being 1:6. Next, the mixture was heated up to 260 °C and maintained at a constant temperature for 2.5 h in a protective N_2 atmosphere. Finally, to remove remaining unreacted chemicals, the solution was washed with ethanol three times *via* centrifuge separation

(10,000 rpm, 10 min) and ultrasound re-dispersion. The obtained PEG-coated BiNPs were stored in ethanol until the synchrotron microCT measurements. The BiNPs possess a mean diameter of 194 nm and a surface charge of $- 3.5$ mV (Zetasizer Nano ZS, Malvern Instruments Ltd., Malvern, UK). Prior to measurements, the BiNPs were separated from the solution by centrifuging the BiNP-ethanol solution at 10,000 rpm for 5 min. Then, the NPs were dispersed in distilled water using ultrasound. Subsequently, the centrifuging and re-dispersion process was repeated similarly to ensure that all ethanol was completely washed out from the solution. After the preparation, the NPs were immediately mixed with the other contrast agents and the samples were immersed in the mixture.

Two contrast agent mixtures were prepared; a dual contrast agent and a triple contrast agent. The isotonic (~ 308 mOsm/kg) dual contrast agent composed of a mixture of iodinated cationic contrast agent (CA4+, $q = + 4$, $M = 1499.88$ g/mol) and gadolinium-based, electrically neutral contrast agent (gadoteridol, $q = 0$, $M = 558.69$ g/mol, ProHance[TM], Bracco Diagnostic Inc., Monroe Twp., NJ, USA) was diluted in PBS. In the dual contrast agent, the iodine (I) concentration was 5 mg I/mL and gadolinium (Gd) 10 mg Gd/mL. Moreover, the solution was supplemented with proteolytic inhibitors [5 mM ethylenediaminetetraacetic acid (EDTA, VWR International, France) and 5 mM benzamidine hydrochloride hydrate (Sigma-Aldrich Inc., St Louis, MO, USA)] to suppress general protein degradation in cartilage tissue. Triple contrast agent was otherwise similar to dual contrast agent but BiNPs, with the concentration of 10 mg/mL of BiNPs, were added to the solution. The stability of the BiNPs in the triple contrast agent was analyzed *via* monitoring the particle diameter change during different time periods. The results (Fig. 3) indicate that the BiNPs are stable in the mixed triple contrast agent for more than 24 h.

Synchrotron-based microCT imaging was performed with a third-generation synchrotron-based X-ray source. MicroCT images were acquired by combining 1:1 magnifying visible light optics microscope (Optique Peter, France), a 300 μm thick scintillator (LuAg, CRYTUR spol.s.r.o., Czech Republic), and a scientific complementary metal–oxide–semiconductor (sCMOS) detector (pco.Edge 5.5, PCO AG, Germany). Two monochromatic X-ray energies of 32 and 34 keV from both sides of iodine k-edge (33.2 keV) were selected to maximize the difference in the mass attenuation coefficients of iodine (CA4+). A double-multilayer monochromator with a spectral bandwidth of about 2–3% was used. Imaging geometry resulted in an isometric voxel size of $6.5 \times 6.5 \times 6.5 \ \mu m^3$ and a field of view (FOV) of $16.6 \times 3.5 \ mm^2$. The radiation

exposure was minimized by applying an off-beam alignment system.[33]

Before measuring the bovine samples, a set of CA4+ and gadoteridol phantoms with varying concentrations in distilled water were measured with both X-ray energies to determine the mass attenuation coefficients of the contrast agent compounds. The iodine concentrations in CA4+ phantoms were 3, 6, 12, 18, 24, 30, and 36 mg I/mL and gadolinium concentration in gadoteridol phantoms 6, 9, 12, 15, and 18 mg Gd/mL. Based on these calibration measurements, CA4+ and gadoteridol concentrations within the cartilage tissue can be calculated using QDECT. To validate this technique, contrast agent mixture phantoms having iodine/gadolinium concentrations of 3/18,
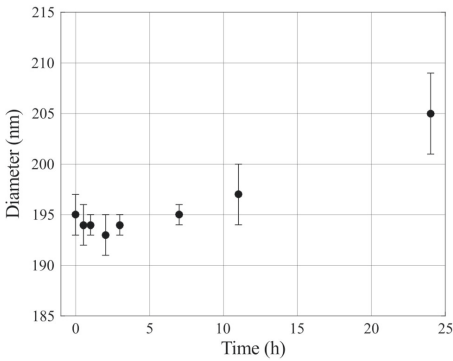

FIGURE 3. The stability of the bismuth nanoparticles was determined by measuring the particle diameter after the CA4+ and gadoteridol were added to the triple contrast agent mixture. The particle diameter change was not significant within 24 h according to the statistical analysis with the One-way ANOVA model ($p > 0.05$), as compared with the original particle diameter.

6/16, 10/14, 16/12, 20/10, 26/8, 32/6, and 40/3 mg/mL were imaged (Fig. 4).

Prior to the contrast agent immersion, non-contrast images of all quarter cartilage samples ($n = 54$) were acquired in the air with 32 and 34 keV X-ray energies. After acquiring the baseline image, the quarter sample pairs obtained from the same patellae were immersed either in dual ($n = 27$) or triple ($n = 27$) contrast agent bath (24 mL, ≥ 100 times the cartilage volume) at $+7\ °C$. After 2 h, all the samples ($n = 54$) were imaged three times, first with 34 keV X-ray beam, then with 32 keV, and again with 34 keV, to minimize the effect of ongoing diffusion by averaging the two 34 keV images. The acquisition time was approximately 129 s with time difference between the subsequent acquisitions being 331 s on average. Highly optimized algorithm based on Fourier methods was used in image reconstruction.[36] The measurement set up is explained in more detail in our previous paper by Saukko *et al.*[46]

The absorbed radiation dose on the samples was evaluated by measuring the X-ray flux with calibrated, passivated, and implanted planar silicon (PIPS) diodes.[33] The measured X-ray flux for 32 keV was 9.8×10^{10} photons/mm^2/s and for 34 keV 1.0×10^{11} photons/mm^2/s. To calculate the absorbed dose, the cartilage samples were modelled as soft tissue (ICRU-44)[56] according to the X-ray mass energy-absorption coefficient from the NIST database.[14] The presence of contrast agent was neglected. The absorbed doses were 0.47 Gy for 32 keV and 0.43 Gy for 34 keV.

The articulating surface and bone-cartilage interface at each time point were defined manually using a segmentation software (Seg3D, version 2.2.1, 2015, University of Utah, Salt Lake City, UT, USA) along a protocol described in more detail in our previous paper.[45] A cylindrical volume of interest (VOI, $d = 1313\ \mu m$, h = cartilage thickness) was delineated
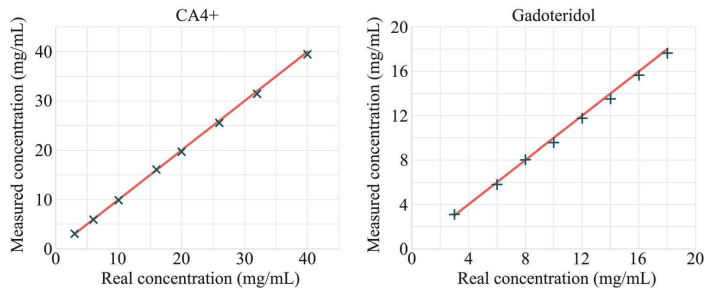
FIGURE 4. The synchrotron microCT measured CA4+ (×) and gadoteridol (+) concentrations with dual energy technique, and the real concentrations (solid line) within mixture phantoms. The relative mean error in measured concentrations were 1.5 and 2.6% for CA4+ and gadoteridol, respectively.

from the center of the bovine sample using a custom-made MATLAB (R2017b, The MathWorks, Inc., Natick, MA, USA) code. The cracks in the mechanically injured samples were removed by thresholding. Then, the depth-wise X-ray attenuation profiles were calculated, and the profiles obtained from the 34 keV acquisitions were averaged to minimize the error caused by ongoing diffusion. The native X-ray attenuation profiles of the cartilage obtained from the non-contrast-enhanced images were subtracted from the contrast-enhanced profiles. Finally, the depth-wise iodine (CA4+) and gadolinium (gadoteridol) partitions within cartilage were determined in two steps: (1) the mass attenuation coefficients of iodine and gadolinium were determined based on the CA4+ and gadoteridol phantoms; (2) Beer-Lambert law and Bragg's rule were used to calculate the concentrations of iodine and gadolinium partitions in the cartilage[43]:

$$\alpha_E = \mu_{I,E} C_I + \mu_{Gd,E} C_{Gd}, \tag{1}$$

where α_E is the X-ray attenuation with energy E, $\mu_{I,E}$ and $\mu_{Gd,E}$ are the mass attenuation coefficients, and C_I and C_{Gd} the concentrations of iodine (I) and gadolinium (Gd), respectively. By applying two energies (32 and 34 keV), the concentrations of iodine and gadolinium at each point can be solved as follows:

$$C_I = \frac{\alpha_{34\,keV}\mu_{Gd,32\,keV} - \alpha_{32}\mu_{Gd,34\,keV}}{\mu_{I,34\,keV}\mu_{Gd,32\,keV} - \mu_{I,32\,keV}\mu_{Gd,34\,keV}} \tag{2}$$

$$C_{Gd} = \frac{\alpha_{32\,keV}\mu_{I,34\,keV} - \alpha_{34\,keV}\mu_{I,32\,keV}}{\mu_{I,34\,keV}\mu_{Gd,32\,keV} - \mu_{I,32\,keV}\mu_{Gd,34\,keV}}. \tag{3}$$

In the analysis, the decrease of the contrast agent concentrations in the surrounding bath due to diffusion was taken into consideration. Moreover, the determined iodine (CA4+) partition profiles were normalized with that of gadolinium (gadoteridol) to reduce the effect of water content and steric hindrance on CA4+ partition and, thereby, to improve the detection of PG content. Further, X-ray attenuation profiles through cartilage depth were divided into superficial (0–10%), middle (10–40%) and deep (40–100%) zones, 0% denoting the articulating surface and 100% the cartilage-bone interface, to compare the contrast agent partition values between the groups (reference, PG-depleted and mechanically injured) and to the corresponding PG distribution (optical density) in each zone.

DD measurements were performed on the second half of the samples to calculate the optical density (OD) by first thawing and subsequently fixing the samples in 10% formalin. Then, ascending series of ethanol and EDTA were used to dehydrate and decalcify the samples, respectively. The samples were embedded in paraffin and cut into 3 μm thick sections. Subsequently, the paraffin was removed, and the samples were stained with Safranin-O which is a cationic dye stoichiometrically binding to the negative fixed charge in cartilage.[19] To examine the spatial FCD distribution in the cartilage, the optical density (i.e., PG distribution) of the samples were measured using quantitative DD. The equipment included a light microscope (Nikon Microphot-FXA, Nikon Co., Japan) equipped with a monochromatic light source (wavelength 492 ± 8 nm) and a 12-bit CCD camera (ORCA-ER, Hamamatsu Photonics K.K., Japan). The system was calibrated using neutral density filters (Schott, Germany) covering OD range from 0 to 2.6. An average of three sections was used to calculate the depth-wise PG content.

Pearson correlation was used to determine the statistical dependency between the contrast agent partitions and PG distribution within cartilage zones. The significance of enhancement, established by normalization, to CA4+ correlations with PG distribution was tested based on Steiger.[52] In addition, the significance of the differences in contrast agent partition values between reference samples and conditioned samples were obtained with Wilcoxon signed-rank test. The difference was defined to be significant when $p < 0.05$. The statistical analyses were conducted using SPSS (v. 25.0 SPSS Inc., IBM Company, Armonk, NY, USA).

RESULTS

The triple contrast agent enhanced the image contrast at the bath-cartilage interface and allowed accurate segmentation of the articulating surfaces at the 2-h time point (Fig. 5). Visual detection of cracks on the cartilage surface of the mechanically injured samples was possible with use of the BiNPs. With the dual contrast agent, the visualization of the bath-cartilage interface and cracks on the cartilage surface was limited. The stability of the BiNPs was measured after mixing the BiNPs, CA4+, and gadoteridol, by determining mean particle diameter at the 2-h time point (193 ± 2 nm; Fig. 3) as well as the 7 and 24-h time points. No change in particle diameter was noted at the 7-h time point, however at the later time point, the diameter of BiNPs slightly increased to 205 ± 4 nm. Even though particle diameter at 24 h was increased, the change was not significant according to the statistical analysis with the One-way ANOVA model ($p > 0.05$) as compared with the original particle diameter. The nanoparticles possessed good colloidal stability in aqueous solution due to the coating with polyethylene glycol (PEG).[40]
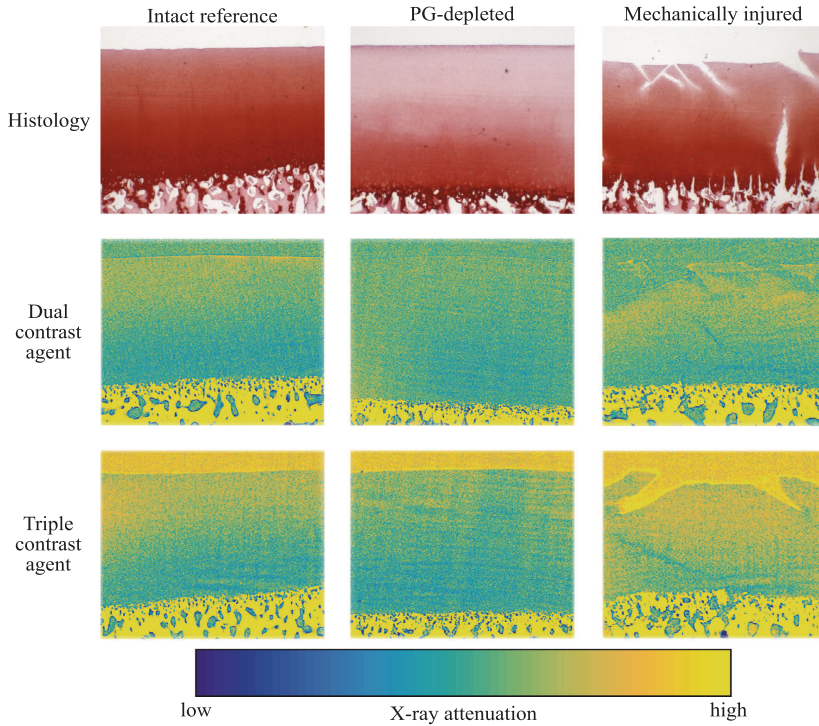
BMES BIOMEDICAL ENGINEERING SOCIETY

FIGURE 5. Safranin-O stained histological sections and synchrotron microCT (32 keV) images (average of five consecutive 6.5 μm thick slices) of the intact reference, PG-depleted, and mechanically injured samples imaged with dual and triple contrast agents 2 h after the contrast agent immersion. Articulating surface and cracks are better visualized with the triple contrast agent owing to better contrast induced by bismuth nanoparticles (BiNPs) that, due to their size, are too large to diffuse into cartilage. The enhancement caused by the BiNPs was similar for 34 keV synchrotron microCT images (not shown). CT images were selected to closely match the locations of the histological sections.

The uptake of CA4+ into intact healthy reference samples was higher as compared with PG-depleted samples, especially at the superficial and middle zones where the difference was significant (Table 1; Fig. 6). A significant difference in CA4+ uptake between intact reference and mechanically injured samples was observed in the superficial and deep zones with the dual contrast agent and in the superficial zone with the triple contrast agent. The normalization of CA4+ partition with that of gadoteridol increased the difference between the intact reference and PG-depleted and mechanically injured samples. In the PG-depleted samples, gadoteridol uptake was significantly higher in all zones for the dual contrast agent while it was greatest in middle and deep zones for the triple contrast agent. In the mechanically injured samples, gadoteridol uptake was greatest in middle and deep zones for the dual agent,

and in all zones with triple agent. A statistically significant ($p < 0.05$) difference between the full thickness partitions of the dual and triple contrast agents were observed for CA4+ (reference and mechanically injured samples), normalized CA4+ (mechanically injured samples), and gadoteridol (reference and mechanically injured samples; Table 1). Statistically significant correlations ($0.504 < r < 0.766$, $0.0001 < p < 0.007$) were found between CA4+ partition and PG distribution with both contrast agent mixtures in superficial and middle zones. Gadoteridol partition correlated significantly ($-0.442 < r < -0.428$, $0.021 < p < 0.026$) with PG distribution only in the deep zone and whole cartilage thickness with dual contrast agent. The normalization significantly improved the correlation between the CA4+ and PG distribution in the middle zone with both contrast agents.

TABLE 1. Full thickness contrast agent partitions, standard deviations and optical density (OD) for intact reference, PG-depleted and mechanically injured samples.

	Contrast agent	Reference	PG-depleted	Mechanical injury
CA4+	Dual	111.7 ± 28.8	86.3 ± 12.1	143.7 ± 35.6
	Triple	129.8 ± 34.8	88.5 ± 9.6	137.3 ± 37.7
Normalized CA4+	Dual	152.3 ± 26.2	100.1 ± 11.6	182.5 ± 29.1
	Triple	163.1 ± 53.2	92.1 ± 8.8	146.4 ± 30.5
Gadoteridol	Dual	64.8 ± 9.5	77.6 ± 10.5	77.6 ± 12.0
	Triple	79.4 ± 10.2	91.2 ± 11.3	93.1 ± 14.9
OD		1.52 ± 0.26	0.41 ± 0.25	1.16 ± 0.22

Statistically ($p < 0.05$) significant differences between the contrast agent partitions for dual and triple contrast agents are marked with square brackets].
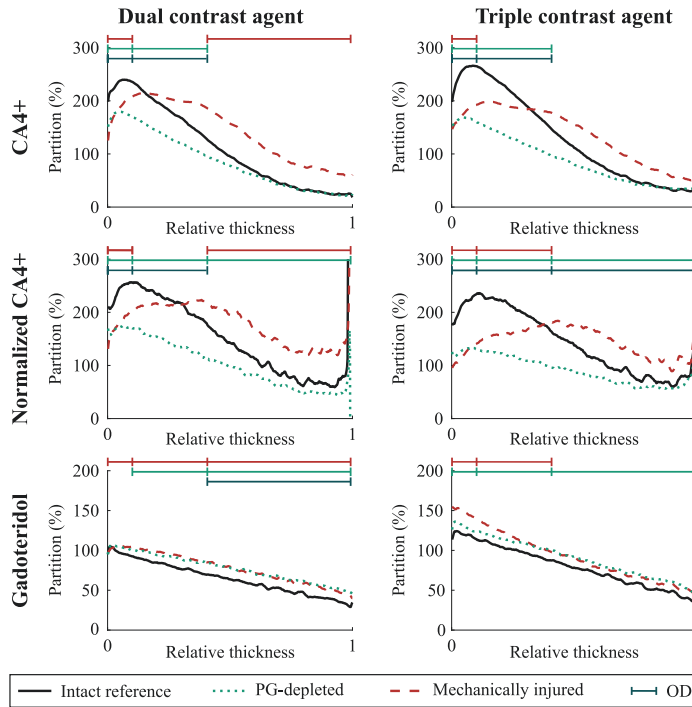
FIGURE 6. Mean ($n = 9$ for each sample group) depth-wise partitions of CA4+, normalized CA4+, and gadoteridol in cartilage 2 h after the immersion in dual or triple contrast agent. |——| represents the statistically significant ($p < 0.05$) difference between the contrast agent partition in the intact reference and proteoglycan (PG)-depleted (turquoise) or mechanically injured (red) sample and statistically significant ($p < 0.05$) correlation with PG distribution (dark green) within the superficial, middle, and deep zones. Partition is defined as contrast agent concentration in the cartilage divided by the concentration of the immersion bath. 0 denotes the articulating surface and 1 the cartilage-bone interface.

BMES BIOMEDICAL ENGINEERING SOCIETY

DISCUSSION

This study evaluates the potential of CECT using the triple contrast agent for assessment of cartilage degeneration and acute injury. We hypothesize that the triple contrast agent will provide a solution for two shortcomings of the current technique. Firstly, simultaneous loss of PGs and decrease in steric hindrance in degenerating cartilage afford opposite effects on CA4+ diffusion, leading to a loss of diagnostic sensitivity at early, clinically feasible, time points. Secondly, contrast at the synovial fluid-cartilage interface is diminished due to contrast agent diffusion into the cartilage, thus limiting detection of this tissue boundary. Accordingly, the triple contrast agent will yield enhanced diagnostic sensitivity for articular cartilage injury and evaluation of cartilage degeneration with lower radiation dose.

Higher CA4+ uptake was seen in reference cartilage samples compared with PG-depleted samples using the dual and triple contrast agents in the superficial and middle zones. During 2 h of diffusion, only a minor portion of the contrast agent molecules have reached the deepest parts of the cartilage and therefore, almost similar CA4+ uptake of contrast agent in intact and PG-depleted samples is observed (Fig. 6). In addition, regardless of the trypsin treatment, some PG molecules remain in the deepest cartilage in the PG-depleted samples. Normalization of CA4+ partition with that of gadoteridol, diminishing the effect of variation in water content on the contrast agent diffusion, increases the difference between the CA4+ partitions of PG-depleted and reference samples. Since nearly all PGs were depleted during the trypsin treatment, the PG-depleted samples bound less CA4+ compared with the intact reference samples with higher PG concentrations in the superficial zone. However, as in this study, imaging was conducted at 2 h after the diffusion afar from the diffusion equilibrium. The contrast agent distribution along the cartilage thickness is not equivalent to that of the PG content (Fig. 5). These results are in agreement with literature.[2,11,24,54]

The uptake of CA4 + into mechanically injured samples, when compared with the intact reference samples, was lower near the articulating surface of the cartilage and higher in deeper with both contrast agent mixtures. This is most probably due to cracks (having exactly 100% partition for CA4+ and gadoteridol) on the cartilage tissue caused by the mechanical impact. Even though the cracks are mostly removed by thresholding, a small margin was left to ensure that no data within cartilage was excluded. Therefore, small parts of the cracks with lower CA4+ partition, when compared with the tissue next to it, are averaged to mean partition in the superficial zone, causing the lower partition than in reference samples at the surface. However, the cracks also facilitate CA4+ diffusion, through the crack walls, into the cartilage, therefore increasing the diffusion surface area, while the diffusion into the reference samples occurs only through the articulating surface.

The uptake of gadoteridol into PG-depleted and mechanically injured samples is higher compared to intact reference samples. This result is a consequence of reduced steric hindrance due to depletion of PGs, disruption of collagen network, and increased water content due to mechanical impact.[9,21] These changes increase the tissue porosity allowing easier penetration of the contrast agent molecules. As the cracks in the mechanically injured samples increase the surface area for diffusion, the uptake of gadoteridol and the gadoteridol partition also increase.

The shapes of the mean ($N = 9$) partition profiles of CA4+ and gadoteridol are similar when using triple or double contrast agents. However, statistically significant ($p < 0.05$) difference between dual and triple contrast agents' full thickness partitions were found in the reference and mechanically injured samples. The contrast agent partitions for triple contrast agent were slightly higher in the reference and mechanically injured samples (Table 1). These higher partitions of the triple contrast agent's CA4+ and gadoteridol are most probably due to reconstruction-based increase (in the superficial and middle zones) in attenuation near the articulating surface where the attenuation level drastically changes when the triple contrast agent is used. Moreover, the different halves of the samples were used for dual and triple contrast agent imaging causing minor variation in the cartilage height, due to natural curvatures of the cartilage surfaces leading to a minor difference in the contrast agent partitions. Thus, the significantly lower normalized CA4+ partition for the mechanically injured samples was observed as the slightly lower CA4+ partition was normalized with significantly higher gadoteridol partition. We have ruled out the possibility of BiNPs (particle diameter = 193 nm) to diffuse into cartilage and being responsible for these differing results since BiNPs remains stable for 24 h (Fig. 3) and do not diffuse into cartilage having pore size around 6 nm.[31,45,49] As the CA4+ and gadoteridol partitions are slightly higher with the triple contrast agents, BiNPs are not interfering with the diffusion of the other contrast agents. A similar result was observed by Saukko *et al.* with another dual contrast agent (ioxaglate and BiNPs).[45]

In the triple contrast agent, the BiNPs enhanced the contrast between the cartilage tissue and the surrounding contrast agent bath. This enhancement significantly improved the delineation of the articulating

surfaces and the detection of surface lesions caused by a mechanical impact compared with dual contrast agent (Fig. 5).

The present triple contrast imaging protocol has three limitations. First, QDECT is based on two image acquisitions conducted simultaneously using two different energies. The energies are selected based on the attenuating elements of the contrast agents, and, the selected energies must straddle both sides of the other elements' k-edge (in this study we chose iodine, 33.2 keV). In the present study, imaging with two energies was performed consecutively with in average 331 s time difference between acquisitions. This difference allows the progression of diffusion within cartilage violating the basic assumption of simultaneous dual energy imaging. However, as imaging was performed first with 34 keV X-ray beam, then with 32 keV, and again with 34 keV, the effect of ongoing diffusion on results was minimized by averaging the 34 keV images. Further, as the image acquisition took approximately 129 s, the obtained attenuation profiles are expected to represent an average over the scan time rather than an exact value at a specific imaging time point. Regardless of this, the results and conclusions are expected to contain no major errors as samples were imaged using the same imaging protocol and as the sample thicknesses were relatively similar. Furthermore, as dual-energy and photon-counting CT scanners become more available, the execution of QDECT technique will become easier and straightforward. Second, the observed minor agglomeration of the BiNPs indicates that BiNPs and the triple contrast agent mixture needs to be prepared just before the immersion/injection, as was done in this study. Third, the technique requires the administration of three contrast agents, and the safety of this combined formulation will need to be addressed. Alone, gadoteridol has been widely used in the clinic, and it is known to possess a very low incidence (1.4%)[13] of acute adverse reactions. A preliminary study reported the safety of CA4+ on articulating tissues.[53,54] Evaluation of the safety regarding the use of BiNPs is still ongoing. However, bismuth is known to exhibit low toxicity.[37]

To conclude, the triple contrast method enables simultaneous evaluation of PG and water contents, providing information on degenerative changes of articular cartilage. Furthermore, triple contrast agent allows, for the first time, the evaluation of cartilage condition and accurate segmentation of articulating surfaces simultaneously at 2 h post administration. Moreover, taking the advantage of monochromatic X-ray beams with high resolution offered by a synchrotron microCT system, artefacts and limitations related to conventional CT systems are minimized in determining the degenerative state of cartilage.

Therefore, this method may enable accurate evaluation of joint health with one image acquisition. As the dual contrast technique with CA4+ and gadoteridol successfully images articular cartilage and provides an assessment of proteoglycan and water content in human articular cartilage with a clinical full-body CT,[12] we are optimistic that the triple contrast method will perform well also in the clinical setup. However, further studies with ex vivo knee joints at early diffusion time points and using a full-body CT device are needed to optimize the imaging parameters and imaging time point. These experiments are important in order to reveal the clinical potential of the triple contrast method to detect acute injuries and PTOA related changes in cartilage condition. An extensive time series can be conducted with ex vivo setup, as the patient dose is not limiting factor, and with clinical CT system the image acquisition is very fast (< 1 min). Finally, the optimal imaging time point needs to be confirmed with in vivo measurements.

OPEN ACCESS

BMES BIOMEDICAL ENGINEERING SOCIETY

REFERENCES

[1]Anderson, D. D., S. Chubinskaya, F. Guilak, J. A. Martin, T. R. Oegema, S. A. Olson, and J. A. Buckwalter. Post-traumatic osteoarthritis:improved understanding and opportunities for early intervention. *J. Orthop. Res.* 29:802–809, 2011.

[2]Bansal, P. N. N., R. C. C. Stewart, V. Entezari, B. D. D. Snyder, and M. W. W. Grinstaff. Contrast agent electrostatic attraction rather than repulsion to glycosaminoglycans affords a greater contrast uptake ratio and improved quantitative CT imaging in cartilage. *Osteoarthr. Cartil.* 19:970–976, 2011.

[3]Bartholomew, J. S., C. J. Handley, and D. A. Lowther. The effects of trypsin treatment on proteoglycan biosynthesis by bovine articular cartilage. *Biochem. J.* 227:429–437, 1985.

[4]Bay-Jensen, A.-C., S. Hoegh-Madsen, E. Dam, K. Henriksen, B. C. Sondergaard, P. Pastoureau, P. Qvist, and M. A. Karsdal. Which elements are involved in reversible and irreversible cartilage degradation in osteoarthritis? *Rheumatol. Int.* 30:435–442, 2010.

[5]Bhattarai, A., J. T. J. Honkanen, K. A. H. Myller, M. Prakash, M. Korhonen, A. E. A. Saukko, T. Virén, A. Joukainen, A. N. Patwa, H. Kröger, M. W. Grinstaff, J. S. Jurvelin, and J. Töyräs. Quantitative dual contrast CT technique for evaluation of articular cartilage properties. *Ann. Biomed. Eng.* 46:1038–1046, 2018.

[6]Borthakur, A., E. Mellon, S. Niyogi, W. Witschey, J. B. Kneeland, and R. Reddy. Sodium and T1rho MRI for molecular and diagnostic imaging of articular cartilage. *NMR Biomed.* 19:781–821, 2006.

[7]Buckwalter, J. A. Mechanical injuries of articular cartilage. *Iowa Orthop. J.* 12:50, 1992.

[8]Burgin, L. V., and R. M. Aspden. Impact testing to determine the mechanical properties of articular cartilage in isolation and on bone. *J. Mater. Sci. Mater. Med.* 19:703–711, 2008.

[9]Ewers, B., V. Jayaraman, R. Banglmaier, and R. C. Haut. Rate of blunt impact loading affects changes in retropatellar cartilage and underlying bone in the rabbit patella. *J. Biomech.* 35:747–755, 2002.

[10]Harris, E. D., H. G. Parker, E. L. Radin, and S. M. Krane. Effects of proteolytic enzymes on structural and mechanical properties of cartilage. *Arthr. Rheumatol.* 15:497–503, 1972.

[11]Honkanen, J. T. J., M. J. Turunen, J. D. Freedman, S. Saarakkala, M. W. Grinstaff, J. H. Ylärinne, J. S. Jurvelin, and J. Töyräs. Cationic contrast agent diffusion differs between cartilage and meniscus. *Ann. Biomed. Eng.* 44:2913–2921, 2016.

[12]Honkanen, M. K. M., M. Hanna, J. T. J. Honkanen, A. Bhattarai, M. W. Grinstaff, A. Joukainen, H. Kröger, J. S. Jurvelin, and J. Töyräs. Imaging of proteoglycan and water contents in human articular cartilage with full-body CT using dual contrast technique. *J. Orthop. Res.* 37:1059–1070, 2019.

[13]https://www.accessdata.fda.gov/drugsatfda_docs/label/2017/020131s027lbl.pdf.

[14]Hubbel J. H., S. Seltzer. X-ray mass attenuation coefficient—NIST Standard Reference Database 126. 2004. https://doi.org/10.18434/T4D01F.

[15]Jeffrey, J. E., D. W. Gregory, and R. M. Aspden. Matrix damage and chondrocyte viability following a single impact load on articular cartilage. *Arch. Biochem. Phys.* 322(1):85–87, 1995.

[16]Joshi, N. S., P. N. Bansal, R. C. Stewart, B. D. Snyder, and M. W. Grinstaff. SI: effect of contrast agent charge on visualization of articular cartilage using computed tomography: exploiting electrostatic interactions for improved sensitivity. *J. Am. Chem. Soc.* 131:S1–S6, 2009.

[17]Kallioniemi, A. S., J. S. Jurvelin, M. T. Nieminen, M. J. Lammi, and J. Töyräs. Contrast agent enhanced pQCT of articular cartilage. *Phys. Med. Biol.* 52:1209–1219, 2007.

[18]Karhula, S. S., Finnilä, M. A., Freedman, J. D., Kauppinen, S., Valkealahti, M., Lehenkari, P., Pritzker, K. P. H., Nieminen, H. J., Snyder, B. D., Grinstaff, M. W., Saarakkala, S. Micro-scale distribution of CA4+ in ex vivo human articular cartilage detected with contrast-enhanced micro-computed tomography imaging. Front. Phys. 5(38):1–8, 2017.

[19]Kiviranta, I., J. Jurvelin, A.-M. Säämänen, and H. J. Helminen. Microspectrophotometric quantitation of glycosaminoglycans in articular cartilage sections stained with Safranin O. *Histochemistry* 82:249–255, 1985.

[20]Koivisto, J., T. Kiljunen, J. Wolff, and M. Kortesniemi. Assessment of effective radiation dose of an extremity CBCT, MSCT and conventional X ray for knee area using MOSFET dosemeters. *Radiat. Prot. Dosimetry* 157:515–524, 2013.

[21]Kokkonen, H. T. T., J. S. S. Jurvelin, V. Tiitu, and J. Töyräs. Detection of mechanical injury of articular cartilage using contrast enhanced computed tomography. *Osteoarthr. Cartil.* 19:295–301, 2011.

[22]Kokkonen, H. T., A. S. Aula, H. Kroger, J.-S. Suomalainen, E. Lammentausta, E. Mervaala, J. S. Jurvelin, and J. Toyras. Delayed computed tomography arthrography of human knee cartilage in vivo. *Cartilage* 3:334–341, 2012.

[23]Kokkonen, H. T., J.-S. Suomalainen, A. Joukainen, H. Kröger, J. Sirola, J. S. Jurvelin, J. Salo, and J. Töyräs. In vivo diagnostics of human knee cartilage lesions using delayed CBCT arthrography. *J. Orthop. Res.* 32:403–412, 2014.

[24]Lakin, B. A. B. A., D. J. Grasso, R. C. Stewart, J. D. Freedman, B. D. Snyder, and M. W. Grinstaff. Contrast enhanced CT attenuation correlates with the GAG content of bovine meniscus. *J. Orthop. Res.* 31:1765–1771, 2013.

[25]Lakin, B. A., D. J. Grasso, R. C. Stewart, P. N. Bansal, J. D. Freedman, M. W. Grinstaff, B. D. Snyder, S. S. Shah, R. C. Stewart, P. N. Bansal, J. D. Freedman, M. W. Grinstaff, and B. D. Snyder. Cationic agent contrast-enhanced computed tomography imaging of cartilage correlates with the compressive modulus and coefficient of friction. *Osteoarthr. Cartil.* 21:60–68, 2013.

[26]Lakin, B. A., B. D. Snyder, and M. W. Grinstaff. Assessing cartilage biomechanical properties: techniques for evaluating the functional performance of cartilage in health and disease. *Annu. Rev. Biomed. Eng.* 19:27–55, 2017.

[27]Li, X., V. Pedoia, D. Kumar, J. Rivoire, C. Wyatt, D. Lansdown, K. Amano, N. Okazaki, D. Savic, M. F. Koff, J. Felmlee, S. L. Williams, and S. Majumdar. Cartilage T1ρ and T2 relaxation times: longitudinal reproducibility and variations using different coils, MR systems and sites. *Osteoarthr. Cartil.* 23:2214–2223, 2015.

[28]Lin, P. M., C.-T. C. Chen, and P. A. Torzilli. Increased stromelysin-1 (MMP-3), proteoglycan degradation (3B3- and 7D4) and collagen damage in cyclically load-injured articular cartilage. *Osteoarthr. Cartil.* 12:485–496, 2004.

[29]Ling, W., R. R. Regatte, G. Navon, and A. Jerschow. Assessment of glycosaminoglycan concentration in vivo by

chemical exchange-dependent saturation transfer (gag-CEST). *Proc. Natl. Acad. Sci. USA* 105:2266–2270, 2008.

[30]Link, T. M., J. Neumann, and X. Li. Prestructural cartilage assessment using MRI. *J. Magn. Reson. Imaging* 45:949–965, 2017.

[31]Linn, F. C., and L. Sokoloff. Movement and composition of interstitial fluid of cartilage. *Arthritis Rheum*. 8:481–494, 1965.

[32]Lotz, M. K. New developments in osteoarthritis. Post-traumatic osteoarthritis: pathogenesis and pharmacological treatment options. *Arthritis Res. Ther.* 12:211, 2010.

[33]Lovric, G., R. Mokso, C. M. Schlepütz, and M. Stampanoni. A multi-purpose imaging endstation for high-resolution micrometer-scaled sub-second tomography. *Phys. Med.* 32:1771–1778, 2016.

[34]Lusic, H., and M. W. Grinstaff. X-ray-computed tomography contrast agents. *Chem. Rev.* 113:1641–1666, 2013.

[35]Madry, H., E. Kon, V. Condello, G. M. Peretti, M. Steinwachs, R. Seil, M. Berruto, L. Engebretsen, G. Filardo, and P. Angele. Early osteoarthritis of the knee. *Knee Surg. Sport Traumatol. Arthrosc.* 24:1753–1762, 2016.

[36]Marone, F., M. Stampanoni, and IUCr. Regridding reconstruction algorithm for real-time tomographic imaging. *J. Synchrotron Radiat*. 19:1029–1037, 2012.

[37]Mohan, R. Green bismuth. *Nat. Chem.* 2:336, 2010.

[38]Moody, H. R., C. P. Brown, J. C. Bowden, R. W. Crawford, D. L. S. McElwain, and A. O. Oloyede. In vitro degradation of articular cartilage: does trypsin treatment produce consistent results? *J. Anat.* 209:259–267, 2006.

[39]Myller, K. A. H., M. J. Turunen, J. T. J. Honkanen, S. P. Väänänen, J. T. Iivarinen, J. Salo, J. S. Jurvelin, and J. Töyräs. In vivo contrast-enhanced cone beam CT provides quantitative information on articular cartilage and sub-chondral bone. *Ann. Biomed. Eng.* 45:811–818, 2017.

[40]Näkki, S., J. Rytkönen, T. Nissinen, C. Florea, J. Riikonen, P. Ek, H. Zhang, H. A. Santos, A. Närvänen, W. Xu, and V. P. Lehto. Improved stability and biocompatibility of nanostructured silicon drug carrier for intravenous administration. *Acta Biomater.* 13:207–215, 2015.

[41]Olson, S. A., B. D. Furman, V. B. Kraus, J. L. Huebner, and F. Guilak. Therapeutic opportunities to prevent post-traumatic arthritis: lessons from the natural history of arthritis after articular fracture. *J. Orthop. Res.* 33:1266–1277, 2015.

[42]Palmer, A. W., R. E. Guldberg, M. E. Levenston, and G. W. Woodruff. Analysis of cartilage matrix fixed charge density and three-dimensional morphology via contrast-enhanced microcomputed tomography. *Proc. Natl. Acad. Sci. USA* 103:19255–19260, 2006.

[43]Rangacharyulu, C. Physics of Nuclear Radiations: Concepts, Techniques and Applications. Boca Raton: CRC Press, 2013.

[44]Rieppo, J., J. Töyräs, M. T. Nieminen, V. Kovanen, M. M. Hyttinen, R. K. Korhonen, J. S. Jurvelin, and H. J. Helminen. Structure-function relationships in enzymatically modified articular cartilage. *Cells Tissues Organs* 175:121–132, 2003.

[45]Saukko, A. E. A., J. T. J. Honkanen, W. Xu, S. P. Väänänen, J. S. Jurvelin, V. P. Lehto, and J. Töyräs. Dual contrast CT method enables diagnostics of cartilage injuries and degeneration using a single CT image. *Ann. Biomed. Eng.* 45:2857–2866, 2017.

[46]Saukko, A. E. A., M. J. Turunen, M. K. M. Honkanen, G. Lovric, V. Tiitu, J. T. J. Honkanen, M. W. Grinstaff, J. S. Jurvelin, and J. Töyräs. Simultaneous quantitation of cationic and non-ionic contrast agents in articular cartilage using synchrotron microCT imaging. *Sci. Rep.* 9:1–9, 2019.

[47]Silvast, T. S., J. S. Jurvelin, M. J. Lammi, and J. Töyräs. pQCT study on diffusion and equilibrium distribution of iodinated anionic contrast agent in human articular cartilage - associations to matrix composition and integrity. *Osteoarthr. Cartil.* 17:26–32, 2009.

[48]Silvast, T. S., H. T. Kokkonen, J. S. Jurvelin, T. M. Quinn, M. T. Nieminen, and J. Töyräs. Diffusion and near-equilibrium distribution of MRI and CT contrast agents in articular cartilage. *Phys. Med. Biol.* 54:6823–6836, 2009.

[49]Sophia, A. J., A. Bedi, and S. A. Rodeo. The basic science of articular cartilage: structure, composition, and function. *Sports Health* 1:461–468, 2009.

[50]Stampanoni, M., A. Groso, A. Isenegger, G. Mikuljan, Q. Chen, D. Meister, M. Lange, R. Betemps, S. Henein, and R. Abela. TOMCAT: a beamline for TOmographic Microscopy and Coherent rAdiology experimenTs. *AIP Conf. Proc.* 879:848–851, 2007.

[51]Stampanoni, M., F. Marone, P. Modregger, B. Pinzer, T. Thüring, J. Vila-Comamala, C. David, R. Mokso, and K. K. W. Siu. Tomographic Hard X-ray Phase Contrast Micro- and Nano-imaging at TOMCAT. *AIP Conf. Proc.* 1266:13–17, 2010.

[52]Steiger, J. H. Tests for comparing elements of a correlation matrix. *Psychol. Bull.* 87:245–251, 1980.

[53]Stewart, R. C., P. N. Bansal, V. Entezari, H. Lusic, R. M. Nazarian, B. D. Snyder, and M. W. Grinstaff. Contrast-enhanced CT with a high-affinity cationic contrast agent for imaging ex vivo bovine, intact ex vivo rabbit, and in vivo rabbit cartilage. *Radiology* 266:141–150, 2013.

[54]Stewart, R. C., A. N. Patwa, H. Lusic, J. D. Freedman, M. Wathier, B. D. Snyder, A. Guermazi, and M. W. Grinstaff. Synthesis and preclinical characterization of a cationic iodinated imaging contrast agent (CA4 +) and its use for quantitative computed tomography of ex vivo human hip cartilage. *J. Med. Chem.* 60:5543–5555, 2017.

[55]Turunen, M. J., J. Töyras, H. T. Kokkonen, and J. S. Jurvelin. Quantitative evaluation of knee subchondral bone mineral density using cone beam computed tomography. *IEEE Trans. Med. Imaging* 34:2186–2190, 2015.

[56]White, D. R., J. Booz, R. V. Griffith, J. J. Spokas, and I. Wilson. ICRU Report 44: tissue substitutes in radiation dosimetry and measurement. *J ICRU* 1989. https://doi.org/10.1093/jicru/os23.1.Report44.

Paper **IV**

Saukko, A. E., Nykänen, O., Sarin, J., Nissi, M., te Moller, N. C., Weinans, K., Mancini., I. A., Visser, J., Brommer, H., van Weeren, P. R., Malda, J., Grinstaff, M. & Töyräs, J.
"Dual contrast CT technique can reveal equine post-traumatic osteoarthritis *in vitro*"
Journal of Orthopaedic Research
2021

RESEARCH ARTICLE

Dual-contrast computed tomography enables detection of equine posttraumatic osteoarthritis in vitro

Annina E. A. Saukko[1,2] ⓘ | Olli Nykänen[1,3] ⓘ | Jaakko K. Sarin[1,4] ⓘ |
Mikko J. Nissi[1,3] ⓘ | Nikae C. R. te Moller[5] ⓘ | Harrie Weinans[6,7] |
Irina A. D. Mancini[5] | Jetze Visser[7] | Harold Brommer[5] |
P. Réné van Weeren[5] ⓘ | Jos Malda[5,7] | Mark W. Grinstaff[8] ⓘ | Juha Töyräs[1,4,9,10]

[1]Department of Applied Physics, University of Eastern Finland, Kuopio, Finland

[2]Department of Medical Physics, Turku University Hospital, Turku, Finland

[3]Research Unit of Medical Imaging Physics and Technology, University of Oulu, Oulu, Finland

[4]Diagnostic Imaging Center, Kuopio University Hospital, Kuopio, Finland

[5]Department of Clinical Sciences, Faculty of Veterinary Medicine, Utrecht University, Utrecht, The Netherlands

[6]Department of Biomechanical Engineering, Delft University of Technology (TU Delft), Delft, The Netherlands

[7]Department of Orthopedics, University Medical Center Utrecht, Utrecht, The Netherlands

[8]Departments of Biomedical Engineering, Chemistry, and Medicine, Boston University, Boston, Massachusetts, USA

[9]School of Information Technology and Electrical Engineering, The University of Queensland, Brisbane, Australia

[10]Science Service Center, Kuopio University Hospital, Kuopio, Finland

Correspondence
Annina E. A. Saukko, MSc (Tech.),
Department of Applied Physics, University of
Eastern Finland, Kuopio 70210, Finland.
Email: annina.saukko@uef.fi

Funding information
Jenny and Antti Wihuri Foundation; Dutch
Arthritis Association, Grant/Award Numbers:
LLP-12, LLP-22; Jorma ja Märtha Sihvola
Foundation; Academy of Finland,
Grant/Award Numbers: 285909, 293970,
307932; Doctoral Program in Science,
Technology and Computing (SCITECO,
University of Eastern Finland)

Abstract

To prevent the progression of posttraumatic osteoarthritis, assessment of cartilage composition is critical for effective treatment planning. Posttraumatic changes include proteoglycan (PG) loss and elevated water content. Quantitative dual-energy computed tomography (QDECT) provides a means to diagnose these changes. Here, we determine the potential of QDECT to evaluate tissue quality surrounding cartilage lesions in an equine model, hypothesizing that QDECT allows detection of posttraumatic degeneration by providing quantitative information on PG and water contents based on the partitions of cationic and nonionic agents in a contrast mixture. Posttraumatic osteoarthritic samples were obtained from a cartilage repair study in which full-thickness chondral defects were created surgically in both stifles of seven Shetland ponies. Control samples were collected from three nonoperated ponies. The experimental ($n = 14$) and control samples ($n = 6$) were immersed in the contrast agent mixture and the distributions of the agents were determined at various diffusion time points. As a reference, equilibrium moduli, dynamic moduli,

and PG content were measured. Significant differences ($p < 0.05$) in partitions between the experimental and control samples were demonstrated with cationic contrast agent at 30 min, 60 min, and 20 h, and with non-ionic agent at 60 and 120 min. Significant Spearman's rank correlations were obtained at 20 and 24 h ($\rho = 0.482–0.693$) between the partition of cationic contrast agent, cartilage biomechanical properties, and PG content. QDECT enables evaluation of posttraumatic changes surrounding a lesion and quantification of PG content, thus advancing the diagnostics of the extent and severity of cartilage injuries.

KEYWORDS

articular cartilage, cationic contrast agent, contrast-enhanced computed tomography, dual-contrast agent, dual-energy computed tomography, posttraumatic osteoarthritis

1 | INTRODUCTION

Osteoarthritis (OA) is a progressive joint disease characterized by a breakdown of articular cartilage and underlying bone, pain, stiffness, and impairment of joint function. Single and multiple traumas to the joint cause focal damage, and more specifically lead to abnormal mechanical function and biochemical alterations of cartilage. Trauma may not only lead to a local chondral defect but can also trigger changes in the surrounding cartilage, predisposing patients to developing posttraumatic OA (PTOA). To prevent or delay the progression of an acute injury into PTOA, surgical and pharmaceutical interventions are needed.[1,2] However, injuries must be first detected and assessed. After the injury, the time to develop clinical PTOA varies highly from as short as 2–5 years but for some injuries, the timeframe can be even longer.[1] The earlier the cartilage degeneration can be detected in the preclinical phase, the better are chances for effective treatment. The focus of this study is to evaluate a new contrast-enhanced computed tomography (CECT) technique for the detection of the initial changes in cartilage adjacent to chondral defects.

Magnetic resonance imaging (MRI) is an important imaging tool in cartilage damage diagnostics as it features excellent soft-tissue contrast and can assess proteoglycan (PG) content, collagen orientation, and water content.[3,4] Unfortunately, MRI has a relatively low spatial resolution in vivo (1–2 mm) and long image acquisition times with the length of a typical knee MRI protocol varying from 20 to 30 min.[4,5] As an alternative to MRI, CECT enables the detection of cartilage degeneration in acute injuries[6–10] and has recently been introduced in the clinic. The advantages of CECT over MRI include better spatial resolution (0.5–0.625 mm), shorter acquisition time (<1 min), lower costs, and better availability. Furthermore, changes in the bony structures are better visualized in computed tomographic (CT) images.

The CECT of the knee typically involves two subsequent CT scans acquired immediately (arthrography) and 45 min (delayed arthrography) after the intra-articular injection of a contrast agent.[6,7,10] The first scan allows segmentation of the articulating surface and lesions, while the second scan reveals internal cartilage changes related

to the initiation of PTOA (e.g., increased water content and decreased PG content). In CECT, contrast agents enhance the contrast at the synovial fluid-cartilage interface since the natural contrast at this interface is almost nonexistent in CT. Contrast agents also enable the detection of degenerative changes by examining their uptake and partitioning in the cartilage.[11–16] The early degenerative changes of cartilage include PG loss, disruption of the superficial collagen network, and increased water content.[17,18] These changes increase the uptake of anionic contrast agent (most commonly ioxaglate), enabling the evaluation of the internal cartilage changes and degeneration.[19]

A recently introduced cationic contrast agent (CA4+) has a superior sensitivity for revealing tissue PG content at diffusion equilibrium compared with the currently used anionic contrast agents.[13,20–22] Cationic contrast agents distribute in cartilage proportionally to the PG content due to the electrostatic attraction caused by the negative fixed charge density of the PG molecules. At the onset of diffusion, cationic contrast agent diffusion is also controlled by two other degeneration-related factors: increased water content and decreased steric hindrance (i.e., the physical diffusion barrier formed by the dense collagen network and the interspersed PGs in the matrix). Degeneration of the extracellular matrix has opposite effects on the diffusion of cationic agents: the loss of PGs decreases the diffusion while the increased water content and decreased steric hindrance increase the diffusion. This phenomenon diminishes the sensitivity of detecting cartilage injuries and osteoarthritic degeneration at clinically feasible imaging time points (30 min up to 2 h after the administration of the contrast agent[6]).

We previously reported that this weakness in clinically feasible time points is minimized by employing a quantitative dual-energy CT (QDECT) technique, together with a contrast agent mixture consisting of cationic, iodinated contrast agent (CA4+) and nonionic, gadolinium-based contrast agent (gadoteridol).[23,24] In the mixture, the cationic contrast agent is sensitive to the changes in PG content and the non-ionic contrast agent is sensitive to the tissue water content and altered steric hindrance. Thus, with non-ionic agent, the effect of water content and altered steric hindrance into CA4+ diffusion can be assessed.

QDECT is based on dual-energy CT that exploits the "absorption k-edges," that is, sharp element-specific changes in the photo-electric X-ray absorption spectrum. In this method, the energies and filtration of the X-ray beam are selected so that the resulting X-ray energy spectra fall on both sides of either gadolinium (50.2 keV) or iodine (33.2 keV) k-edge. The technique enables simultaneous quantification of the uptake of cationic and non-ionic contrast agents in cartilage and, thus, improved diagnosis of cartilage degeneration and injuries.[23,24]

Previous research on QDECT has focused on studying car-tilage injuries in lesion sites of osteoarthritic human cartilage and bovine cartilage with artificial injuries and degeneration ex vivo.[23–27] In this study, we extend our examinations from the lesion site to the surrounding tissue to evaluate the capability of the technique to reveal changes related to PTOA. This is of in-terest because the changes in the adjacent tissue are usually not as prominent as in the lesion site and, thus, the sensitivity of the QDECT method needs to be validated in this setting. Ad-ditionally, this is the first time the QDECT technique is being evaluated in an equine model. Specifically, we investigate the potential of the QDECT technique for monitoring posttraumatic degeneration in the cartilage surrounding surgically repaired le-sions in the equine stifle joint. We hypothesize that simultaneous quantification of the cationic and non-ionic contrast agent parti-tions using the QDECT technique enables the detection of posttraumatic, degeneration-related changes in the tissue sur-rounding the lesions at clinically relevant diffusion time points and, hence, QDECT improves the quantitative diagnosis of posttraumatic degeneration.

2 | METHODS

2.1 | Sample extraction

In both femoropatellar joints of Shetland ponies ($N = 7$, age = 8.8 ± 3.5 years, 6 females and 1 male) two full-thickness cylindrical chondral lesions ($d = 9$ mm) were surgically created on the medial femoral ridges. The experiments were carried out in a surgical theater at the Equine Division of the Department of Clinical Sciences, Utrecht University, The Netherlands. The lesions were treated with different combinations of chondrons and mesenchymal stem cells in different carrier hydrogels. After a 12-month treatment period, the ponies were euthanized. Osteochondral samples, includ-ing the lesions and surrounding tissue, were extracted postmortem from the medial femoral ridge (Figure 1). In addition, to obtain a representative sample population, equivalent osteochondral samples were extracted from femoropatellar joints of healthy ponies ($N_{control} = 3$, age = 10.3 ± 4.7 years) obtained from a local abattoir (Van de Veen, Nijkerk, The Netherlands), resulting in a total of 20 samples (14 experimental and 6 control). Extracted samples were frozen at $-20°C$ until biomechanical testing. We expect that, based on literature, this freeze-thaw cycle did not induce substantial changes in the structure, composition, or biomechanical properties of cartilage.[28] The number of samples was based on power calculations of the original cartilage repair study.[29] The measurement protocol was evaluated and approved by the Ethics Committee of Utrecht University for Animal Experiments in compliance with the Institu-tional Guidelines on the Use of Laboratory Animals (Permission DEC 2014. III.11.098).
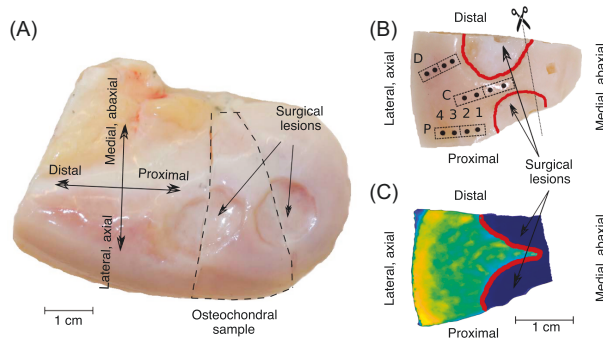

FIGURE 1 Sample extraction and anatomical locations. (A) Medial view of a left trochlea showing the locations of the surgically repaired lesions and the extraction site of an experimental sample. (B) Photograph of an experimental sample. Red lines indicate the locations of the surgically induced and repaired lesions. The boxes illustrate the locations where the histological samples were extracted, and the black dots illustrate the anatomical locations of the biomechanical measurement points. Letters P, C, and D (proximal, central, and distal) and numbers 1–4 denote the naming of the anatomical locations, for example, P1 is the proximal and closest location from the surgically repaired lesion. The line with scissors shows where the samples were trimmed before the microCT measurements. (C) Corresponding view of the CA4+ partition map [Color figure can be viewed at wileyonlinelibrary.com]

2.2 | Biomechanical testing

Biomechanical properties of cartilage were examined using indentation testing. Twelve biomechanical testing locations were examined from proximal (P), central (C), and distal (D) anatomical locations (Figure 1). Each anatomical location included four testing locations with the closest to a lesion denoted as location 1 and the farthest as location 4. A total of 235 locations were tested biomechanically (two samples had less than 12 locations due to the shape of the sample).[30] The indentation system utilized a 250 g load cell (accuracy ± 0.25%, Model 31; Honeywell Sensotec Sensors) and an actuator (displacement resolution 0.1 µm, PM500-1 A; Newport). During the measurements, the samples were glued to a custom-made sample holder and a perpendicular alignment with the face of a plane-ended nonporous cylindrical indenter (d = 0.53 mm) was ensured using a goniometer (Model #55-841; Edmund Optics Inc.). To begin with, the indenter was brought into contact with the sample. The contact was confirmed by indenting the sample five times using 2% strain. First, four stress-relaxation steps with 5% strain and a ramp velocity of 100%/s were performed using a relaxation time of 600 s in between the steps. Thereafter, dynamic sinusoidal loading (f = 1.0 Hz) with a strain amplitude of 1% was applied. The linear region of the stress-relaxation curve was used to determine the equilibrium modulus using Poisson's ratio of ν = 0.1. The dynamic modulus was calculated as a ratio of the stress and strain amplitudes obtained from the sinusoidal loading using a Poisson's ratio of ν = 0.5.[31,32] Measuring adjacent points with distances varying between 3 and 4 mm was feasible, as the diameter of the employed indenter was sufficiently small (~0.5 mm).

2.3 | MicroCT imaging

The QDECT measurements were conducted using a microCT scanner (Quantum FX; Perkin Elmer). The samples were scanned at room temperature using two X-ray tube voltages (90 and 50 kV) with a tube current of 200 µA and isotropic voxel size of $59 \times 59 \times 59$ µm³. Custom-made 2 mm and 0.588 mm copper filters were used in 90 and 50 kV scans, respectively. Each scan included seven calibration phantoms. These phantoms comprised of one distilled water phantom, three CA4 + (q = +4, M = 1499.17 g/mol) phantoms with iodine concentrations of 8, 16, and 32 mg I/ml, and three gadoteridol (q = 0, M = 558.69 g/mol, ProHance, Bracco Diagnostic Inc.) phantoms with gadolinium concentrations of 8, 16, and 32 mg Gd/ml. CA4+ was synthesized as reported previously.[14]

Before imaging, the sides and bottom of the osteochondral samples were sealed carefully using cyanoacrylate (Loctite, Henkel Norden AB), which served as a barrier and allowed the contrast agent diffusion only through the articulating surface. The X-ray attenuation within the cartilage was determined by imaging the osteochondral sample in air with both tube voltages. After baseline data acquisition, the samples were immersed in an isotonic (~308 mOsm/kg) mixture of CA4+ and gadoteridol diluted in phosphate-buffered saline (PBS). The iodine concentration in the

solution was 10 mg I/ml, and the gadolinium concentration was 20 mg Gd/ml. The solution was supplemented with proteolytic inhibitors (5 mM ethylenediaminetetraacetic acid [EDTA; VWR International] and 5 mM benzamidine hydrochloride hydrate Sigma-Aldrich Inc.]) and penicillin–streptomycin (100 units/ml penicillin, 100 µg/ml streptomycin; Life Technologies) to prevent general protein degradation in the tissue. The samples were kept immersed in a contrast agent for 24 h in a bath volume of 20 ml at 7°C while the bath was stirred gently. The uptake of the dual-contrast agent in articular cartilage was imaged at five time points following an immersion period of 30 min, 1 h, 2 h, 20 h, and 24 h. The samples were imaged in air and the atmosphere in the imaging tube was kept moist during imaging using saline-soaked gauze. The image acquisition time was 2.6 min for both energies. Late imaging time points (20 and 24 h) are not clinically relevant but were used here as comparison data points since the diffusion of contrast agents is presumed to be at diffusion equilibrium at these imaging time points. After microCT imaging, the samples were frozen at −20°C.

2.4 | Digital densitometry

Preceding sample preparation for histological digital densitometry (DD) analysis of the PG content, the contrast agent was washed out from the cartilage tissue by immersing the samples in PBS for a total of 48 h at 7°C, including the change of the PBS bath after 24 h. MicroCT imaging was conducted to confirm that all contrast agent was washed out from the sample. Next, the samples were prepared for DD from twelve locations corresponding with the biomechanical testing locations. Sample blocks, including two biomechanical testing locations, were extracted with matching distances from the edges of the block to ensure correct locations for DD measurements. The extracted samples were fixed in formalin and subsequently decalcified in EDTA to soften them for histological sectioning. Samples were fixed in paraffin and three DD sections with a thickness of 3 µm from each measurement location were prepared using a microtome.[33] The DD sections were stained using safranin-O and measured with a DD measurement system to quantify the depth-wise PG content in cartilage. Safranin-O is a cationic stain that binds specifically and stoichiometrically to the PGs.[34] The DD measurement system was composed of a light microscope (Nikon Microphot-FXA; Nikon Co.) equipped with a monochromatic light source and a 12-bit CCD camera (ORCA-ER; Hamamatsu Photonics K.K.). System calibration was performed using neutral density filters of 0–3.0 optical density. Before determining the optical density of the cartilage at each biomechanical measurement point, the subchondral bone was manually segmented from the images. Then the optical density profiles perpendicular to the articulating surface were determined and the profiles were interpolated to 100 points. The analysis was performed with a custom-made Matlab script (Matlab 2016b; Mathworks, Inc.). A more detailed description of the biomechanical and histological analysis and results can be found in our previous studies.[30,33]

2.5 | Data analysis

MicroCT images were coregistered by first delineating the bone volumes using Stradwin (v. 5.2, Department of Engineering, University of Cambridge) and subsequently matching the orientations of the bone volumes with that of the 0-min, 90 kV baseline image using an open-source software wxRegSurf (v. 16, Department of Engineering, University of Cambridge, UK). After co-registration, the cartilage volumes were traced using ITK-SNAP software (v. 3.8.0, www.itksnap.org) and a custom-made MATLAB script was used to calculate the partitions of iodine and gadolinium in the cartilage based on the equations described below.

The concentrations of two components in a mixture can be solved based on Bragg's additive rule for the mixtures:

$$\alpha_E = \mu_{I,E} C_I + \mu_{Gd,E} C_{Gd}, \tag{1}$$

where α_E is the attenuation coefficient in the medium at an energy E, $\mu_{I,E}$, and $\mu_{Gd,E}$ the mass attenuation coefficients, and C_I and C_{Gd} the concentrations of iodine (I) and gadolinium (Gd) in the mixture. From this equation, iodine and gadolinium concentrations can be solved from the dual-contrast images based on the X-ray attenuation with two tube voltages (here 90 and 50 kV) as follows:

$$C_I = \frac{\alpha_{90}\mu_{Gd,50} - \alpha_{50}\mu_{Gd,90}}{\mu_{I,90}\mu_{Gd,50} - \mu_{I,50}\mu_{Gd,90}} \tag{2}$$

$$C_{Gd} = \frac{\alpha_{50}\mu_{I,90} - \alpha_{90}\mu_{I,50}}{\mu_{I,90}\mu_{Gd,50} - \mu_{I,50}\mu_{Gd,90}}. \tag{3}$$

The attenuation of native cartilage tissue was removed by subtracting the images obtained before the contrast agent immersion from the image obtained at each time point with the same energy. The contrast agent partitions were obtained by dividing the contrast agent concentration inside the cartilage with the concentration in the immersion bath.

In addition, depth-wise contrast agent concentration profiles were calculated from the locations of biomechanical testing to investigate potential differences between the contrast agents' partitioning and DD measurement. To calculate depth-wise contrast agent concentration profiles for iodine and gadolinium, cylindrical regions of interest with 1.416 mm diameter were carefully matched with the histological locations based on microCT measurements having X-ray positive markers on top of the histological location and photographs of the samples.[30] The depth-wise concentration distributions were linearly interpolated into 30 points long depth-wise profiles and afterward used to compare with the depth-wise distribution of PG content. Mean values of contrast-agent concentrations were calculated for full cartilage and superficial cartilage (50% of the total cartilage thickness).

Mann–Whitney U test was used to determine whether statistically significant differences occurred between the contrast agent partitions (CA4+ or gadoteridol) in experimental and control samples. Statistical significance of dependence between DD and CA4+ was calculated using

FIGURE 2 Representative partition maps of CA4+ for three experimental and three control samples. The partitions are presented for both full thickness cartilage and for the superficial layer (50% of the total cartilage thickness). Red lines indicate the locations of the lesions in the experimental samples and the corresponding sites in the control samples. Higher partition of CA4+ is seen in the control samples at 20 and 24 h after contrast agent immersion, indicating higher PG content. In experimental samples, the CA4+ partition at 20 and 24 h time points is the lowest near the lesion site and increased when moving further away [Color figure can be viewed at wileyonlinelibrary.com]
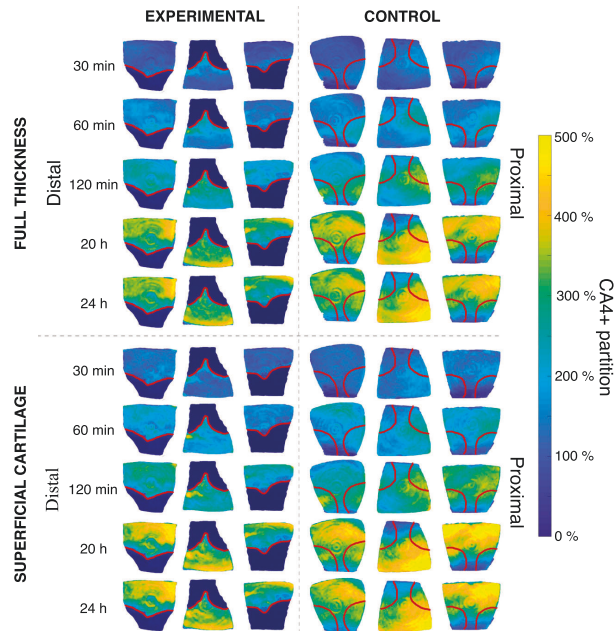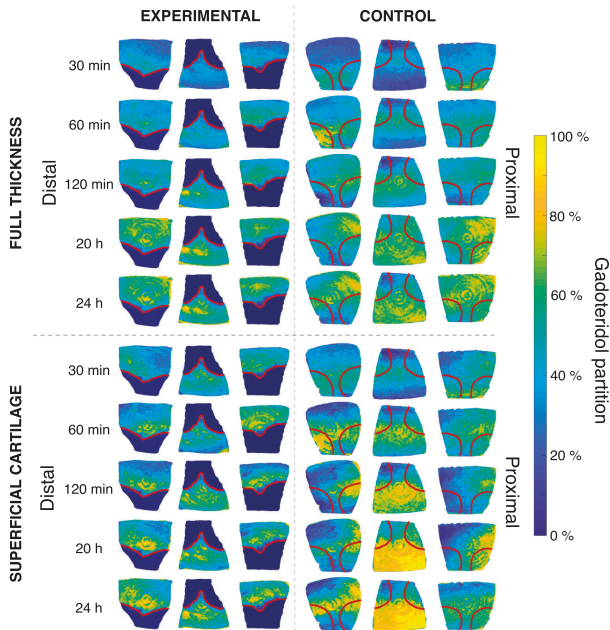
FIGURE 3 Representative partition maps of gadoteridol for three experimental and three control samples. The partitions are presented for both full-thickness cartilage and for the superficial layer (50% of the total cartilage thickness). Red lines indicate the locations of the lesions in the experimental samples and the corresponding sites in the control samples. No distinct differences in gadoteridol partition are seen between the experimental and control samples [Color figure can be viewed at wileyonlinelibrary.com]

Spearman's rank correlation. $p < 0.05$ was considered as the limit for statistical significance. Due to the relatively small sample size and non-normal distribution of the parameters (Shapiro–Wilk test, $p < 0.0001$), nonparametric tests were used. The statistical tests were performed using the SPSS software package (v. 24.0 SPSS Inc., IBM Company).

3 | RESULTS

Mean CA4+ partitions in full thickness cartilage were significantly higher in experimental samples than in control samples at 30 min ($p = 0.004$) and 60 min ($p = 0.028$) after contrast-agent immersion but significantly lower at 20 h ($p < 0.0001$) after immersion. For the superficial cartilage layer, the CA4+ partition was significantly higher at 30 min ($p = 0.001$) and significantly lower at 20 h ($p < 0.0001$) and 24 h ($p < 0.0001$). The partition of gadoteridol in full-thickness cartilage was significantly lower in experimental samples compared with the control samples at 60 min ($p < 0.0001$) and 120 min ($p = 0.002$) after the immersion. In the superficial cartilage layer, gadoteridol partition was lower in experimental samples at 30 min ($p = 0.003$), 60 min ($p < 0.0001$), and 120 min ($p < 0.0001$). No significant differences in gadoteridol partition at 20 or 24 h were found. The partition maps of the full thickness and superficial cartilage layer, respectively, are shown in Figures 2 and 3.

TABLE 1 Spearman's rank correlations of CA4+ partition and reference parameters (optical density, equilibrium, and dynamic moduli)

| | Optical density | | Equilibrium modulus | | Dynamic modulus | |
	Full cartilage Thickness	Superficial cartilage	Full cartilage Thickness	Superficial cartilage	Full cartilage Thickness	Superficial cartilage
30 min	−0.148*	−0.304*	−0.137*	−0.289*	−0.078	−0.217*
60 min	−0.177*	−0.325*	−0.150*	−0.341*	−0.102	−0.281*
120 min	0.089	−0.014	0.101	−0.043	0.125	0.015
20 h	0.693*	0.660*	0.635*	0.537*	0.610*	0.537*
24 h	0.627*	0.600*	0.553*	0.482*	0.550*	0.517*

*Indicates that correlation is significant at the level $p < 0.05$.

Twelve biomechanical testing locations were examined from proximal, central, and distal cartilage surrounding the lesions in respect to the anatomical location. Biomechanical testing revealed that in the experimental samples, the equilibrium and dynamic moduli were lower compared with the moduli of the healthy, control samples at all distal locations and most of the central locations ($p < 0.05$). The difference increased toward the distal aspect of the specimens with respect to the joint orientation. The moduli of the control samples decreased toward the medial aspect of the femoral groove. Safranin-O staining revealed a lower overall PG content in the experimental samples compared to the controls. This difference in PG content was greatest near the lesion site and decreased when moving further away in the proximal and distal locations. In contrast, in the central locations, the difference in PG content was greatest farthest away from the lesion site and decreased toward the lesion.

Significant correlations between CA4+ partition and reference parameters (optical density, equilibrium moduli, and dynamic moduli) were obtained at late-diffusion time points of 20 and 24 h (Table 1). Spearman's rank correlations at these time points varied between $\rho = 0.482$ and $\rho = 0.693$. Significant correlations were also obtained at 30 and 60 min time points where the Spearman's rank correlations varied between $\rho = -0.078$ and $\rho = -0.341$.

4 | DISCUSSION

In our previous studies, we showed that QDECT can simultaneously quantify CA4+ and gadoteridol partitions in cartilage, and differentiate healthy from injured cartilage tissue.[23,24,27,35] However, the potential of QDECT to detect posttraumatic degeneration in the tissue surrounding a lesion has remained unknown. To investigate this issue, we examined posttraumatic degeneration in equine cartilage surrounding a surgically created and repaired lesion at different imaging time points and evaluated the diagnostic capacity of QDECT in this laboratory study.

CA4+ partition was greater in the experimental samples compared with the control samples at 30 and 60 min after immersion in the contrast agent mixture. In the beginning, the CA4+ diffusion is governed by the lowered steric hindrance but as it reaches equilibrium, the tissue region with the greater PG content dominates the CA4+ partitioning. CA4+ partitions in full-thickness and superficial cartilage layers were significantly higher at the 20 h imaging time point in control samples compared with experimental samples. This result is in line with previous results,[23,24,26,27] as the PG content dominates the partition of CA4+ at the late diffusion time points. Unexpectedly, no difference in 24 h time point was found. With the experimental cartilage samples, no apparent difference in either contrast agent partition values between 20 and 24 h existed, indicating that diffusion is at equilibrium or nearly approaching it. In contrast, the contrast agents in control samples did not reach diffusion equilibrium at 20 h as a significant difference was seen

between the partition values at 20 and 24 h time points. This incomplete diffusion likely contributes to the observed difference in the partitions between 20 and 24 h in control samples and explains why no statistically significant difference in CA4+ partition could be found between control and experimental samples at the 24 h time point.

Gadoteridol partitions were lower in the experimental than in control samples at the 60 and 120 min time points. Faster diffusion of gadoteridol is consistent with the increases in the water content and permeability of degenerated cartilage. In this context, the lower partition of gadoteridol in the experimental samples at the early diffusion time point is surprising. This result may be explained by the diffusion-related challenges due to possible interactions between gadoteridol and CA4+ molecules. By examining the concentration maps in Figures 2 and 3, the partition of gadoteridol appears to be lower in the areas of high CA4+ partition, suggesting that a repulsive interaction between the two contrast agents may also be occurring. Previous studies have demonstrated that the iodine and gadolinium concentrations can be accurately measured with QDECT,[23,25,27] thus indicating that the technique is functional but may be subject to the above-described challenge in more demanding measurement set-ups. In this study, for example, the size of the samples was bigger, and more tissue is included around the measurement sites whereas the previous studies only included the cartilage with the measured lesions and a small amount of bone underneath.

The present results showed no difference in the partition of the nonionic gadolinium contrast agent between the experimental and control samples at the late-diffusion time points, suggesting that no difference in water content exists. Thus, in the early-diffusion time point, the increased diffusion of the CA4+ with the experimental samples is mostly due to decreased steric hindrance. Alternatively, the differences in water content may be so subtle that these differences are overshadowed by the limitation of conventional microCT, which reduce the sensitivity of QDECT. Conventional microCT systems suffer from beam hardening and other artifacts originating from the polychromatic X-ray beam. The weaknesses of conventional microCT systems can be avoided with synchrotron microCT that implements a narrow energy spectrum, thus minimizing the negative effects of the polychromatic X-ray beam.

A significant positive correlation was seen to exist between the PG content and CA4+ partition at 20 and 24 h time points in both superficial cartilage and full-thickness cartilage. At early diffusion time points (30 and 60 min), the correlations were relatively weak and surprisingly negative. This finding suggests that evaluation of PG content based on CA4+ diffusion in the early diffusion time point in cartilage tissue surrounding the lesion site is unreliable. At 20 and 24 h time points, between equilibrium/dynamic moduli and CA4+ partition, the correlations were positive in both superficial and full cartilage layers. For equilibrium modulus and in the superficial layer for dynamic modulus, weak negative correlations exist in both superficial cartilage and full-thickness at 30 and 60 min time points. The negative correlations are surprising as in previous studies a

positive correlation between CA4+ partition and PG content at early diffusion time points in the lesion sites was reported.[23,26,27] This negative correlation may also arise from the lowered steric hindrance of posttraumatic cartilage, thereby increasing the diffusion of CA4+. Further, reliable quantification of PG and water contents in early-diffusion time points is challenging in species with relatively thick cartilage. In species with thin cartilage (e.g., mice with cartilage thickness of $87 \pm 13 \, \mu m$[36]), mapping of PG and water concentrations is possible after very short diffusion times.

To achieve the most accurate results, data collection with two energies should be performed simultaneously with the shortest possible acquisition time. In this study, the acquisitions at the two energies (90 and 50 keV) were obtained consecutively with the time difference between the acquisition starting points being 4 min 10 s. The acquisition time for one energy was 2.6 min. Immediately after the contrast agent immersion, the diffusion rate of the contrast agent is at its highest, constantly altering the depth-wise partition. Thus, the ongoing diffusion results in an average uptake of the contrast agent over the measurement time rather than an exact uptake value at a certain time point. As the measurement protocols were similar for all samples, the ongoing diffusion has minimal effect on the results or conclusions.

In this study, the samples were images in the air, providing significant contrast, which is unobtainable by imaging joint surfaces ex vivo or in vivo. Loss of contrast at articulating surfaces may lead to incorrect segmentation of cartilage and thus cause misinterpretation of contrast agent partitions. Further, at in vivo imaging, the loss and dilution of contrast agents in the joint capsule occurs rapidly. Thus, the time-dependent contrast agent partitions obtained in this study are greater than can be attained in vivo. The next step forward is to address these limitations in future studies.

In summary, QDECT allows evaluation of cartilage degeneration at diffusion equilibrium and quantification of PG and water contents in the laboratory setting. Additionally, QDECT can differentiate healthy tissue from posttraumatic tissue based on CA4+ partition at 30 and 60 min after contrast agent immersion. However, reliable evaluation of PG content was found challenging at early diffusion imaging time points. The results indicate that evaluation of posttraumatic degeneration in the tissue surrounding the lesions is more complicated than in the lesion site. As indicated above, many challenges still exist and further assessment of QDECT in ex vivo and in vivo models are required to ascertain its limitations and full potential as a diagnostic tool. Given the clinical need for improved diagnostic capabilities for PTOA, the development of QDECT or other such techniques is critical to empower clinicians to choose the optimal treatment modalities for delaying and/or preventing the onset or progression of PTOA.

CONFLICT OF INTERESTS

Dr. Grinstaff reports a patent pending on CA4+ composition. The other authors declare that there are no conflict of interests.

AUTHOR CONTRIBUTIONS

The conception and design of the study was done by Annina EA. Saukko, Irina AD. Mancini, Jetze Visser, Harold Brommer, P Rénévan van Weeren, Jos Malda, Mark W. Grinstaff, Harrie Weinans, and Juha Töyräs. Nikae CR. te Moller, Irina AD. Mancini, Jetze Visser, Harold Brommer, P Rénévan van Weeren, Jos Malda, and Jaakko K. Sarin participated in the sample collection. Biomechanical measurements were performed by Jaakko K. Sarin and Nikae CR. te Moller. Digital densitometry measurements were conducted by Jaakko K. Sarin. Annina EA. Saukko performed microCT measurements. Data analysis was done by Annina EA. Saukko, Olli Nykänen, and Mikko J. Nissi. The data interpretation was done by all the authors. Original draft preparation was done by Annina EA. Saukko and Juha Töyräs. All the authors have critically reviewed and approved the manuscript.

DATA AVAILABILITY STATEMENT

The datasets used and/or analyzed during the current study are available from the corresponding author on reasonable request.

ORCID

Annina E. A. Saukko http://orcid.org/0000-0001-8678-4675
Olli Nykänen http://orcid.org/0000-0001-7329-3463
Jaakko K. Sarin https://orcid.org/0000-0002-6237-9015
Mikko J. Nissi https://orcid.org/0000-0002-5678-0689
Nikae C. R. te Moller http://orcid.org/0000-0001-8675-330X
P. Réné van Weeren https://orcid.org/0000-0002-6654-1817
*Mark W. Grinstaff* http://orcid.org/0000-0002-5453-3668

REFERENCES

1. Anderson DD, Chubinskaya S, Guilak F, et al. Posttraumatic osteoarthritis: improved understanding and opportunities for early intervention. *J Orthop Res.* 2011;29(6):802-809.
2. Olson SA, Furman BD, Kraus VB, Huebner JL, Guilak F. Therapeutic opportunities to prevent post-traumatic arthritis: lessons from the natural history of arthritis after articular fracture. *J Orthop Res.* 2015;33(9):1266-1277.
3. Li X, Pedoia V, Kumar D, et al. Cartilage T1ρ and T2 relaxation times: longitudinal reproducibility and variations using different coils MR systems and sites. *Osteoarthr Cartil.* 2015;23(12):2214-2223.
4. Link TM, Neumann J, Li X. Prestructural cartilage assessment using MRI. *J Magn Reson Imaging.* 2017;45(4):949-965.
5. Lakin BA, Snyder BD, Grinstaff MW. Assessing cartilage biomechanical properties: techniques for evaluating the functional performance of cartilage in health and disease. *Annu Rev Biomed Eng.* 2017;19(1):27-55.
6. Kokkonen HT, Aula AS, Kröger H, et al. Delayed computed tomography arthrography of human knee cartilage in vivo. *Cartilage.* 2012;3(4):334-341.

7. Myller KA, Turunen MJ, Honkanen JT, et al. In vivo contrast-enhanced cone beam CT provides quantitative information on articular cartilage and subchondral bone. *Ann Biomed Eng*. 2017;45(3): 811-818.

8. Yoo HJ, Hong SH, Choi J-Y, et al. Contrast-enhanced CT of articular cartilage: experimental study for quantification of glycosaminoglycan content in articular cartilage. *Radiology*. 2011;261(3):805-812.

9. Stewart RC, Honkanen JTJ, Kokkonen HT, et al. Contrast-enhanced computed tomography enables quantitative evaluation of tissue properties at intrajoint regions in cadaveric knee cartilage. *Cartilage*. 2016;8:391-399.

10. Kokkonen HT, Suomalainen J-S, Joukainen A, et al. In vivo diagnostics of human knee cartilage lesions using delayed CBCT arthrography. *J Orthop Res*. 2014;32(3):403-412.

11. Silvast TS, Kokkonen HT, Jurvelin JS, Quinn TM, Nieminen MT, Töyräs J. Diffusion and near-equilibrium distribution of MRI and CT contrast agents in articular cartilage. *Phys Med Biol*. 2009;54(22): 6823-6836.

12. Kallioniemi AS, Jurvelin JS, Nieminen MT, Lammi MJ, Töyräs J. Contrast agent enhanced pQCT of articular cartilage. *Phys Med Biol*. 2007;52(4):1209-1219.

13. Stewart RC, Bansal PN, Entezari V, et al. Contrast-enhanced CT with a high-affinity cationic contrast agent for imaging ex vivo bovine, intact ex vivo rabbit, and in vivo rabbit cartilage. *Radiology*. 2013; 266(1):141-150.

14. Joshi NS, Bansal PN, Stewart RC, Snyder BD, Grinstaff MW. Effect of contrast agent charge on visualization of articular cartilage using computed tomography: exploiting electrostatic interactions for improved sensitivity. *J Am Chem Soc*. 2009; 131(37):13234-13235.

15. Palmer AW, Guldberg RE, Levenston ME. Analysis of cartilage matrix fixed charge density and three-dimensional morphology via contrast-enhanced microcomputed tomography. *Proc Natl Acad Sci USA*. 2006;103(51):19255-19260.

16. Lusic H, Grinstaff MW. X-ray-computed tomography contrast agents. *Chem Rev*. 2013;113(3):1641-1666.

17. Lin PM, Chen C-TC, Torzilli PA. Increased stromelysin-1 (MMP-3), proteoglycan degradation (3B3- and 7D4) and collagen damage in cyclically load-injured articular cartilage. *Osteoarthr. Cartil*. 2004; 12(6):485-496.

18. Buckwalter JA. Mechanical injuries of articular cartilage. *Iowa Orthop J*. 1992;12:50.

19. Silvast TS, Jurvelin JS, Aula AS, Lammi MJ, Töyräs J. Contrast agent-enhanced computed tomography of articular cartilage: association with tissue composition and properties. *Acta Radiol*. 2009;50(1): 78-85.

20. Bansal PN, Stewart RC, Entezari V, Snyder BD, Grinstaff MW. Contrast agent electrostatic attraction rather than repulsion to glycosaminoglycans affords a greater contrast uptake ratio and improved quantitative CT imaging in cartilage. *Osteoarthr. Cartil*. 2011;19(8):970-976.

21. Lakin BA, Grasso DJ, Stewart RC, Freedman JD, Snyder BD, Grinstaff MW. Contrast enhanced CT attenuation correlates with the GAG content of bovine meniscus. *J Orthop Res*. 2013;31(11): 1765-1771.

22. Lakin BA, Grasso DJ, Shah SS, et al. Cationic agent contrast-enhanced computed tomography imaging of cartilage correlates with the compressive modulus and coefficient of friction. *Osteoarthr. Cartil*. 2013;21(1):60-68.

23. Saukko AEA, Turunen MJ, Honkanen MKM, et al. Simultaneous quantitation of cationic and non-ionic contrast agents in articular cartilage using synchrotron microCT imaging. *Sci Rep*. 2019;9(1):1-9.

24. Honkanen MKM, Matikka H, Honkanen JTJ, et al. Imaging of proteoglycan and water contents in human articular cartilage with full-body CT using dual contrast technique. *J Orthop Res*. 2019;37(5): 1059-1070.

25. Bhattarai A, Honkanen JTJ, Myller KAH, et al. Quantitative Dual Contrast CT Technique for Evaluation of Articular Cartilage Properties. *Ann Biomed Eng*. 2018;46(1038):1-9.

26. Honkanen MKM, Saukko AEA, Turunen MJ, et al. Triple contrast CT method enables simultaneous evaluation of articular cartilage composition and segmentation. *Ann Biomed Eng*. 2020;48(2): 556-567.

27. Honkanen MKM, Saukko AEA, Turunen MJ, et al. Synchrotron microCT reveals the potential of the dual contrast technique for quantitative assessment of human articular cartilage composition. *J Orthop Res*. 2020;38(3):563-573.

28. Qu C, Hirviniemi M, Tiitu V, Jurvelin JS, Töyräs J, Lammi MJ. Effects of freeze-thaw cycle with and without proteolysis inhibitors and cryopreservant on the biochemical and biomechanical properties of articular. *Cartilage. Cartilage*. 2014;5(2):97-106.

29. Bekkers JE, Tsuchida AI, van Rijen MH, et al. Single-stage cell-based cartilage regeneration using a combination of chondrons and mesenchymal stromal cells. *Am J Sports Med*. 2013;41(9):2158-2166.

30. Sarin JK, Nykänen O, Tiitu V, et al. Arthroscopic determination of cartilage proteoglycan content and collagen network structure with near-infrared spectroscopy. *Ann Biomed Eng*. 2019;47(8):1815-1826.

31. Hayes WC, Keer LM, Herrmann G, Mockros LF. A mathematical analysis for indentation tests of articular cartilage. *J Biomech*. 1972; 5(5):541-551.

32. Danso EK, Mäkelä JT, Tanska P, et al. Characterization of site-specific biomechanical properties of human meniscus—importance of collagen and fluid on mechanical nonlinearities. *J Biomech*. 2015; 48(8):1499-1507.

33. Nykänen O, Sarin JK, Ketola JH, et al. T2* and quantitative susceptibility mapping in an equine model of post-traumatic osteoarthritis: assessment of mechanical and structural properties of articular cartilage. *Osteoarthr. Cartil*. 2019;27(10):1481-1490.

34. Kiviranta I, Jurvelin J, Säämänen A-M, Helminen HJ. Microspectrophotometric quantitation of glycosaminoglycans in articular cartilage sections stained with Safranin O. *Histochemistry*. 1985; 82(3):249-255.

35. Bhattarai A, Honkanen JTJ, Myller KAH, et al. Quantitative dual contrast CT technique for evaluation of articular cartilage properties. *Ann Biomed Eng*. 2018;46(7):1038-1046.

36. Malda J, de Grauw JC, Benders KEM, et al. Of mice, men and elephants: the relation between articular artilage thickness and body mass. *PLOS One*. 2013;8(2):e57683.
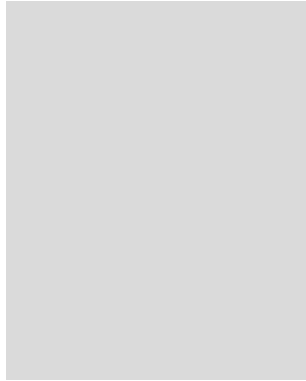
ANNINA SAUKKO

To prevent the onset of osteoarthritis, early detection of post-traumatic changes in articular cartilage is important for selecting the optimal treatment options. This thesis presents a triple-contrast computed tomography technique that improves the characterization of cartilage proteoglycan and water contents and enables the simultaneous and accurate segmentation of the articulating surfaces; thus, the triple-contrast technique provides more comprehensive information for treatment planning.

UNIVERSITY OF
EASTERN FINLAND

uef.fi